Effect of Variations in Metal Inclusion Geometries on the Performance of Meta-DRAs

A Thesis Submitted to the

College of Graduate Studies and Research

In Partial Fulfillment of the Requirements

For the Degree of Master of Science

In the Department of Electrical and Computer Engineering

University of Saskatchewan

Saskatoon

By

Shaon Ganguly

Permission to Use

In presenting this thesis in partial fulfillment of the requirements for a Postgraduate degree from the University of Saskatchewan, I agree that the Libraries of this University may make it freely available for inspection. I further agree that permission for copying of this thesis in any manner, in whole or in part, for scholarly purposes may be granted by the professor or professors who supervised my thesis work or, in their absence, by the Head of the Department or the Dean of the College in which my thesis work was done. It is understood that any copying or publication or use of this thesis or parts thereof for financial gain shall not be allowed without my written permission. It is also understood that due recognition shall be given to me and to the University of Saskatchewan in any scholarly use which may be made of any material in my thesis.

Requests for permission to copy or to make other use of material in this thesis in whole or part should be addressed to:

Head of the Department of Electrical and Computer Engineering

University of Saskatchewan

3B48 Engineering Building

57 Campus Drive, Saskatoon, SK

Saskatoon SK S7N 5A9

Abstract

Antennas that use the radiating mode of a dielectric resonator are called Dielectric Resonator Antennas (DRAs). They are used extensively in microwave communication in today's world. They can be of any three-dimensional shape such as cylindrical, rectangular, hemispherical, etc. Such a resonator typically has low loss (no conductor loss) and frequency bandwidth is dependent on the dielectric permittivity. They are generally smaller in size than an equivalent metallic cavity, and can be incorporated into microwave circuits and coupled to planar transmission lines.

DRAs are much more difficult to batch fabricate along with microwave circuits compared to their metal counterparts. This is due to the fact that most DRAs are generally made of high permittivity ceramics, which require high temperature firing which is not generally compatible with microwave fabrication processes. The fabrication of miniature DRAs for high frequency bands is even more challenging. Machining of the extremely hard ceramics becomes difficult. This resulted in a new approach proposed in the research group, which enabled one to fabricate DRAs using lower permittivity 'soft' polymer materials. These so called 'meta-DRAs' were formed by incorporating metal inclusions within a polymer base material. The polymer-base has a very low permittivity, and hence does not naturally resonate as a DRA in the 20-60 GHz region. In order to achieve resonance at the desired frequencies, the relative permittivity of the DRA has to be increased considerably. This was done by introducing metal inclusions in the polymer base of the DRA to affect the electric flux density. In this thesis, a wide variety of such meta-DRAs have been designed and simulated considering various structural design parameters. The simulations have been done using HFSS version 15.0 and a layout for fabrication was developed with the help of AutoCAD and ADS. The antennas were designed for two principal resonating frequencies, 24 GHz and 60 GHz. Various

designs were evaluated and the ones with the best results were included in the layout. Small physical variations such as lateral metal width and gap have been carried out. The height of the inclusions was also altered. The layout was used to fabricate an X-Ray mask at the Karlsruhe Institute of Technology (KIT), Germany. Using this mask, X-Ray lithography and metal electroplating were used to demonstrate the feasibility of fabricating the proposed structure.

In the thesis, the entire process used to design and simulate these meta-DRAs has been explained and the simulation results have been compared. The primary objective of this project, to demonstrate through simulations an increase in the effective permittivity of a polymer based DRA and the effect on permittivity of varying the inclusion properties, has been successfully satisfied.

Generally, the use of metal inclusions can increase the effective relative permittivity of the DRA in the range of 12-16. Different metal inclusion geometries behave differently. Out of the geometries tested, the “H shaped” inclusions generally perform most favorably. Other geometries include “window” and “half-window”. Certain meta-DRAs with unusual shapes or special meta arrays have been designed and results compared. Varying the gap/width of the meta inclusions affects the resonance. This also depends on the number of elements (metal inclusions) in the polymer base. Some designs have non-uniform metal widths. Non-uniform height of the meta samples results in multiple resonances in some cases.

ACKNOWLEDGMENTS

I would like to take this opportunity and extend my gratitude towards my supervisor, Dr. David M Klymyshyn. His encouragement and support throughout the project has been wonderful. I thank him for giving me an opportunity to pursue my Master's degree here at University of Saskatchewan.

A big thank you to Matt Tayfeh, PhD candidate at University of Saskatchewan, guided by Dr. David M Klymyshyn for his able guidance and constant help. I am also thankful to Dr. Martin Boerner and the micro-fabrication group at KIT, Germany, for their ongoing contribution in fabricating the meta-DRAs.

Also, I would like to thank Randy Hickson, Computer Support Technician, College of Engineering, University of Saskatchewan, for his help in setting up the computer used for the research.

I would like to thank my supervisor and College of Engineering, University of Saskatchewan, for providing funding and financial support for my education.

Finally I would like to thank my family and friends in India for their continuing support. Also I would like to take a moment and remember my grandmother who passed away this year. Her ideals continue to inspire me. A big thank you to my extended family here in Canada who have given me so much love and encouragement during my research here.

Table of Contents

LIST OF TABLES

LIST OF FIGURES

LIST OF ABBREVIATIONS

ADS	Advanced Design System
CAD	Computer Aided Design
dB	Decibel
dBW	Decibel-watt
DRA	Dielectric Resonator Antenna
D-XRL	Deep X-Ray Lithography
EM	Electromagnetic
f_0	Central Frequency
FEM	Finite Element Method
HFSS	High Frequency Structure Simulator
KIT	Karlsruhe Institute of Technology
L	Length
LC	Inductor and Capacitor
LCP	Liquid Crystal Polymers
LHM	Left Handed Media
NIM	Negative Index Material
PMMA	Polymethylmethacrylate
PRA	Polymer Resonator Antenna
RDRA	Rectangular Dielectric Resonator Antenna
S_{11}	Reflection Coefficient in terms of S-Parameters
Si	Silicon

SoP	System-on-Package
S-Parameters	Scattering Parameters
TE	Transverse Electric
TEM	Transverse Electromagnetic
TM	Transverse Magnetic
TLs	Transmission Lines
V_g	Group Velocity
ε_r	Relative Permittivity
$\boldsymbol{\lambda_0}$	Wavelength at resonant frequency
μ	Magnetic Permeability

Chapter I
Introduction

1.1 Motivation

Dielectric Resonator Antennas have immense potential in the communication industry due to their attractive features such as small size, high radiation efficiency, wide bandwidth and high power handling capability. The size of DRAs can be reduced by increasing the dielectric constant of the resonator (ε_r) resulting in compact antennas. ε_r also affects the frequency bandwidth, defined as the percentage of the operating frequency where a certain acceptable impedance is maintained. For instance, a DRA with ε_r of 10 can provide approximately 10 percent impedance bandwidth, whereas a metal microstrip patch antenna typically provides only a few percent. DRAs can be excited by various feeding mechanisms which are not so complex. The radiation efficiency of a lossy DRA is much higher than that of a typical microstrip patch antenna. They also can provide different radiation patterns due to their varied geometry or resonance modes.

Even though DRAs have advantages, microstrip patch antennas are used more widely for practical purposes. This is mainly because DRAs are made of high permittivity materials such as ceramics. As a result, they are more difficult to fabricate and integrate in a compatible process with microwave circuitry. Microstrip patch antennas are however much easier to process due to compatibility with printed-circuit technology. The problem becomes much worse at the millimetre-wave frequencies where the size of the resonator is in the lower millimetre region and the tolerance for manufacturing errors becomes even smaller. Due to these shortcomings DRAs are not widely used in commercial applications, which is unfortunate given the fact that they are more capable and could make a massive impact in communication industries.

To overcome the fabrication complexity of the DRAs, polymer based DRAs have been proposed and fabricated by Dr. David Klymyshyn's research group at the University of Saskatchewan [1,2]. These DRAs are made of polymer materials, which can dramatically simplify the fabrication process of DRAs. But by replacing a high permittivity material like ceramic with a very low permittivity polymer, the DRA is difficult to excite and typically resonates at very high frequencies (millimeter waves) for small geometries. To overcome this difficulty, metal inclusions were introduced in the polymer-base of the DRA (meta-DRA) [1]. A polymer typically has a low permittivity, ε_r, in the range of 2-3. By introducing various metal inclusions in a certain pattern, the permittivity could be increased to ~16 [1]. This would emulate a high permittivity material like ceramic and also ease the process of fabrication. With the help of photosensitive polymers, a lithographic process can be used. This thesis is a parametric study of the effects of varying the metal inclusion geometries similar to those shown in [1]. The polymer assumed for the design and study of the meta-DRAs in this thesis had a relative permittivity of 2.5 with a dielectric loss tangent of 0.01. Nickel was assumed as the material for the metal inclusions. Figure 1.1 shows the top view of a typical polymer-based DRA with metal inclusions.

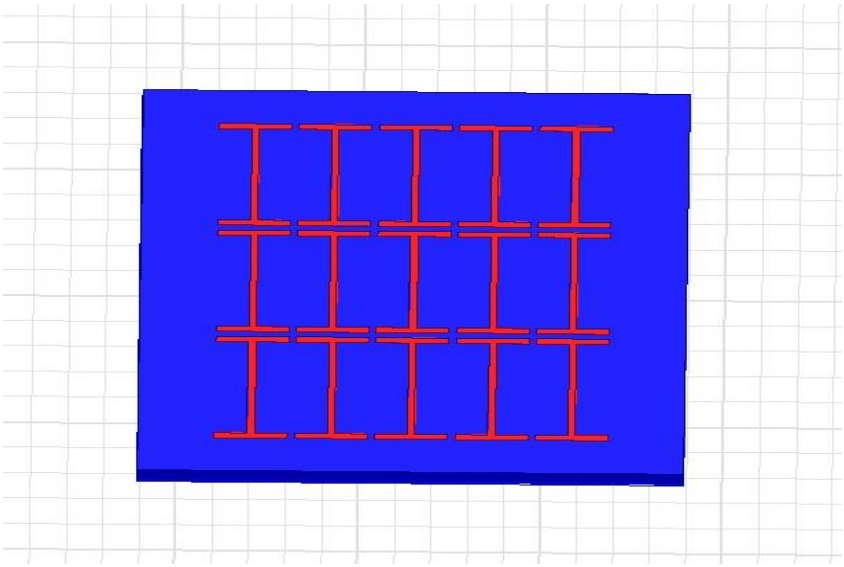

Figure 1.1. Example of a polymer based DRA with metal inclusion.

1.2. Background and Literature Review

Meta-DRAs, a new approach towards resonator antennas, was introduced by the research team led by Professor David Klymyshyn at the University of Saskatchewan in their work in [1]. Metamaterials are defined in several books and journals as artificially structured materials composed of periodic arrays of resonant sub-wavelength metallic structures. Their magnetic and electrical properties provide a freedom to alter dielectric properties, which may not exist in conventional materials. The field of metamaterials generated a lot of interest due to the prospect of obtaining a negative index of refraction. Veselago [3] predicted that in a negative index material (NIM), refraction would occur at negative angles, energy would flow in a direction opposite to the direction of wave front propagation (phase velocity), and the Doppler Effect (the effect on the frequency of a wave due to the change in proximity of the source and/or receiver) would be reversed. A negative index material can be created by combining a negative electric permittivity (ε) material and a negative magnetic permeability (μ) material. Such a medium has been implemented with a combination of magnetically resonant antenna and electrically excitable medium.

By changing the geometrical parameters of the constituent structure of a metamaterial, the realized dielectric or magnetic properties can be engineered. As a result, metamaterials enable the design of materials with choice of electromagnetic properties [4]. The electromagnetic properties of any material can be characterized by its electric permittivity and magnetic permeability. These are governed by a set of vector equations defined by Maxwell and are commonly known as Maxwell's equations [5]:

$$\nabla \times E = -\frac{\partial B}{\partial t}$$

$$\nabla \times H = J + \frac{\partial D}{\partial t} \qquad (1.1)$$

$$\nabla . D = \rho$$

$$\nabla . B = 0$$

Where,

E is the electric field intensity (volt/m),

H is the magnetic field intensity (ampere/m),

D is the electric flux density (coulomb/m^2),

B is the magnetic flux density, also known as magnetic induction (tesla),

J is the electric current density of any external charges (ampere/m^2), and

ρ is the volume charge density of any external charges (coulomb/m^3).

SI units represent all the units of the above expressions. In free space, the electric and magnetic flux densities can also be represented in terms of electric permittivity and magnetic permeability as follows:

$$D = \varepsilon_0 E \qquad (1.2)$$

$$B = \mu_0 H \qquad (1.3)$$

Where,

ε_0 = 8.854 x 10^{-12} farad/m and

μ_0 = 4Π x 10^{-7} Henry/m.

The above expressions are true only for a free space environment. But in practicality, material bodies are often present in the environment, which complicates the analysis.

In a dielectric medium, the E field causes a polarization of the particles given by P that produces electric dipole moments. This adds to the total flux density of the medium given by

$$D = \varepsilon_0 E + P. \tag{1.4}$$

The polarization vector P can be denoted as

$$P = \varepsilon_0 \mathcal{X}_e E, \tag{1.5}$$

where, $\mathcal{X}_e$ is the electric susceptibility and can be complex. Hence equation 1.4 becomes

$$D = \varepsilon_0 \varepsilon_r E = \varepsilon E \tag{1.6}$$

where, $\varepsilon_r = 1 + \mathcal{X}_e$ is the relative permittivity and $\varepsilon = \varepsilon_0(1 + \mathcal{X}_e)$ is the complex permittivity of the medium. The complex permittivity accounts for the vibration losses like damping, which does not happen in free space.

Hence it is clear that the dielectric properties of a DRA are resulted from the phenomenon called dielectric polarization that occurs when electromagnetic fields pass through them. A DRA at rest contains randomly oriented permanent electric dipoles. When an external field is applied, the dipoles align themselves in the direction of the field and the material is said to be polarized.

Similar analysis can be done for the magnetic materials. Magnetic dipole moments are produced on application of a magnetic field in a magnetic material, which results in a magnetic polarization of P_m. This is also known as magnetization. The magnetic flux density is given by

$$B = \mu_0 (H + P_m). \tag{1.7}$$

For a linear material, the magnetic polarization is linearly related to H as follows:

$$P_m = \mathcal{X}_m H, \tag{1.8}$$

where, $\mathcal{X}_m$ is the complex magnetic susceptibility. Combining the above equations and simplifying, the following expression is obtained:

$$B = \mu_0 (1 + \mathcal{X}_m) H = \mu H \tag{1.9}$$

Where, $\mu = \mu_0 (1 + \mathcal{X}_m)$ is the complex magnetic permeability of the medium. The complex part of the μ or $\mathcal{X}_m$ accounts for the loss that occurs due to damping. The equations (1.2) and (1.3) can now be written as:

$$D = \varepsilon E \tag{1.10}$$

$$B = \mu H \tag{1.11}$$

For wave propagation, the charge and current densities are localized in space. They are restricted to flow on an antenna. These are considered as sources of the electromagnetic fields and due to their restriction, the region of space is taken to be as source-free. This gives rise to the source-free Maxwell's equations. The set of equations in (1.1) can now be rewritten as:

$$\nabla \times E = -\frac{\partial B}{\partial t}$$

$$\nabla \times H = \frac{\partial D}{\partial t} \tag{1.12}$$

$$\nabla . D = 0$$

$$\nabla . B = 0$$

From the above set of equations, it can be noted that the densities J and ρ are considered as zero. The source-free Maxwell's equations could be applied to a region and a solution with unknown coefficients could be obtained. These unknown factors could be computed using certain boundary conditions of the region.

In [6], a polymer based DRA for millimeter-wave applications was discussed by the research team led by Professor David Klymyshyn at the University of Saskatchewan. As stated earlier, the fabrication of DRAs in complicated geometries and array patterns is challenging due to the fact that they are composed of ceramics, which are naturally hard materials. Hence they are

difficult to machine. This is where polymer based resonator antennas (PRAs) can immensely simplify the fabrication process [7]. Polymers are rapidly becoming important among materials for microwave and electronic applications whether used in pure form or combined with ceramic powders [8]. For example, in opto-electronics, polymers have been used to produce mechanically flexible "electronic paper" [9] and high-efficiency light emitting diodes [10]. Liquid crystal polymers (LCPs) have been proposed for system-on-package (SoP) applications, displaying attractive properties like low loss, low water absorption, and low cost [11]. In [12], polymer-ceramic composites were proposed as substrate materials for a scanning antenna, and, in [13], polymer-ceramic mixtures were used for thin-film capacitors. Important to note is that although polymers are not intrinsically functional as microwave materials, their properties can be altered and made to function and also their 'soft' nature (unlike crystalline materials) enables fabrication of flexible free-standing shapes.

1.3 Research Objectives

The objectives of this thesis are based on the original meta-DRA concepts developed during the PhD work of Mr. Matt Tayfeh Aligodarz at the University of Saskatchewan, supervised by Dr. David Klymyshyn [1]. The main purpose was to expand on this work to design and simulate meta-DRAs with different metal inclusion geometries resonating at very high frequencies. The batches of meta-DRAs were primarily designed to resonate around frequencies of 24 GHz and 60 GHz. Variations in design such as altering the size of number of inclusions, the width of the inclusions, and the gap between each metal inclusions of the meta-DRA were carried out and the effect on resonance and radiation were observed. Various styles of inclusions were also investigated. The antennas with best reflection coefficients (most negative dB value) and absolute gains were selected to form a layout. This layout was sent to KIT, Germany, for fabrication of an X-ray mask.

Then micro fabrication of meta-DRAs was demonstrated using deep X-ray lithography technique. The primary objectives of this research can be summarized as follows:

1. Select the shape/geometry of the metal inclusion to form the meta-DRAs and develop a set of parameters to vary for the parametric performance study.
2. Design and simulate the meta-DRAs in a three dimensional (3D) full-wave electromagnetic simulator. Define various parameters needed for design and obtain the dB reflection coefficient of the antenna.
3. Evaluate resonant frequency, radiation patterns, and absolute gain obtained from the antennas to assess the effects of inclusion geometries.
4. Compare the results obtained and choose best samples for developing a layout.
5. Have structural demonstrator devices fabricated using D-XRL technology to demonstrate the fabrication feasability.

1.4 Thesis Organization

The thesis is organized into five chapters. Chapter 2 covers the theory on DRAs and metamaterials. This chapter helps understand the various modes of a rectangular DRA antenna and also the feeding mechanism used to excite the antennas in this project. There is a detailed discussion on the history and development of metamaterials over the years and their applications. An example meta-DRA simulation has been compared with a high permittivity DRA simulation to demonstrate similarities.

Chapter 3 starts with a detailed overview of the electromagnetic simulator (HFSS) and how to use it to design and excite an antenna. Later in the chapter, all the variables and structural parameters used to design the meta-DRAs for this project have been explained. Subsequently, a meta-DRA design example has been provided. The mask or layout formation has also been explained

in detail using layout software (ADS). A brief explanation on the D-XRL process, which was used to fabricate the antennas, has been given. At the end of the chapter, a few fabricated antennas from KIT have been discussed.

Chapter 4 gives detailed simulation results obtained from various meta-DRA designs implemented in this project. Also the dB(S_{11}) (reflection coefficient) versus frequency plots are used to compare the resonance. The radiation plots have been explained in detail. All the designs have been compared to try and find out if there exists a pattern in the deviation of the resonant frequency with the alteration of the gap/width of the metal inclusions. The variation in the performance of the meta-DRAs due to change in the length of the feedline underneath the antenna was observed as well.

Chapter 5 is the final chapter of the thesis. The performance results of the meta-DRAs are summarized and the future work involved in this project is described.

Chapter 2

DRA Background and Introduction to Meta-DRA

2.1 General Theory

Dielectric resonators (DRs) have variable feed arrangement, high radiation efficiency, simple geometry, small size and the capability to produce different radiation patterns using different modes. Due to these merits, they are considered ideal for the design of a radiating antenna arrangement [14]. DRA is an open resonating structure, fabricated from a low loss microwave dielectric material. These antennas can be excited with the help of feeding techniques such as a microstrip line, which enable them to integrate with microwave printed circuit technology.

Additionally, DRAs avoid some limitations of the metal microstrip patch antenna including the high conductor losses at millimeter-wave frequencies, sensitivity to tolerances, and narrow bandwidth. DRAs of cylindrical, hemispherical and rectangular shapes are most widely used and investigated. The rectangular shape is typically easier to fabricate and one or more dimensional parameters are available as degrees of freedom for the design [15]. Impedance bandwidth varies over a wide range with resonator parameters. It can be as small as a few percent with high ε_r material or over 20% with small ε_r in conjunction with certain geometries and resonant modes. Different far field radiation patterns can be generated. For a given DRA geometry, the radiation pattern can be modified by exciting different modes.

Systematic experimental investigations on dielectric resonator antennas (DRAs) were first carried out by Long et al. [16]–[18]. Since then, theoretical and experimental investigations have been reported by many investigators on DRAs of various shapes such as spherical, cylindrical (or cylindrical ring), rectangular, etc. (e.g., [19], [20]–[25]). DRAs have been designed to operate over a wide frequency range (1 GHz to 44 GHz). There is no inherent conductor loss for a DRA, only

dielectric loss. High radiation efficiency is thus possible, which is especially attractive for high frequency millimeter wave applications, where the loss from metallic antennas can be high.

The size of the DRA is roughly proportional to $\lambda_0/\sqrt{\varepsilon_r}$, where λ_0 is the wavelength at resonant frequency and ε_r is the dielectric constant of the DRA. Thus for the same frequency, there is a natural reduction in size by increasing ε_r. Also, different values of ε_r (ranging from about 4 to up to 100) can be used, thus allowing flexibility in controlling the size and bandwidth. In this chapter, the TE and TM modes of rectangular DRAs are discussed, along with excitation method used in this project. Later in the chapter, a detailed study on metamaterials is carried out. In the final section of this chapter, the transmission and resonance of a designed meta-DRA is compared with a high permittivity antenna and the feasibility of the project is established.

2.2 Modes of a DRA

Transmission lines are a kind of waveguide that channel electromagnetic energy along a certain path. If they consist of two or more conductors, they may support transverse electromagnetic (TEM) waves, characterized by the lack of longitudinal field components. TEM transmission lines have uniquely defined voltage, current, and characteristic impedance. They are theoretically broadband and without cutoff frequency. Waveguides often consisting of a single conductor support transverse electric (TE) and/or transverse magnetic (TM) wave and are characterized by the presence of longitudinal magnetic or electric field components, respectively [5]. Such TLs can have lower loss and dispersion at high frequencies compared to practical TEM TLs, however they have a low frequency cut-off below which waves do not propagate. Dielectric waveguides, using dielectric slabs or rods, could guide the waves in a particular direction according to Maxwell's equations. If the waveguide is of finite length, upon excitation it can resonate in various modes depending on the

geometrical structure. In this thesis, the theory behind rectangular waveguide resonators has been considered.

2.2.1 Rectangular DRAs (RDRAs)

Rectangular DRAs offer practical advantages over cylindrical and spherical shapes. The mode degeneracy of an antenna could enhance its cross-polar levels, thus limiting its performance. In the case of rectangular DRAs, mode degeneracy could be avoided by properly choosing the three dimensions of the resonator. It may be noted that mode degeneracy always exists in the case of a spherical DRA [26] and in the case of hybrid modes of a cylindrical DRA [27]. Further, for a given resonant frequency, two aspect ratios of a rectangular DRA (height/length and width/length) can be chosen independently. Since the bandwidth of a DRA also depends on its aspect ratio(s), a rectangular-shaped DRA provides more flexibility in terms of bandwidth control [19].

A rectangular DRA theoretically supports two type of modes, TM and TE, but TM modes have never been observed experimentally [19]. Figure 2.1 shows a rectangular DRA placed on a finite ground plane with length = d, width = w, height = h and relative permittivity = ε_r. It also depicts the corresponding rectangular coordinate system. The resonant modes can be TE to any dimension, denoted as TE^x, TE^y, or TE^z. For the calculations in this section, the DRA is considered as an x-directed short magnetic dipole.

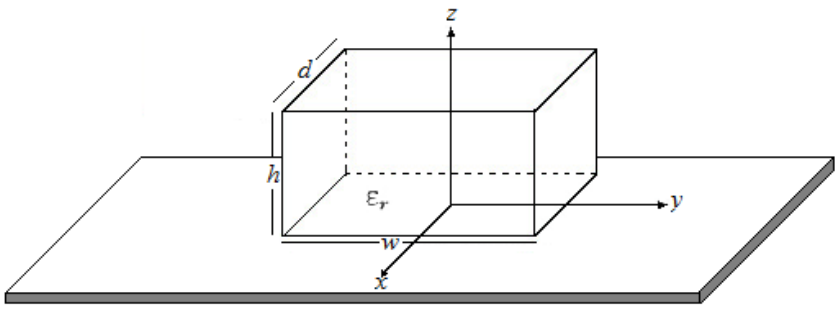

Figure 2.1 Geometry of a RDRA on a finite ground plane.

The modes of a DRA can therefore, be TE to any of three dimensions. Referring to the DRA with dimensions $w > b$ or d (where $b = 2h$) and the coordinate system shown in Figure 2.1, the lowest order mode will be $TE^{x}\delta_{11}$. Using the dielectric waveguide model, this leads to the following fields within the DRA [19]:

$$H_x = \frac{(k_y^2+k_x^2)}{j\omega\mu_0}\cos(k_x x)\cos(k_y y)\cos(k_z z) \tag{2.1}$$

$$H_y = \frac{(k_y^2+k_x^2)}{j\omega\mu_0}\sin(k_x x)\sin(k_y y)\cos(k_z z) \tag{2.2}$$

$$H_z = \frac{(k_z k_x)}{j\omega\mu_0}\sin(k_x x)\cos(k_y y)\sin(k_z z) \tag{2.3}$$

$$E_x = 0 \tag{2.4}$$

$$E_y = k_z\cos(k_x x)\cos(k_y y)\sin(k_z z) \tag{2.5}$$

$$E_z = -k_y\cos(k_x x)\sin(k_y y)\cos(k_z z) \tag{2.6}$$

where,

$$k_x \tan\left(\frac{k_x d}{2}\right) = \sqrt{(\varepsilon_r - 1)k_0^2 - k_x^2} \tag{2.7}$$

and

$$k_0 = \frac{2\pi f_0}{c} \tag{2.8}$$

$$k_x^2 + k_y^2 + k_z^2 = \varepsilon_r k_0^2 \tag{2.9}$$

where f_0 is the resonant frequency and c is the speed of light in vacuum (3×10^8 m/s).

The $e^{j\omega t}$ time dependence is suppressed in the above equations. Assuming magnetic walls along air-dielectric interfaces parallel to the z-axis, then

$$k_y = \frac{m\pi}{w} \quad \text{and} \quad k_z = \frac{n\pi}{b} \tag{2.10}$$

where m, n are positive integers.

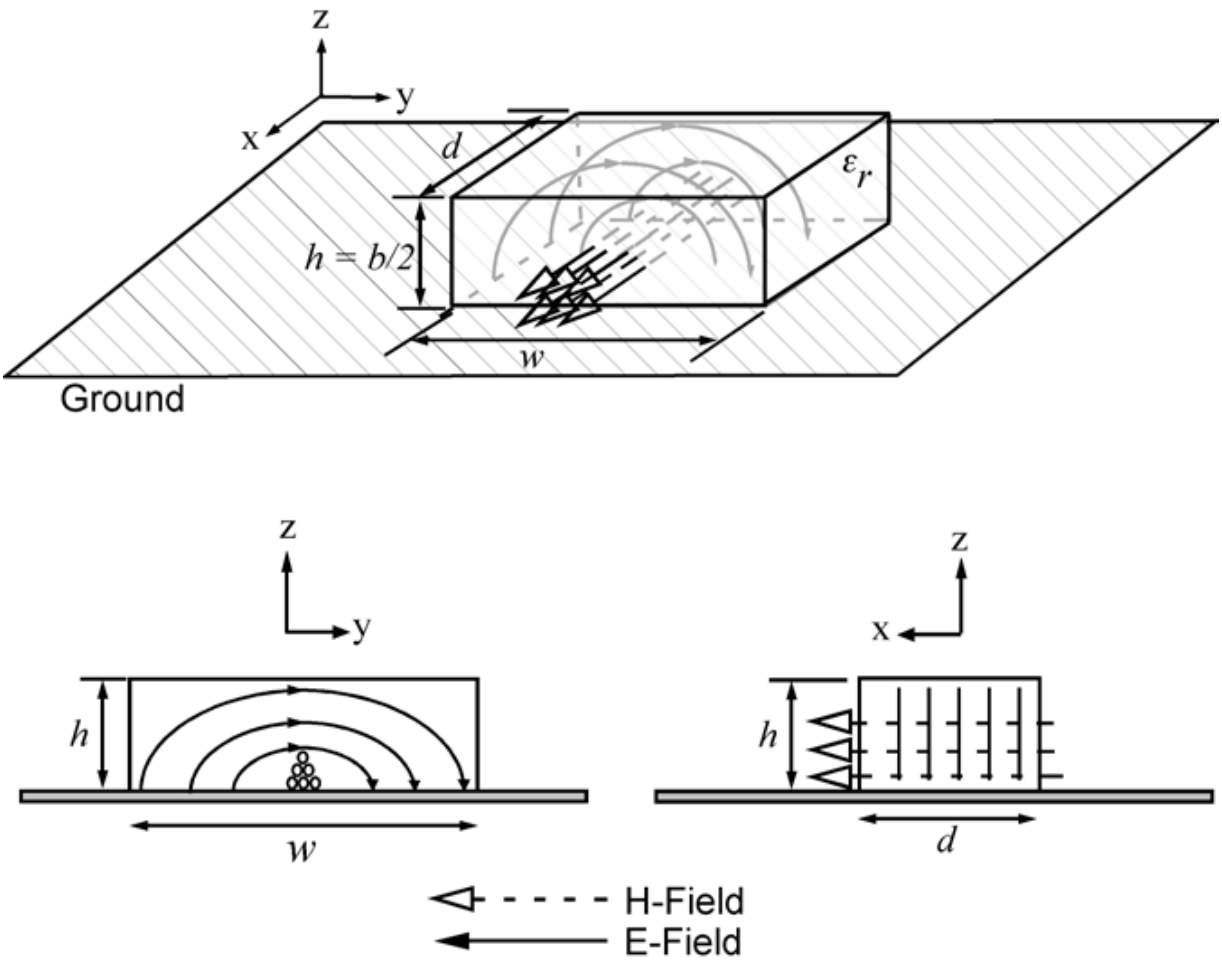

Figure 2.2 Sketch of the fields for the $TE^{x}_{\delta 11}$ mode of the rectangular DRA. [28]

The value δ can be defined as the fraction of a half-cycle of the field variation in the *x*-direction and is given by

$$\delta = \frac{k_x}{\pi/d}\,, \tag{2.10}$$

For the lowest order mode (m = n = 1), a sketch of the field configuration is shown in Figure 2.2. The H_z component of the magnetic field is dominant along the center of the DRA, while the E-Fields (predominantly E_y and E_z) circulate around the H_z component. These fields are similar to those

produced by a short magnetic dipole. A plot of the relative amplitudes of the electric and magnetic fields in the *x*-*y* plane of the DRA is shown in Figure 2.3. A knowledge of the relative amplitudes of these fields as a function of location within the DRA is important for determining where to place the feed mechanism to efficiently excite the DRA.

Higher-order modes of rectangular DRAs can also be excited for certain aspect ratios, with internal field patterns as shown in Figure 2.4. These produce radiation patterns similar to the $TE^{x}_{\delta 11}$ mode, having a peak in the broadside direction (along the *z*-axis), while the $TE^{x}_{\delta 21}$ mode will have a null at broadside. (Note that the $TE^{x}_{\delta 12}$ mode cannot exist for the case of the DRA mounted on the ground plane, due to the boundary condition that forces the tangential E-field to zero at $z = 0$, since the $TE^{x}_{\delta 12}$ would require the E-field to be maximum at that location.) By properly combining one or

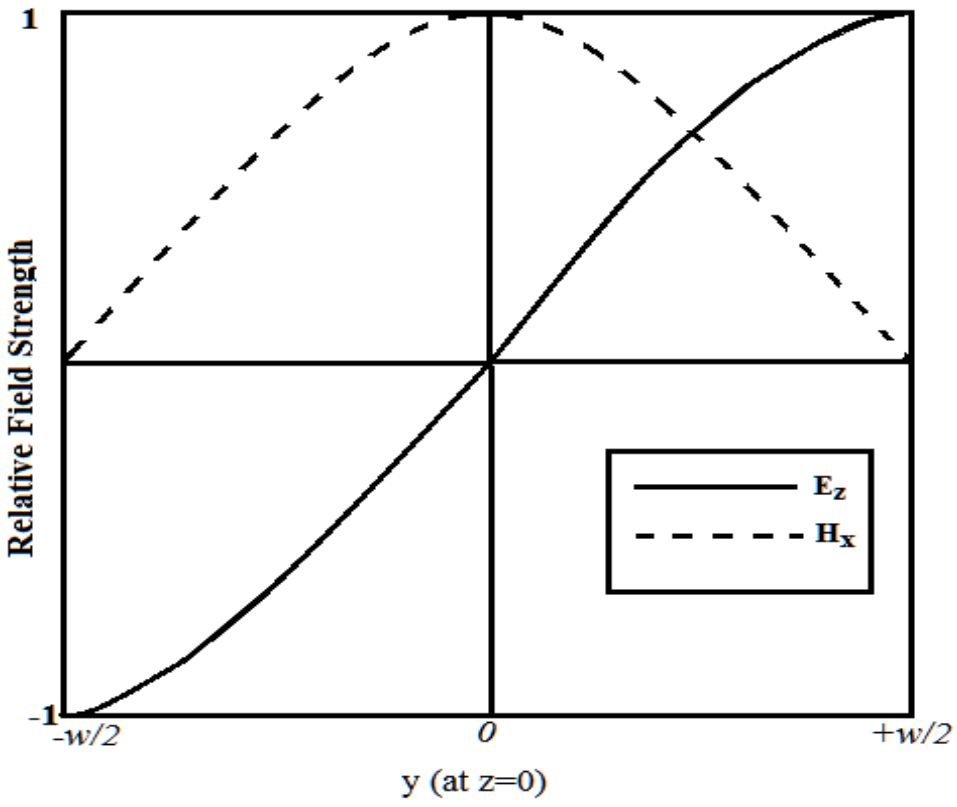

Figure 2.3 Relative field strength of the $TE^{x}_{\delta 11}$ mode within the rectangular DRA. [28]

more of the higher-order modes with the fundamental mode, a wider bandwidth or dual-band operation can be achieved [29].

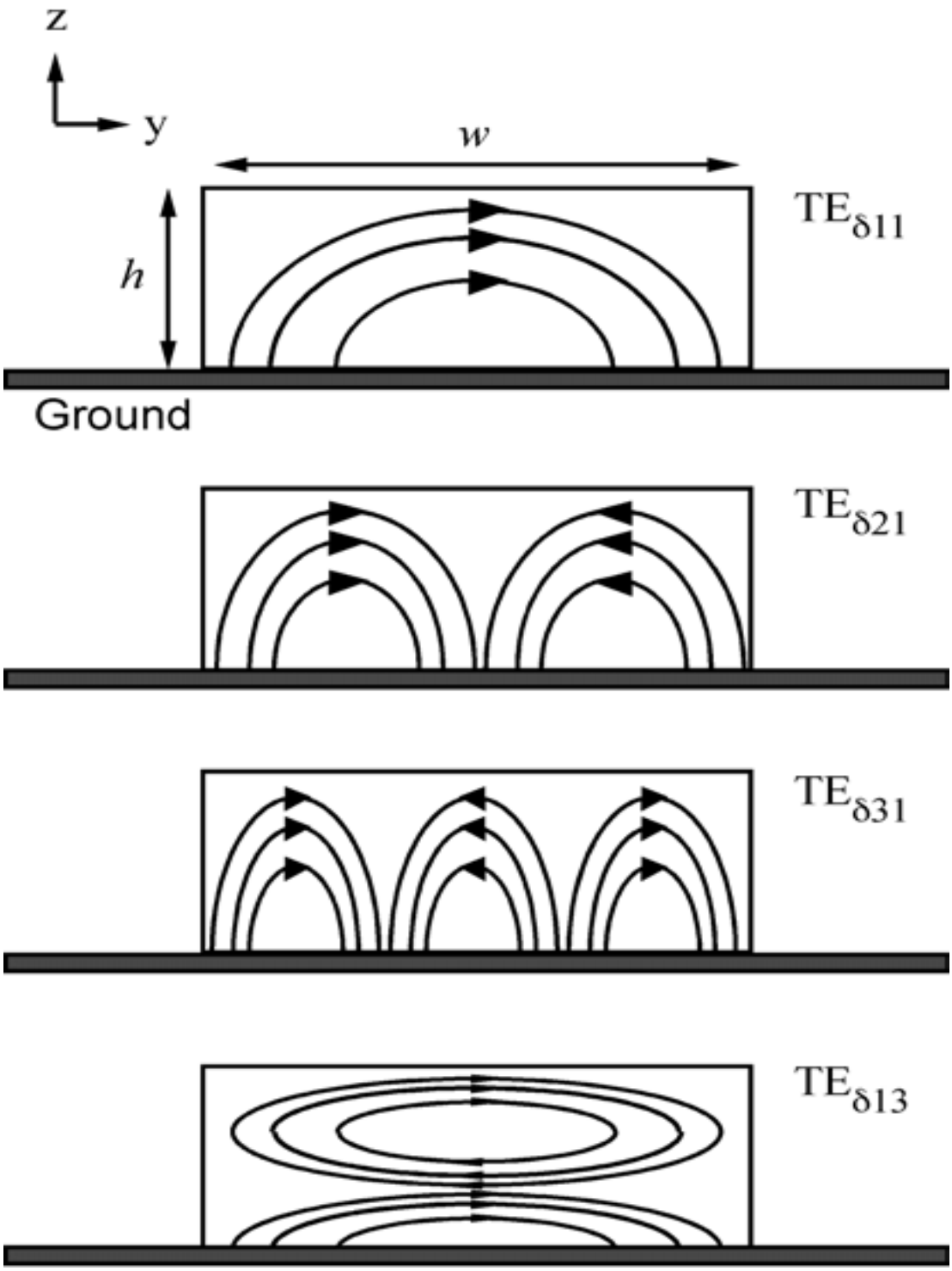

Figure 2.4 Sketches of the E-fields for selected higher-order modes within the rectangular DRA. [28]

2.3 Feeding Mechanisms for a DRA

In order to excite an antenna or in other words transfer power into it (to make it resonate and radiate) various feeding techniques can be used. Dielectric antennas are commonly fed by a coaxial probe through a slot in the ground plane or a microstrip line. Several new feeding mechanisms have been developed for the DRAs as they have radiating elements on one side of the dielectric substrate [28], [30]. Some feeding techniques are easy to fabricate where as others are difficult, and some feeding techniques can enhance the bandwidth. The microstrip feed-line, which was used to excite the DRAs, will now be presented.

2.3.1 Microstrip Transmission Line

A simple method of exciting or energizing a DRA is by using a microstrip feed-line on the same substrate as that of the antenna. In this type of feeding technique, a conducting strip is connected directly to the edge of the DRA or inserted under the DRA. A common method called proximity coupling is used to provide excitation with a microstrip line. The amount of coupling from the microstrip line to the DRA can be controlled to a certain degree by adjusting the spacing between the DRA and the line for the side-coupled case or the length of the line underneath the DRA for the direct-coupled case [28]. The coupling is also affected by the dielectric constant of the DRA. The higher the value of dielectric constant, the higher will be the value of the coupling. This is the simplest feeding scheme and it provides ease of fabrication. It also simplifies the modeling as well as impedance matching. As the thickness of the dielectric substrate of the DRA increases, surface waves and spurious feed radiation also increase, so the thickness of the substrate should be minimized [28]. Figure 2.5 (a) shows the magnetic field lines formed by the microstrip feed-line to excite the DRA. The direct-coupled method (Figure 2.5 (b)) is used in this thesis.

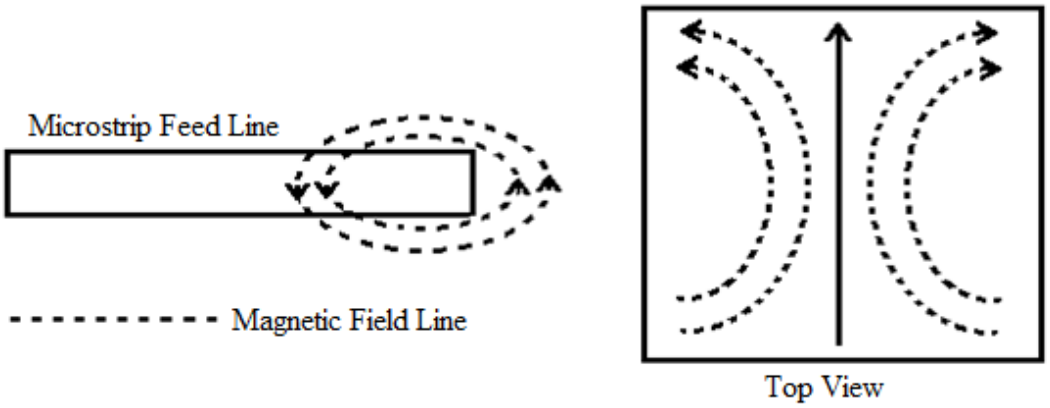

(a)

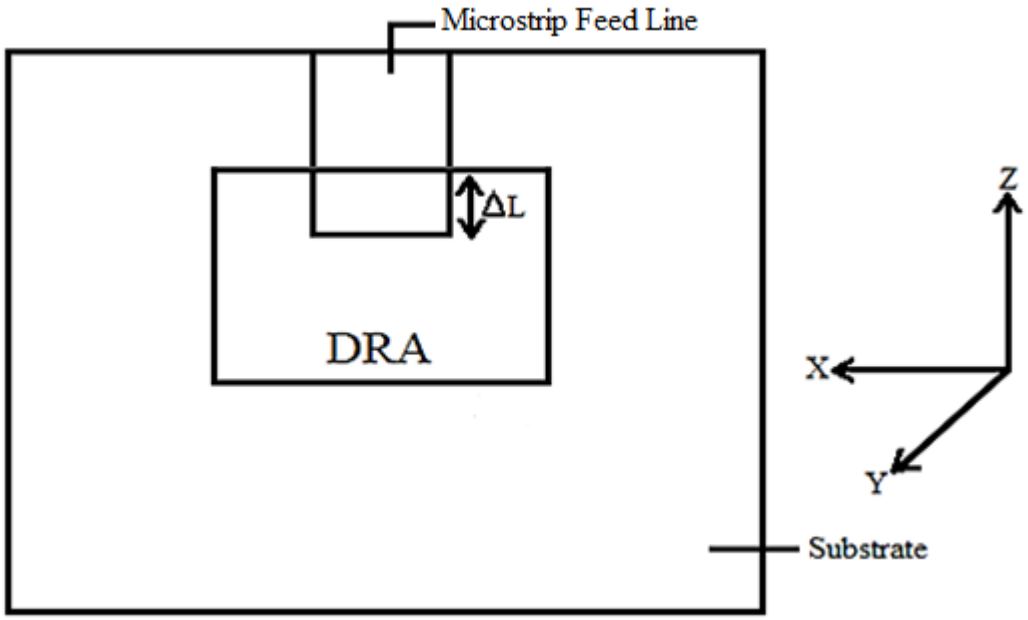

(b)

Figure 2.5 (a) Magnetic field lines formed by a microstrip feed line on a DRA. (b) Direct method coupling for meta-DRA with a variable length of feed line underneath (top-view).

2.4 Theory Behind Meta-DRAs

2.4.1 Metamaterials

Metamaterials were defined as, "Macroscopic composites having a synthetic, three-

dimensional, periodic cellular architecture designed to produce an optimized combination, not available in nature, of two or more responses to specific excitation", by Rodger M. Walser, University of Texas at Austin. Another popular definition for metamaterials is "a material, which gains its properties from its structure rather than directly from its composition." [31]

The above definitions reflect certain natures of metamaterials, but not all. Metamaterials were also defined by Tie Jun Cui, David Smith and Ruopeng Liu in their book, *Metamaterials: Theory, Design and Applications* [32] as "a macroscopic composite of periodic or non-periodic structure, whose function is due to both the cellular architecture and the chemical composition."

2.4.2 A Brief History of Metamaterials

Metamaterials have found applications in optics. J.B. Pendry introduced an ambitious concept of a perfect lens using metamaterials [33]. For such a "lens" an artificial medium has to be designed, which would possess specific properties, not observed in natural materials. The material for this perfect lens should be a medium with both negative permittivity and permeability in the same frequency range. In fact, V. G. Veselago [3] previously considered the study of the light focusing on the planar lens seen previously [33]. This review paper was devoted to phenomena that would occur in strange "left-handed" media (media with $\varepsilon < 0$ and $\mu < 0$). An experiment was carried out to form homogenous magnetic semiconductors, which were fabricated chemically but none of them had doubly negative material parameters and this failure was reported in [34]. In [35], it was stated that such media should act as strong resonant composites. Figure 2.6 shows the variation in the wave propagation within the materials having various ε and μ polarities.

In [3], it was pointed out that a slab under the condition $\varepsilon = \mu = -1$ will focus a diverging light beam. Under the condition $d = 2D$, where d is the thickness of the left-handed slab and D is the

distance from the slab interface to the source, the light will be focused at the point distanced by *D* from the back interface without aberrations and reflections.

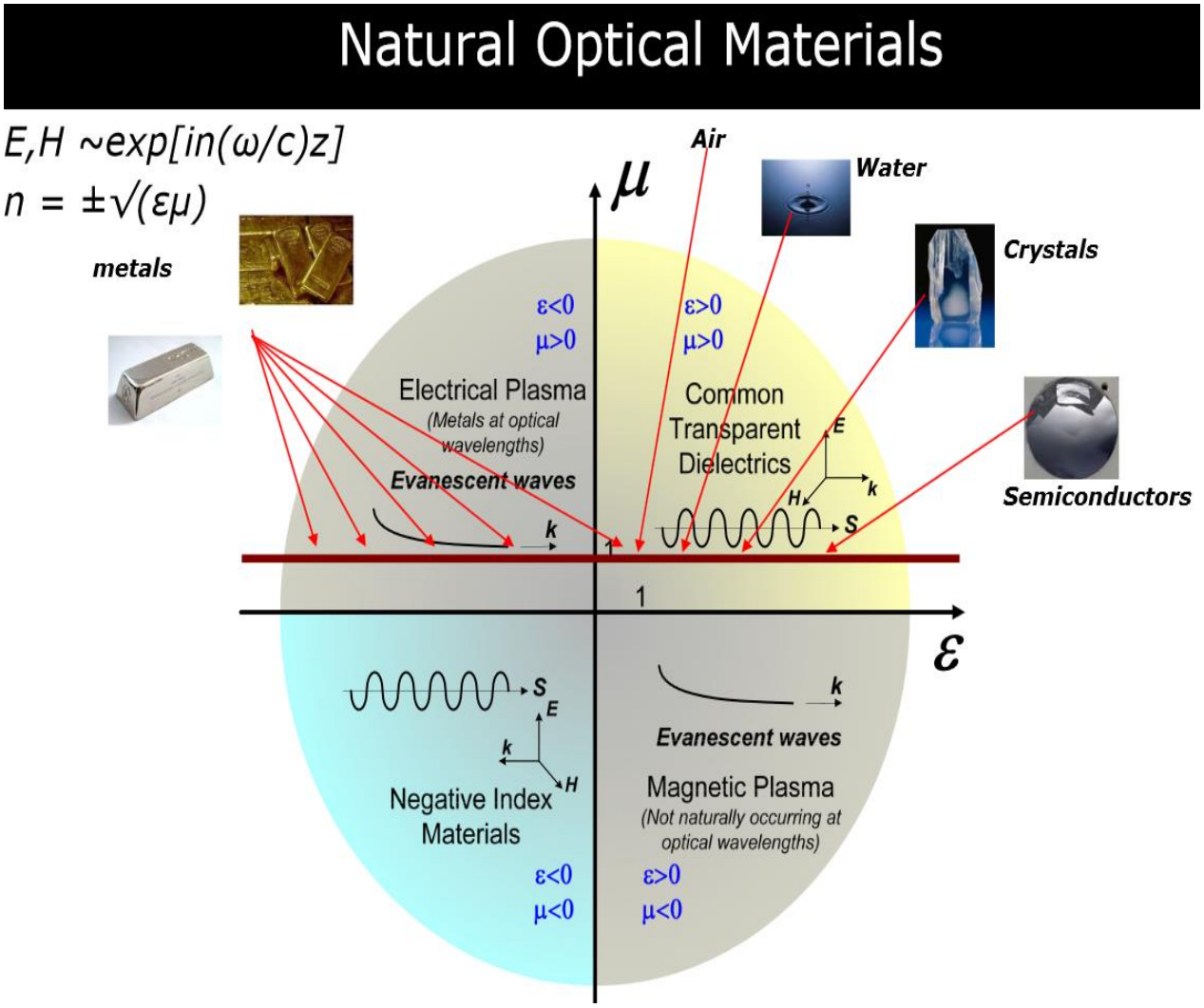

Figure 2.6 A description of optical materials in terms of ε and μ. [36]

J. B. Pendry studied the pseudo-lens design suggested by V. G. Veselago, and revealed the mechanism to redistribute the evanescent (near-zone) fields in the space. This allowed the evanescent waves to be transported far from the source and take part in the formation of the far-field image. This was exciting for specialists in photolithography, recording and reading optical information and also for experts in all domains where the near-field scanning technique cannot be practically used. The ideas in [33] went a long way in developing artificial materials with doubly negative constitutive

parameters. The first design of a structure with $\varepsilon < 0$ and $\mu < 0$ was suggested in the paper [34] and numerically studied. These two publications were instrumental in establishing concepts of the electromagnetics of metamaterials. Since then, there have been various publications on metamaterials. The practical and theoretical potential of metamaterials are still being discovered. Some of the applications of metamaterials include backward waves in bulk media [3]. The meta-DRAs utilize properties of metamaterials to create artificial dielectrics. The following sections take a closer look into these applications of metamaterials.

2.4.2.1 Backward Waves in Bulk Media

Professor L. I. Mandelshtam in his lecture notes had explained the phenomenon of backward electromagnetic waves and negative refraction [37]. Lamb and Pocklington discussed waves in media with negative group velocity as early as 1904 and 1905 respectively [38]. Mandelshtam however had a much simpler approach. In isotropic media, the absolute value of the wave vector is fully determined by the frequency. Therefore, the group velocity is directed along vector **k** or opposite to it, depending on the sign of the derivative dω/ dk. It is given by:

$$\mathrm{v_g} = \frac{d\omega(\mathrm{k})}{d\boldsymbol{k}} = \frac{\boldsymbol{k}}{k}\frac{d\omega}{dk} \qquad (2.11)$$

Mandelshtam mentioned that in the case of negative dispersion the wave in the medium is backward and the negative refraction should occur at an interface with such a medium. Lamb "gave examples of fictitious 1D media with negative group velocity" of the acoustic wave in 1904. A physical example of a 3D structure supporting backward electromagnetic waves was later presented by Mandelshtam [39]. The material was inhomogeneous with periodically varying permittivity in space. Essentially, this effort predicted the negative refraction in photonic crystals that was later rediscovered by Notomi [40]. A model for backward-wave microwave tubes by using the series-capacitance/shunt-inductance equivalent circuit model was developed by Brillouin [41] and Pierce

[42] during 1946-50. They also mentioned the propagation of antiparallel phase/group velocities. In 1951, Malyuzhinets (unaware of works [41] and [42]) generalized this concept to the 3D case in a paper on the Sommerfeld radiation condition in hypothetic backward-wave media [43]. Malyuzhinets noted that in such media the phase velocity of waves at infinity should point from infinity to the source. An equivalent one-dimensional (1D) analogue of these media was artificial transmission lines depicted by Malyuzhinets and shown in Figure 2.7 (compare with [44], [55]). Materials with negative parameters as backward-wave materials were mentioned by Sivukhin in 1957 [46]. He was probably the first who noticed that media with double negative parameters are continuous and homogeneous backward-wave media. Simultaneously he stated that ". . . media with $\varepsilon < 0$ and $\mu < 0$ are not known. The question on the possibility of their existence has not been clarified" [46]. During the 1960s, 1D backward-wave structures were very much studied in connection with the design of microwave tubes and slow-wave periodic systems [47].

Referring to an interesting paper by Silin (1959) [48], where the negative refraction phenomenon in periodical two-dimensional (2D) media was discussed, such media are often called left handed media (LHM) or Veselago media. The first term is related with the fact that the triad of vectors E, H, and k is left handed (the vector product E x H determines the Poynting vector and it is opposite to the wave vector, since the Poynting vector direction in low-loss linear media coincides with that of the group velocity and the wave vector direction coincides with that of the phase velocity). An example is shown in Figure 2.8.

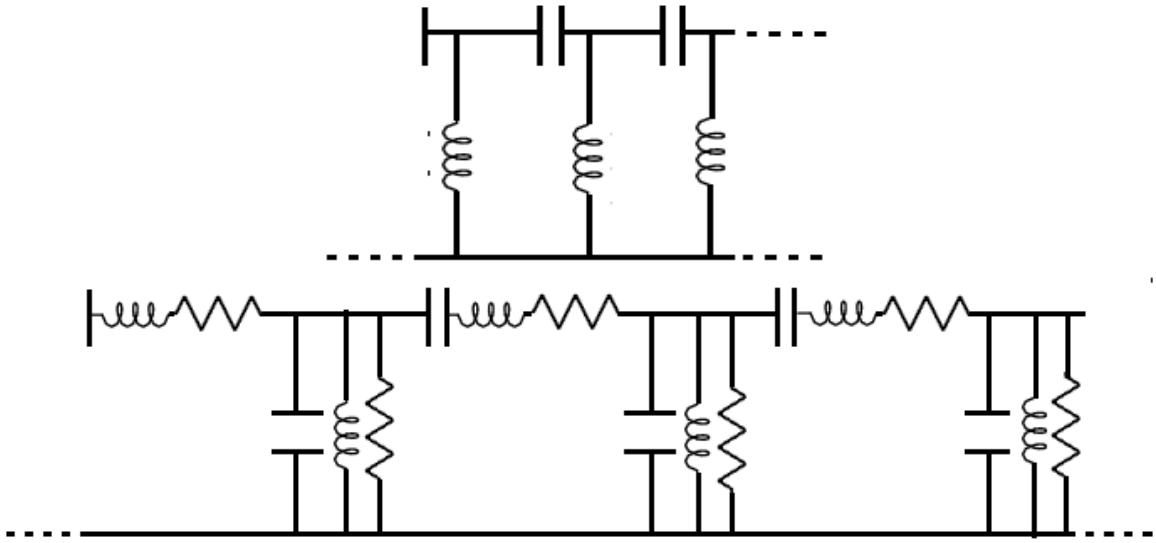

Figure 2.7 Backward-wave transmission lines from a paper by Malyuzhinets (1951) [43]

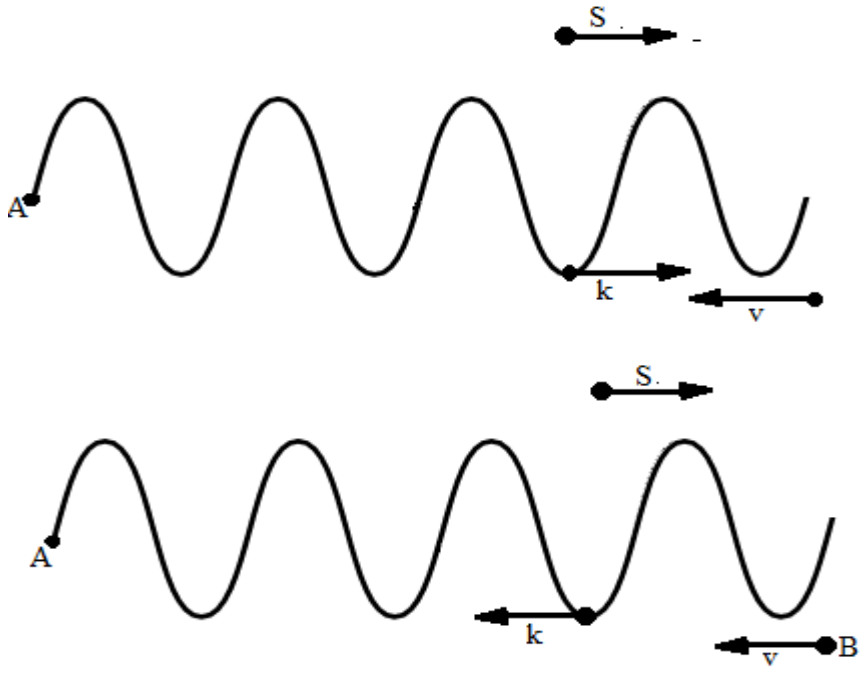

Figure 2.8 Cerenkov radiation in doubly negative medium.

2.4.2.2 Artificial Dielectrics

A major breakthrough in the field of metamaterials occurred in 1948 when Kock proposed to make a dielectric lens lighter by replacing heavy high-permittivity refractive materials with a mixture of small metal spheres in a light-weight medium in [49]. The artificial dielectric material was defined as a composite that had particles, and behaved similar to a usual dielectric. The metallic elements were arranged in a three-dimensional (3D) array or lattice structure in order to replicate the crystalline lattices of dielectric materials. The array formed reacts to radio waves similar to the way a molecular lattice reacts to light waves. Due to the alternating electric field, the free electrons in the metal elements flow back and forth. Metal elements or lattice inclusions become oscillating dipoles similar to the oscillating molecular dipoles of a natural dielectric. Kock used this concept, which was partially introduced by Lord Rayleigh in his work [50] for arrays of metal spheres and implemented it in practical applications. Kharadly and Jackson also developed a similar theory in their work [51]. They studied artificial dielectrics made of metal disks or rods operating at low frequencies and calculated their effective permittivity.

Lens antennas do not use artificial dielectrics with dense packaging of metal inclusions since they possess rather high losses. These are applied in absorbing sheets. Artificial dielectrics have been reviewed in [52]. Their lattices have random formation. The particles may even have a non-uniform concentration. This might cause unusual properties in such composite media [53,54]. Artificial dielectrics develop complex conductivity when the concentration of particles exceeds the so-called percolation threshold (particles touch one another and/or the capacitive coupling between adjacent particles is very strong) [55]. Their conductivity can be engineered by controlling the design parameters and in principle can be adjusted magnetically or electrically. Artificial conductors have

been applied developing electromechanical devices, fuel cells, and other techniques where controlled heating by electric current is needed.

2.5 Metamaterials as DRAs

Artificial dielectric metamaterials are applied in this work as an alternative to ceramic DRAs. Ceramics typically have higher permittivities, which facilitates excitation and resonate at frequencies in the microwave or millimeter wave region. The polymer base of the meta-DRA has a very low permittivity of 2-3 making it difficult to excite directly. Lower permittivity also results in much higher resonant frequencies for small compact geometries, which are not necessarily viable for commercial applications. Hence it is advantageous to increase the overall permittivity of the DRA to a range of 14-16 (usually ceramics have such high permittivity). In order to do this, metal inclusions can be introduced into the polymer base of the DRA. The effective permittivity can be increased by the metal inclusion in the DRA, which tends to direct and focus the electric fields, locally increasing the electric flux density.

$$\lambda_0 = \frac{c_0}{f_0} \tag{2.12}$$

$$c_0 = \frac{1}{\sqrt{\mu_0 \varepsilon_r}} \tag{2.13}$$

From the above equations it can be deduced that,

$$\sqrt{\varepsilon_r} = \frac{1}{f_0} \tag{2.14}$$

Generally speaking, the square root of relative permittivity $\sqrt{\varepsilon_r}$ of the meta-DRA is inversely proportional to the resonant frequency of the antenna. Increased flux density reduces the resonant frequency for the meta-DRA and hence 'increases' the effective ε_r. Figure 2.9 shows the simulated reflection coefficient (dB(S_{11})) for a dielectric resonator antenna made of a high permittivity material; in this case, the material chosen has a relative permittivity of 10. The design and simulation was

performed using HFSS (High Frequency Structure Simulator).

The minimum value in dB(S_{11}) indicates the DRA resonant frequency of 20 GHz, as a function of coupling. More details on scattering parameters are presented in the next chapter.

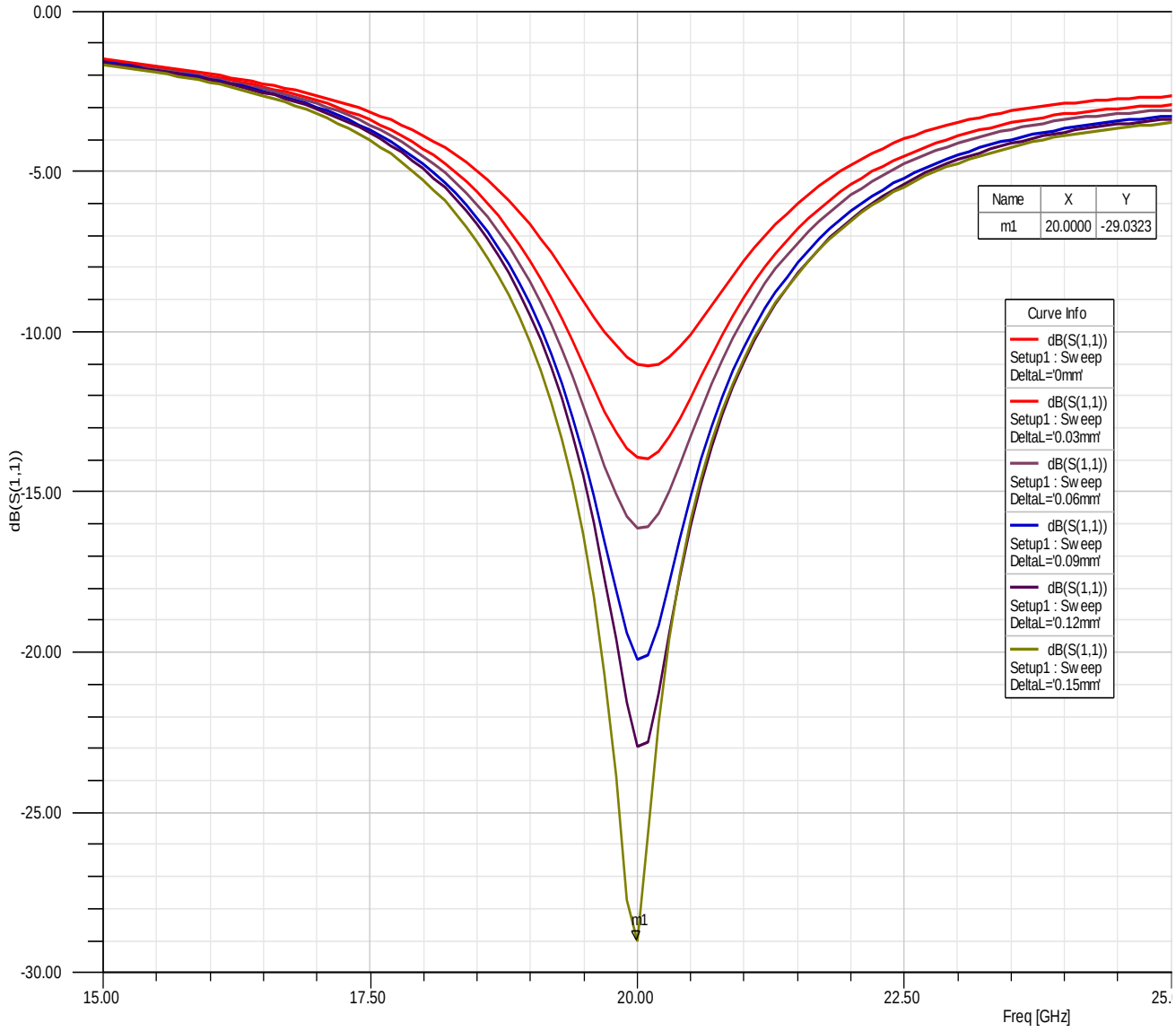

Figure 2.9 dB(S_{11}) versus Frequency plot for a high permittivity material DRA. A reflection coefficient of -29.03 is obtained @ 20 GHz.

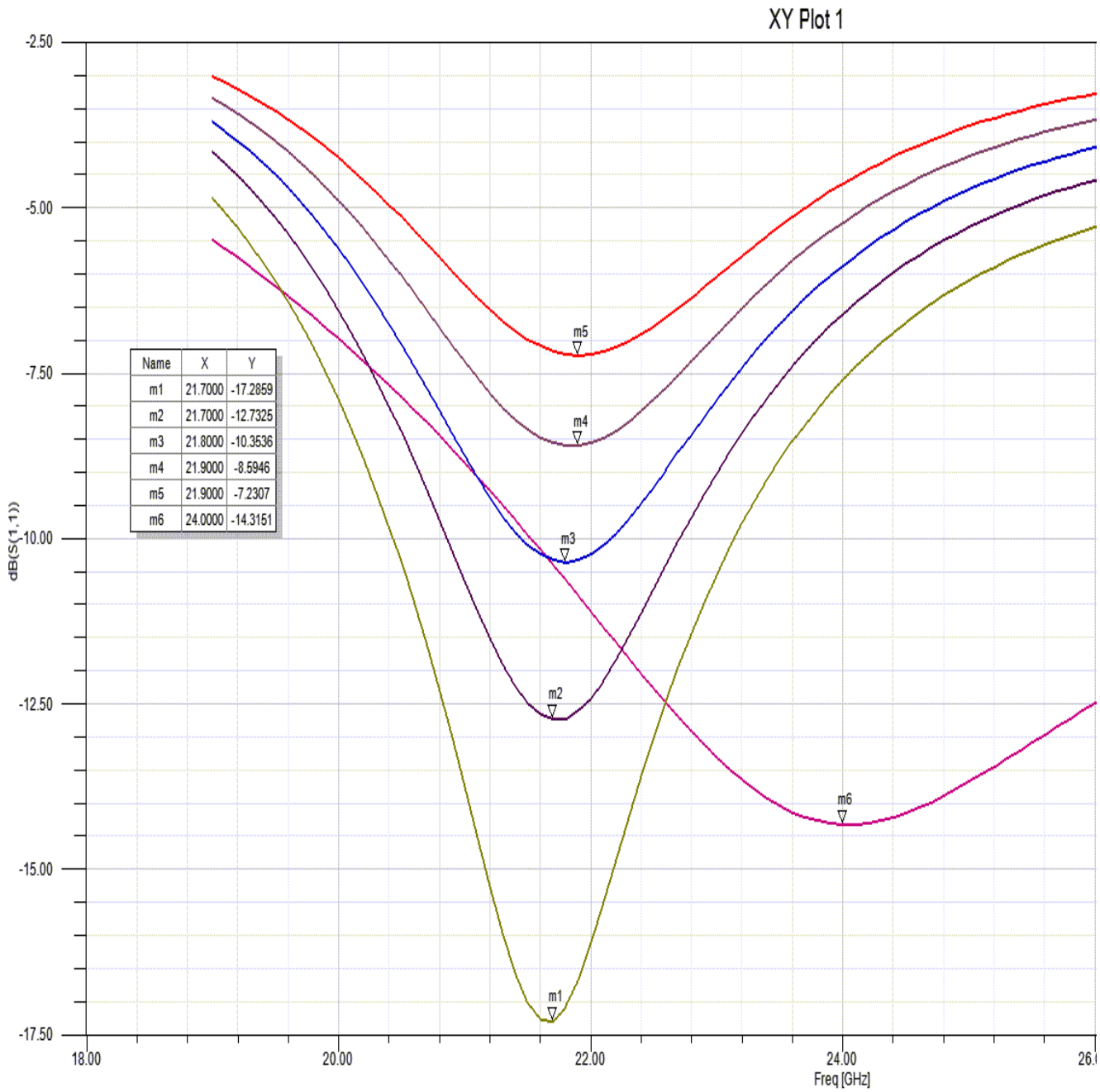

Figure 2.10 dB(S_{11}) versus Frequency plot for a meta-DRA formed by inserting an array of metal (Ni) inclusions inside a low permittivity (ε_r = 2.5) polymer. A reflection coefficient of -17 is obtained @ 21.7GHz, which demonstrates that the design has increased the ε_r of the polymer based DRA.

The dB(S_{11}) versus frequency plot of a comparable meta-DRA is shown in Figure 2.10. For the polymer-base, a material was defined in HFSS having a ε_r of 2.5. The metal assumed as inclusions is nickel (Ni). The following table shows the comparison between the DRAs based on their resonant frequencies and their dB(S_{11}) values.

Type of DRA	**Resonating Frequency (GHz)**	**dB(S_{11}) Value**
Ceramic DRA	20	-29.03
Meta-DRA	21.7	-17.28

Table 2.1 Comparison between ceramic DRA and meta-DRA.

It can be observed that the meta-DRA has a similar resonant frequency and much lower than expected from a pure polymer antenna which would be expected to resonate at approximately 70-90 GHz. This shows the effect of the metal inclusions in the polymer. Hence meta-DRAs can have the same effect as that of the ceramic or high permittivity DRAs in terms of resonance under a given environment.

In the next chapter, a brief introduction to HFSS and the complete design and simulation of a sample meta-DRA is presented. The process of developing a layout for fabrication is also dealt with detail.

Chapter 3

Design and Simulation of Meta-DRAs and Generation of Layout

3.1 An Introduction to HFSS

High Frequency Structure Simulator (HFSS) is a high-performance full-wave electro-magnetic (EM) field simulator for arbitrary 3D volumetric passive device modeling. It integrates simulation, visualization, solid modeling, and automation to solve 3D EM problems. Ansoft HFSS employs the Finite Element Method (FEM) and adaptive meshing, and can be used to calculate parameters such as S-Parameters, resonant frequency, and fields. HFSS is an interactive simulation system whose basic mesh element is a tetrahedron. This allows one to solve any arbitrary 3D geometry, especially those with complex curves and shapes.

3.1.1 Design Windows in HFSS

Figure 3.1 shows the various panels present in HFSS version 15.0. The structure of the entire project is present in the project manager window. It can be also described as a design tree for the project file. It clearly depicts the models in use and their boundaries and excitation. This panel is also used to set-up the analysis and for optimizing the design.

Before simulating a design, it is imperative to run a check on the entire design. Message manger allows one to view any errors or warnings that may occur during simulation. A progress window displays the solution progress.

The property window allows one to change the model parameters and attributes. It is used to define the type of material of the model along with its name, orientation, color and transparency in design.

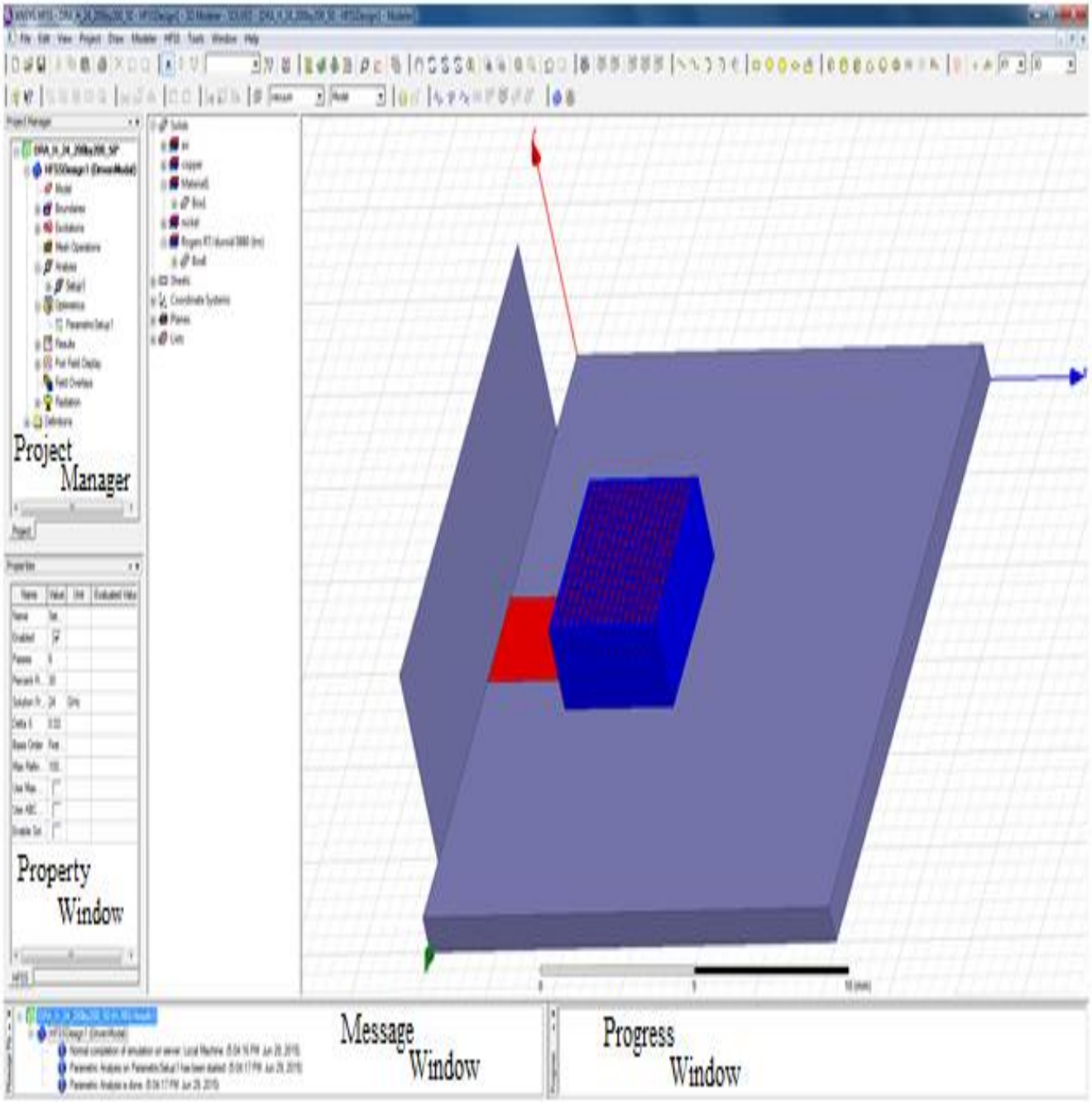

Figure 3.1 Description of various sections in the HFSS window.

3.2 Structure and Design of a Meta-DRA

This section gives a brief description on how to go about designing a DRA in HFSS. Upon

opening the software, click on *Insert HFSS design* icon in the toolbar. This opens the design window for the new project. The subsequent steps are depicted as follows:

3.2.1 Defining the DRA, Substrate and Feedline

Before one starts designing, it should be noted that the axis of the HFSS coordinate system is set to XY and the 3D mode is selected in the Toolbar. In order to design the substrate, DRA and the feed line, the function called *Draw a Box* in HFSS is used. The steps for the design can be summarized as follows:

- Click on the Draw menu from the Toolbar and select the option 'Box'. Set the start point of the base polygon by positioning the active cursor and click the left mouse button.
- Position the active cursor and click the left mouse button to set the second point that forms the base rectangle.
- Set the height by positioning the active cursor and clicking the left mouse button.

The steps above give a cuboid as shown in Figure 3.2. The 3D Modeler design tree now assigns the design as 'Box 1' and the material is assumed to be vacuum. This can be changed by double clicking the 'Box 1' icon in the design tree. Upon doing so, a window such as Figure 3.3 appears. By clicking on Vacuum in the Material attribute, one can edit or change the material. Here, the material has a relative permittivity of 2.5 and a dielectric loss tangent of 0.01. The design specifications for this thesis are described in detail in the following sections. One can also modify the other attributes such as Color and Transparency, but that would not affect the design parameters as such. After defining the material, the new material shows on the design tree instead of vacuum. If any other component is assigned the same material in the future, it will fall under the same category.

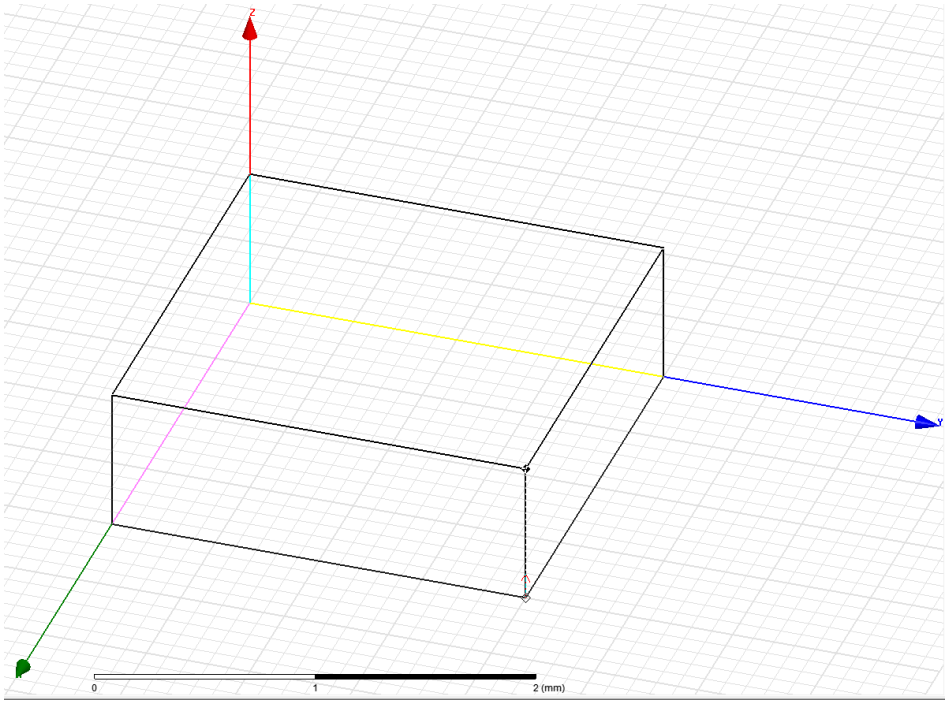

Figure 3.2 Design of a Box in HFSS.

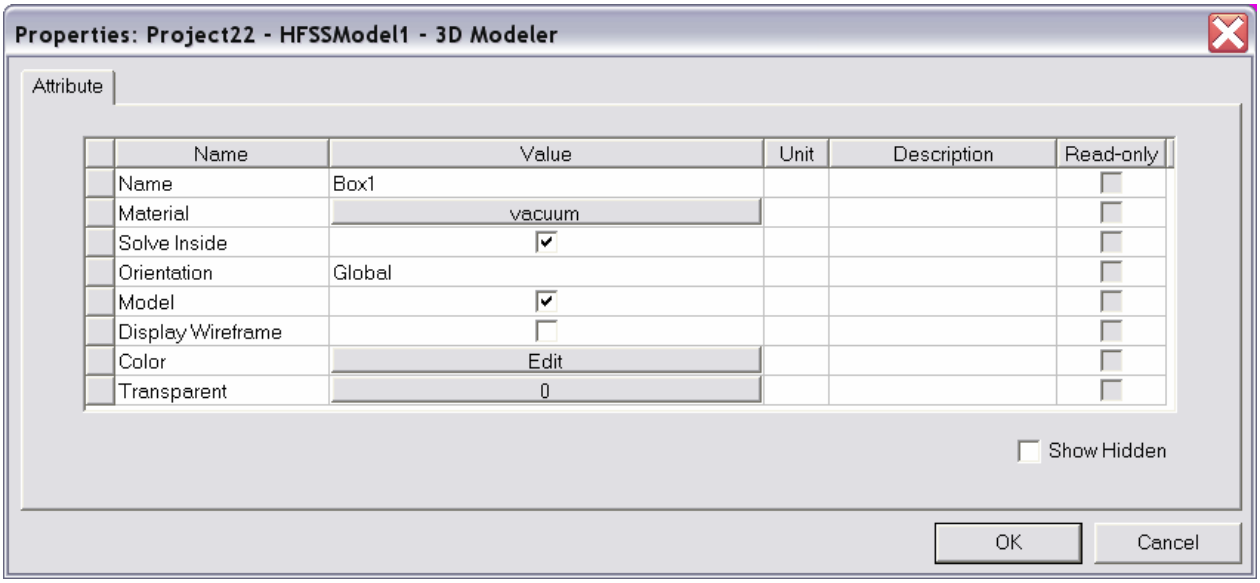

Figure 3.3 Property window of the Box created.

The basic design of the substrate is same as that of the DRA apart from the fact that it has a different size, position and material for obvious reasons. The material assumed for the substrate in

this thesis is Rogers RT/duroid 5880 ™. It has a relative permittivity of 2.2 .

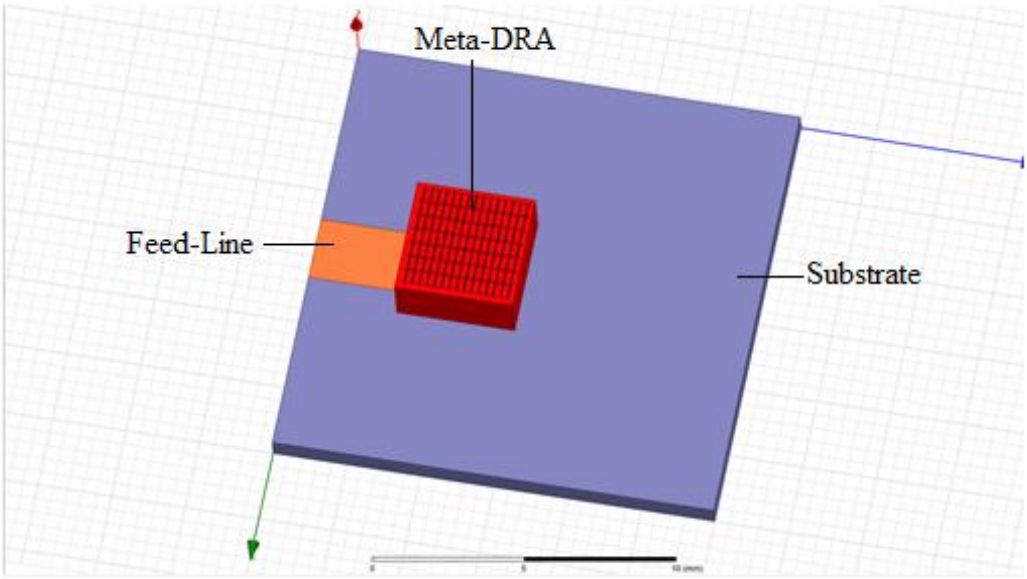

Figure 3.4 The design model of meta-DRA, substrate and feedline.

The feedline used to excite the DRA is a 50 ohm planar microstrip structure made of copper, which has no dielectric loss (dielectric loss tangent, tan $\delta = 0$). The length of the feedline is added as a parametric component in the design and hence it is initially declared as a variable (*DeltaL*). It varies during the simulation from the edge of the meta-DRA to the edge of the first row of metal inclusions. In order to achieve this, the *Optimetrics* tab under the project tree in Project Manager is used. The range of variation and the step size can be defined here. Figure 3.4 shows the DRA with its substrate and feedline.

3.2.2 Defining Boundary Conditions

In order to simulate a DRA, various boundary conditions and excitations need to be defined. A port is an aperture through which a guided-wave mode of some kind propagates. For enclosed transmission lines, port size is merely the waveguide interior carrying the guided field,

rectangular in this case. The port solver only understands conductive boundaries on its borders such as:

- Electric conductors may be finite or perfect (including Perfect E symmetry)
- Perfect E symmetry also understood.
- Radiation boundaries around the periphery of the port do not alter the port edge termination.

3.2.2.1 Microstrip Port Sizing Guidelines

Assume the width of the microstrip trace as *w* and the height of the substrate as *h*. Figure 3.5 shows the design parameters for the wave port in this thesis.

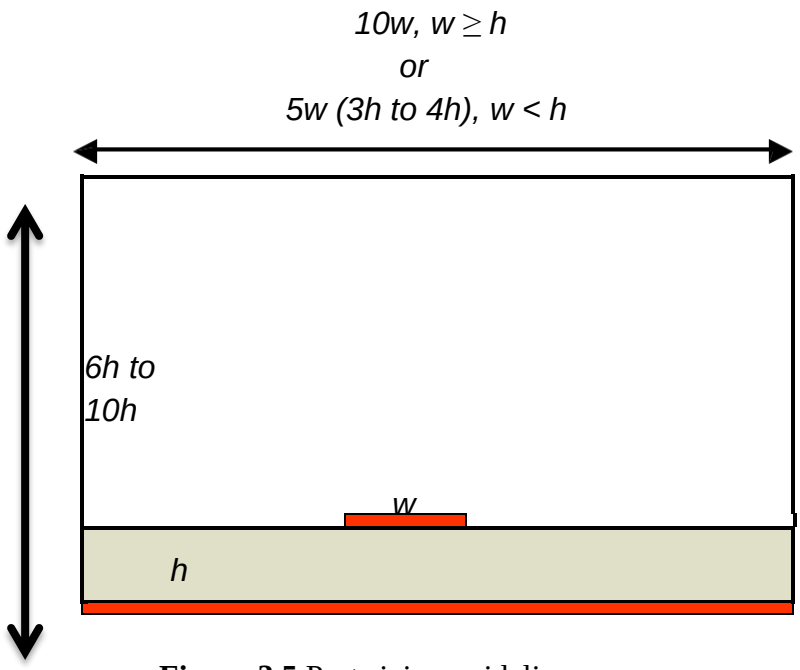

Figure 3.5 Port sizing guidelines.

The guidelines for the wave port are explained below:

Port Height Guidelines:

- It should be between 6*h* and 10*h*.
- Tends towards upper limit as dielectric constant drops and more fields exist in air rather than substrate.
- Bottom edge of port coplanar with the upper face of ground plane.

Port Width Guidelines:

- 10*w*, for microstrip profiles with $w \geq h$.

3.2.2.2 Defining the Excitation Port and Boundaries

In order to form a rectangular excitation port, the starting point and dimension of the port using the above guidelines and design coordinates must be calculated. Once the calculations are done, one can select the Rectangle option from the Draw menu of HFSS and select the starting point as calculated (bottom surface of the substrate). Since the design is in XY coordinates, the rectangular port should be in ZX coordinate. The window shown in Figure 3.6 can be used to define the coordinate and dimension of the port.

Now one selects the rectangle and with the help of a right click, chooses the option *Wave Port* in the *Assign Excitation* field. This will initiate a setup module for the wave port. One can number the wave port if multiple ports are required in the design. Upon clicking *next* in the setup window, the next window allows the user to define a new integration line as shown in Figure 3.7. The integration line is ideally defined from the middle bottom of the port to the height of the substrate as

shown in Figure 3.8. After this process, the window shows the defined integration line and subsequently one can finish the setup for the wave-port design.

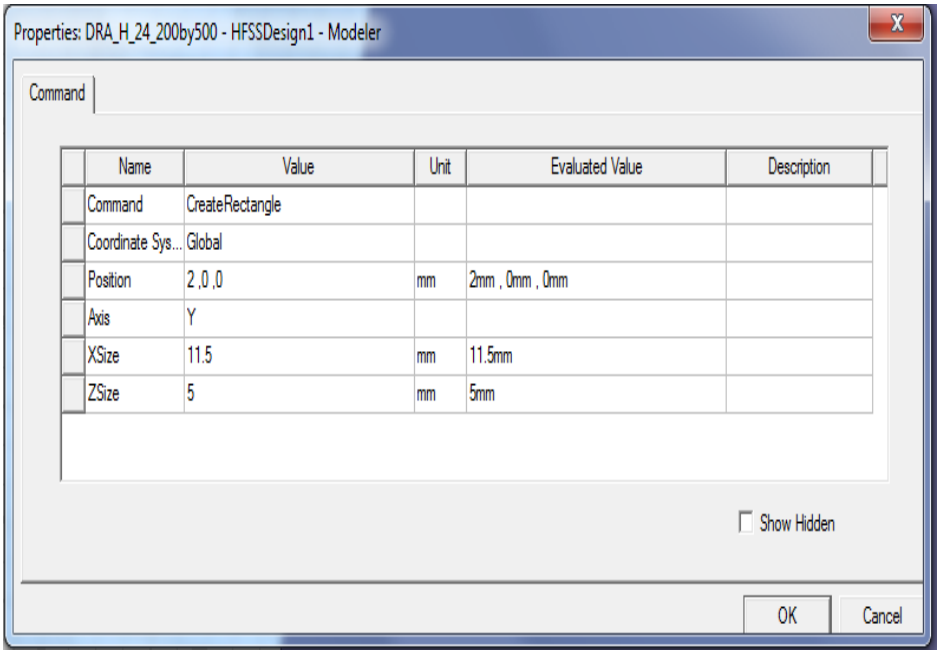

Figure 3.6 Assigning coordinate and dimension of the waveport.

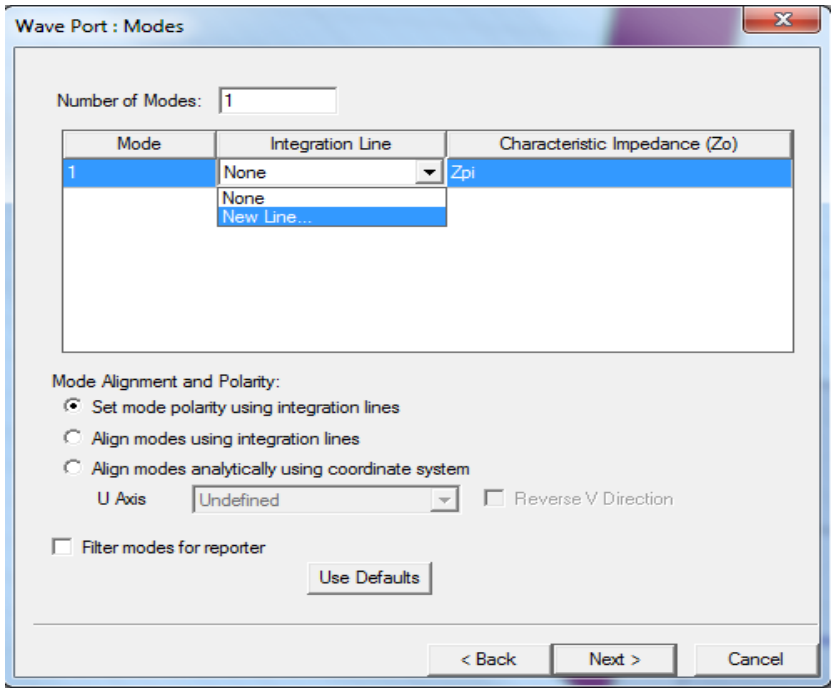

Figure 3.7 Defining integration line of the waveport.

Figure 3.8 After correctly defining the waveport.

Once the waveport is defined, one can now set the lower face of the substrate is set as *Perfect E* by right clicking the surface and choosing *Perfect E* in the *Assign Boundary* field of the drop box menu. The radiation boundary (air box) encloses the entire design. It should be placed λ/10 to λ/4 away from radiating structures. Strong radiators should be λ/4 away. Figure 3.9 shows the radiation boundary around a DRA design for this thesis. The frequency steps and solution setup for the S_{11} and radiation have been dealt with in detail in Chapter 5 of the thesis.

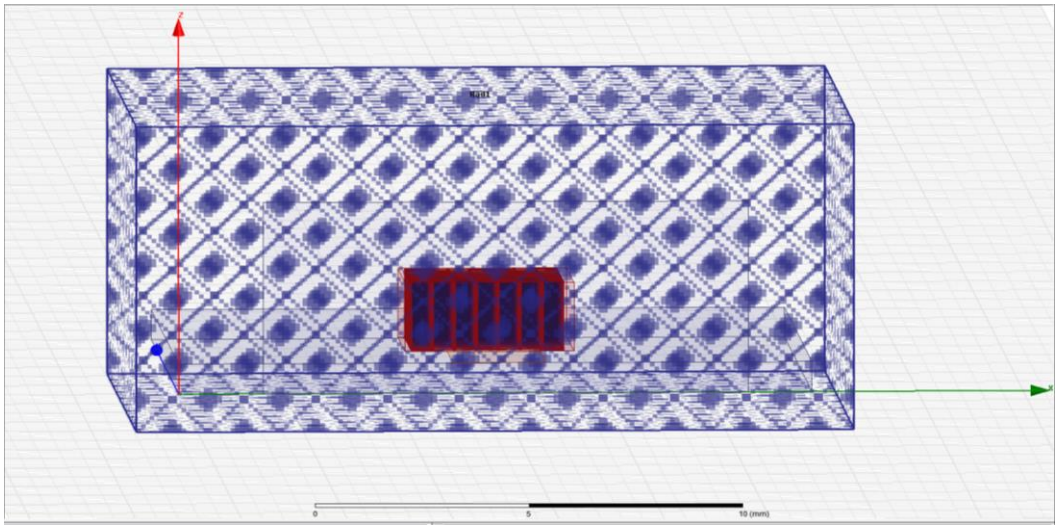

Figure 3.9 The radiation air box around a meta-DRA design.

3.3 Obtaining S-Parameter and Radiation

After defining the waveport and radiation boundary, the design needs to be validated by the software in order to ensure that the meta-DRA design has been set with all boundaries and structures well defined. In order to validate the proper functioning of the antenna, one needs to know two important parameters: the reflection coefficient (S_{11}) in dB and the radiation obtained from the antenna.

3.3.1 Significance of S-Parameter and Plotting in HFSS

The S-parameters describe the input-output relationship between ports (or terminals) in an electrical system. For instance, if there are 2 ports (Port 1 and Port 2), then S_{12} represents the power transferred from Port 2 to Port 1. S_{21} represents the power transferred from Port 1 to Port 2. In general, S_{NM} represents the power transferred from Port M to Port N in a multi-port network.

A port can be loosely defined as any place with voltage and current. So, in a communication system with two radios (radio 1 and radio 2), then the radio terminals (which deliver power to the two antennas) would be the two ports. S_{11} then would be the reflected power radio 1 is trying to deliver to antenna 1. S_{22} would be the reflected power radio 2 is attempting to deliver to antenna 2. And S_{12} is the power from radio 2 that is delivered through antenna 1 to radio 1. Note that in general S-parameters are a function of frequency (i.e. vary with frequency). As an example, consider the two-port network in Figure 3.10. S_{21} represents the power received at antenna 2 relative to the power input to antenna 1. For instance, S_{21} = 0 dB implies that all the power delivered to antenna 1 ends up at the terminals of antenna 2. If S_{21} = -10 dB, then if 1 Watt (or 0 dBW) is delivered to antenna 1, then -10 dBW (0.1 Watts) of power is received at antenna 2.

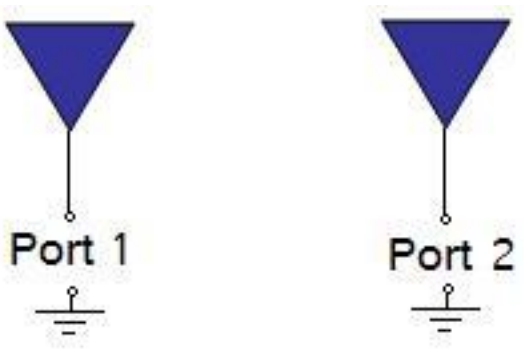

Figure 3.10 A two-port Network

In practice, an important parameter in regards to antennas is S_{11}. S_{11} represents how much power is reflected by the antenna and hence is known as reflection coefficient (sometimes denoted by gamma: Γ or return loss). If S_{11} = 0 dB, then all the power is reflected and nothing is radiated by the antenna. If S_{11} = -10 dB, then it means that if an input power of 3 dBW is given to the antenna, -7 dBW is the reflected power. The remainder of the power was "accepted by" or delivered to the antenna. This accepted power is either radiated or absorbed as losses within the antenna. Since antennas are typically designed to be low loss, ideally the majority of the power delivered to the antenna is radiated.

To be able to plot the S_{11} in HFSS, the frequency sweep has to be defined first. The following steps explain the process of obtaining the plot:

- A solution setup is first defined by right clicking on the *Analysis* option from the Project Manager window. The solution frequency is now defined.

- The setup now appears under the Analysis tab in the Project Manager. By right clicking the setup, one can add a frequency sweep. In this window, the start and end frequencies can be denoted along with the step size (Figure 3.11). Hence the simulation would help obtain a solution within this

frequency range. In this step, it is made sure that the desired operating frequency of the antenna falls under the sweep.

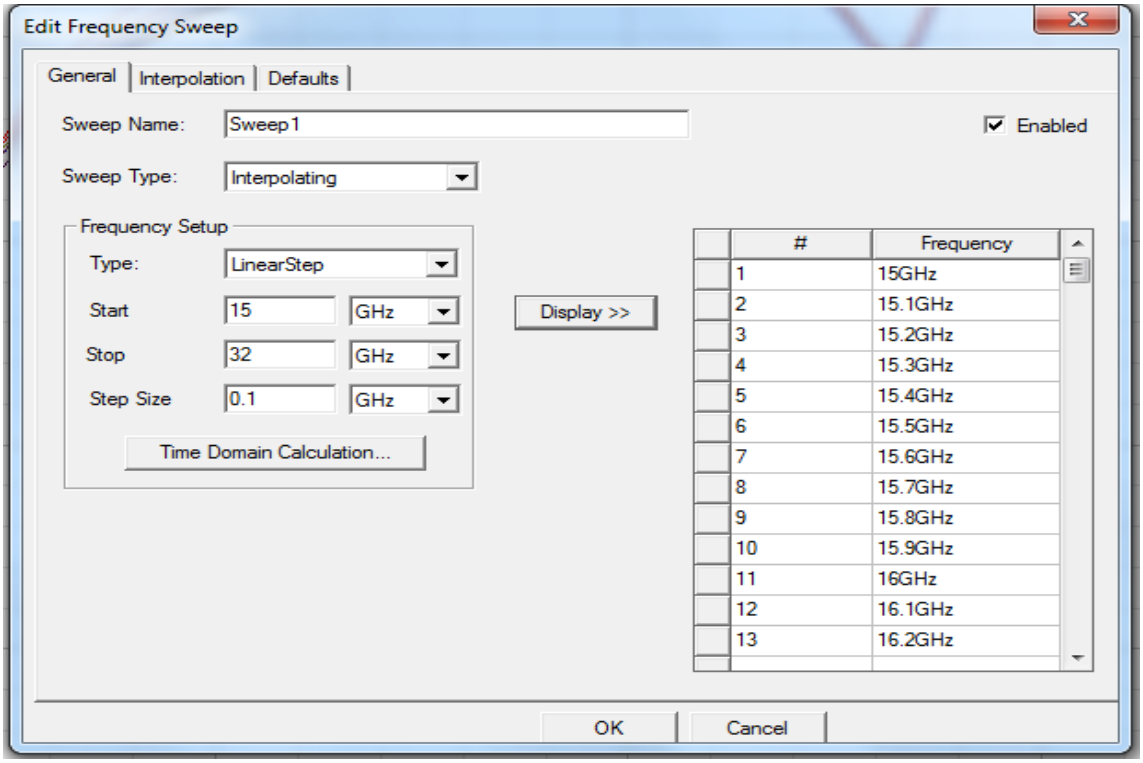

Figure 3.11 Assigning frequency sweep in HFSS for the meta-DRA simulation.

- Once the solution setup is defined, right click on the *Results* tab from the Project Manager tree and select *Create Modal Solution Report* > *Rectangular Plot.* Figure 3.12 shows the dialogue box that appears. The X and Y-axes of the plot can be selected here. In this case a dB(S_{11}) versus Frequency plot is selected. The desired selections are highlighted in the figure.

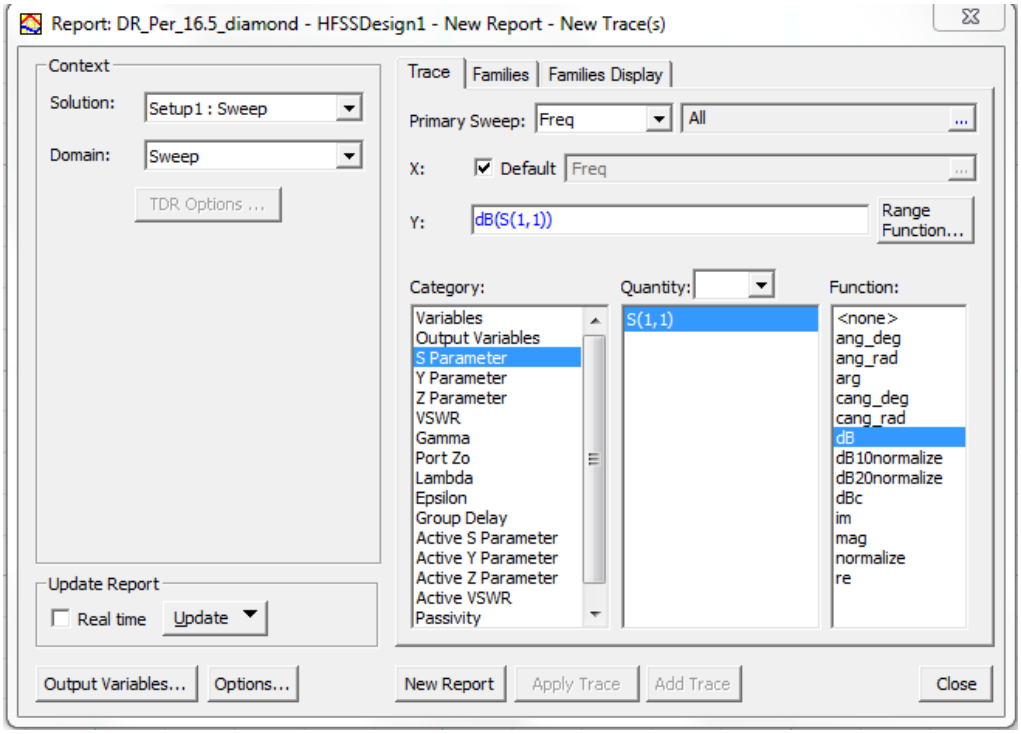

Figure 3.12 Setting up the S_{11} versus Frequency sweep.

Hence the desired reflection coefficient plot is setup by using the above procedure. The following section will deal with obtaining the radiation from the antenna.

3.3.2 Plotting Radiation

The radiation pattern of an antenna can be obtained by defining the far-field setup in HFSS. As shown in Figure 3.13, the Phi and Theta radiation sweep with their step size has to be defined.

After simulation is completed, the radiation pattern produced by the design is plotted. This can be done by selecting *Project Manager> Results> Create Far Field Report> Radiation Pattern*. Figure 3.14 depicts the window that appears. The *dB(GainTheta)* and *dB(GainPhi)* are needed to understand the amount of radiation coming out of the antenna and also the magnitude of the back radiation. In the designs, the gain across *Phi* gives the desired radiation magnitudes. One thing has to

be kept in mind, for plotting the H-Plane, the variable *Phi* is zero degrees and for E-Plane it is ninety degrees. The design resonant frequency and any other parametric variable defined in the design have to be set.

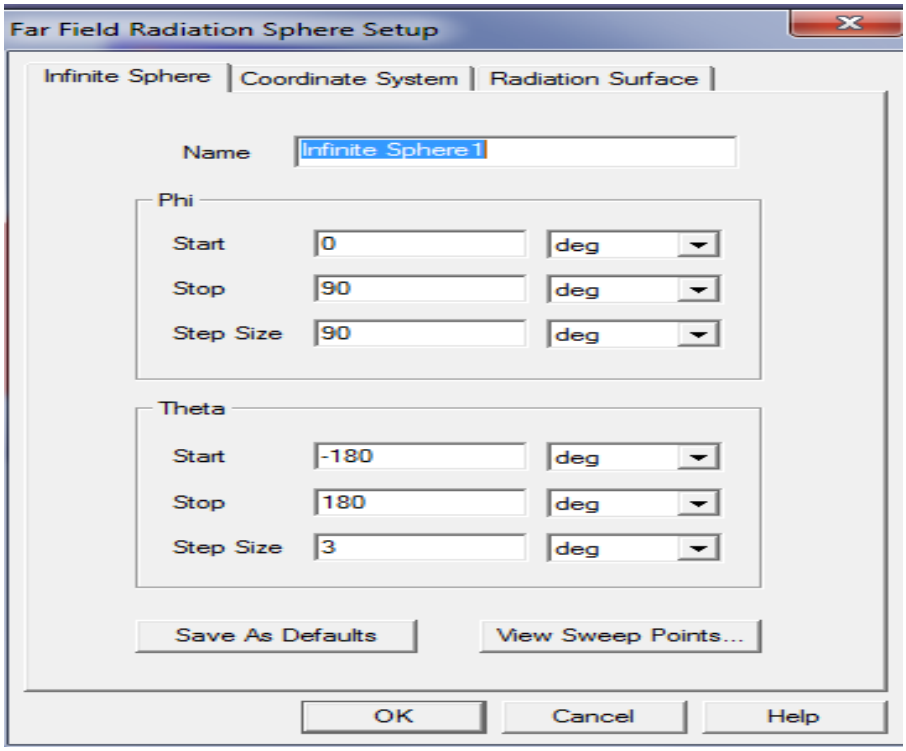

Figure 3.13 The far-field radiation sphere setup.

In order to obtain the 3D radiation plot, the following selections are to be made: *Project Manager> Results> Create Far Field Report> 3D Polar Plot*. The following figures show the window that appears where both *dB(GainTheta)* and *dB(GainPhi)* could be added to the trace.

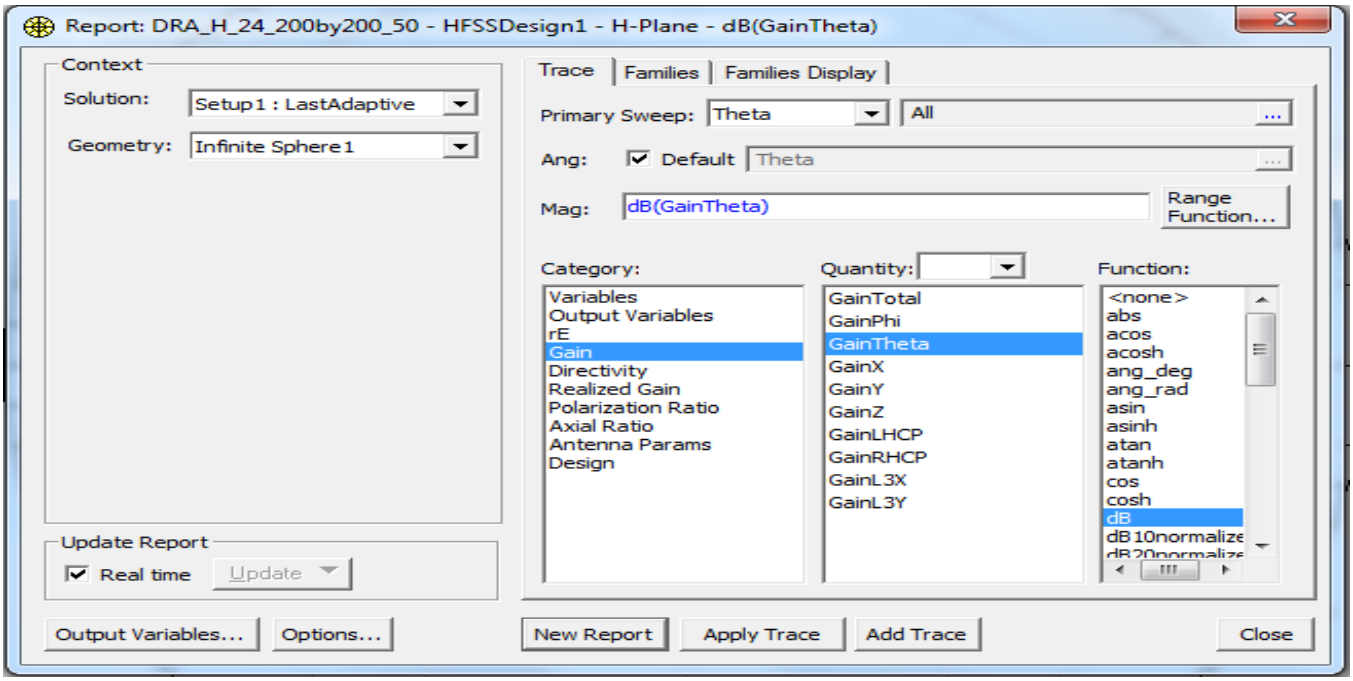

Figure 3.14 Plotting *dB(GainTheta)* in 3D.

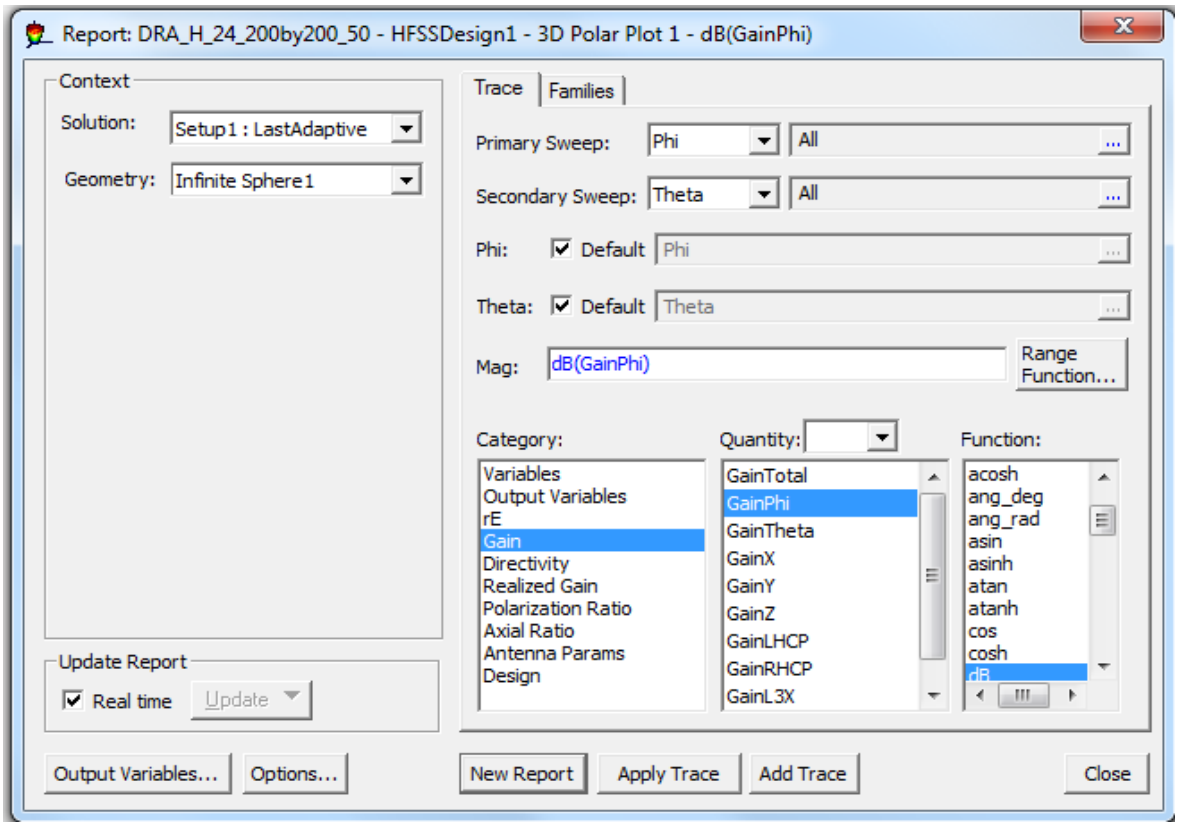

Figure 3.15 Plotting *dB(GainPhi)* in 3D.

3.4 Characteristics of the Meta-DRA Designs

The meta-DRAs designed in the following sections have been constructed with the following variations or attributes:

- Designs were made for two resonating frequencies: 24 GHz and 60 GHz.
- The various meta inclusion shapes include:
    - H
    - Window
    - Half-Window
    - Arrays
    - Special Designs
- Each parameter was generally varied in multiples of: 1, 2, 5 & 10.
- Metal inclusion line width. (20 μm, 25 μm, 30 μm and 50 μm)
- Gap between each inclusion. (20 μm, 25 μm, 30 μm and 50 μm)
- Element Size.

24 GHz	**60 GHz**
200 * 200 μm	100 * 100 μm
200 * 500 μm	100 * 200 μm
500 * 500 μm	

Table 3.1 Element sizes for meta-DRAs.

- Number of inclusions were varied depending on the design.
- Parametric variation of the feedline under the meta DRA.
- Arrays were designed only for a few selected H and Window meta-DRAs.

The lateral metal inclusion shapes (top-view) were as follows:

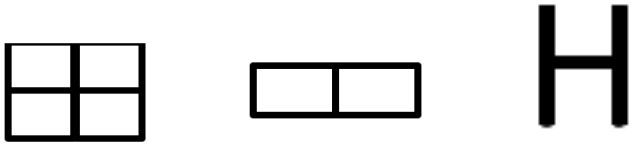

The selection of the meta inclusions depends on the coupling area available in the antenna. Higher coupling results in increasing the permittivity of the meta-DRA. Also, the DRA surface is a square or rectangle, hence similar geometries would result in a more stuctured pattern.

3.5 An Example Meta-DRA Resonating at 24 GHz

In this section, an example simulation of a meta-DRA has been shown. As discussed earlier, various batches of H inclusion meta-DRAs were simulated by changing the parameters such as gap, metal width, etc. This example and is a basis for comparing the reflection coefficients and the resonant frequencies of the designs.

3.5.1 Meta-DRA Structure

The physical structure of the meta-DRA is shown in Figure 3.16. In this case, the dimension of the metal inclusion and other structural details are given as follows:

Element Size: 500 by 500 μm

Gap: 50 μm

Internal Width: 50 μm

The DRA, substrate and micro-strip feed-line were selected as mentioned in Section 3.2.1. After setting up the meta-DRA as described in Section 3.2, the simulation is completed.

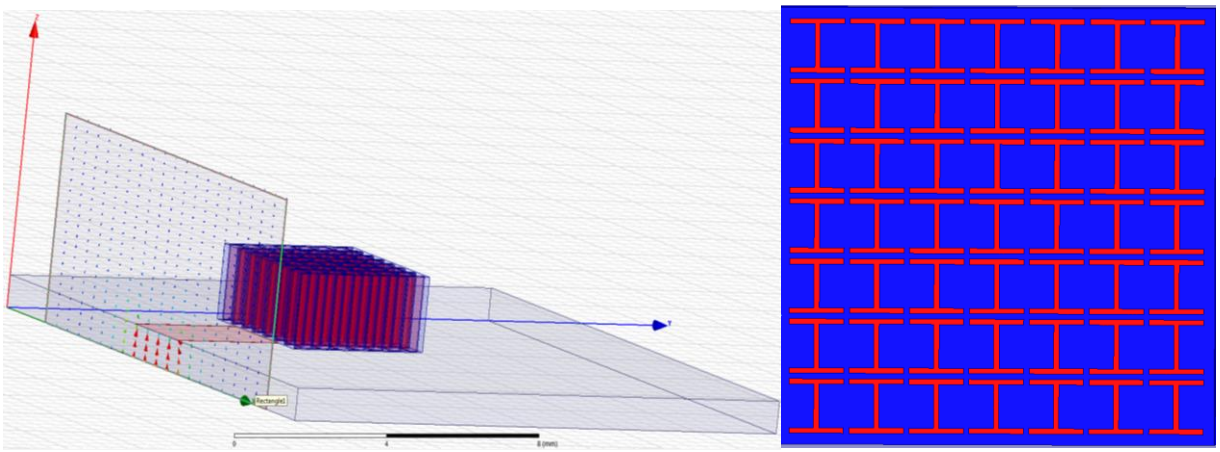

(a) (b)

Figure 3.16 (a) Physical structure of the meta-DRA, feed line, substrate and excitation wave-port.

(b) Top-view of the meta-DRA design.

3.5.2 Simulation Results

From the dB(S_{11}) versus frequency plot in Figure 3.17, one can see that a resonance has been obtained at ~21 GHz. Each curve represents a certain length of the microstrip feedline underneath the meta-DRA. This shows better coupling due to the metal inclusions. The dB(S_{11}) value becomes more negative as the feedline approaches the first row of the metal inclusions. A high negative dB(S_{11}) denotes better power transfer or in other words, no reflection. Hence the meta-DRA with a polymer-base behaves like a high permittivity ceramic DRA which has identical resonance and good transmission. Now the only concern would be the power radiated out of the antenna. This can be examined by studying the radiation plot of the antenna.

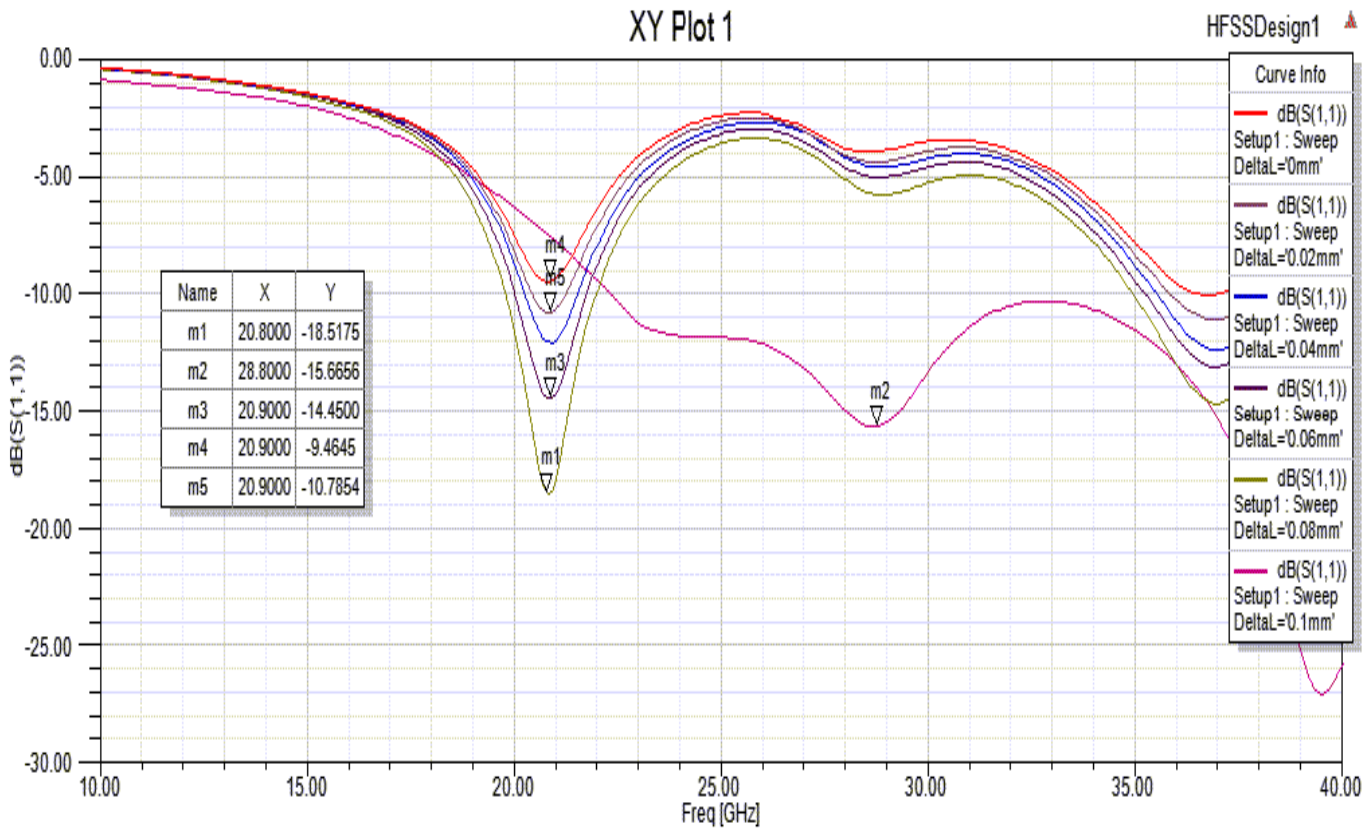

Figure 3.17 The S_{11} parameter vs Frequency plot.

The radiation plot shows the realized gain (considers loss due to reflection) of the antenna. The loss that might occur due to reflection is also accounted for. It can be observed that a gain of ~3.5 dB has been achieved from the meta-DRA design. The *GainPhi* frontal and backward lobes can be seen in the plot and their magnitudes are denoted by markers m_1 and m_3. The difference between these magnitudes gives the front to back radiation of the antenna. The expected gain from a high permittivity DRA is 5 dB. Hence the meta-DRA with a gain of ~3.5 dB could possibly replace the ceramic DRAs in terms of power radiated. Figure 3.19 shows the 3D form of the radiation plot obtained from the meta-DRA. In the next chapter, the simulated designs have been dealt with much greater detail. They have been discussed, compared and inferred.

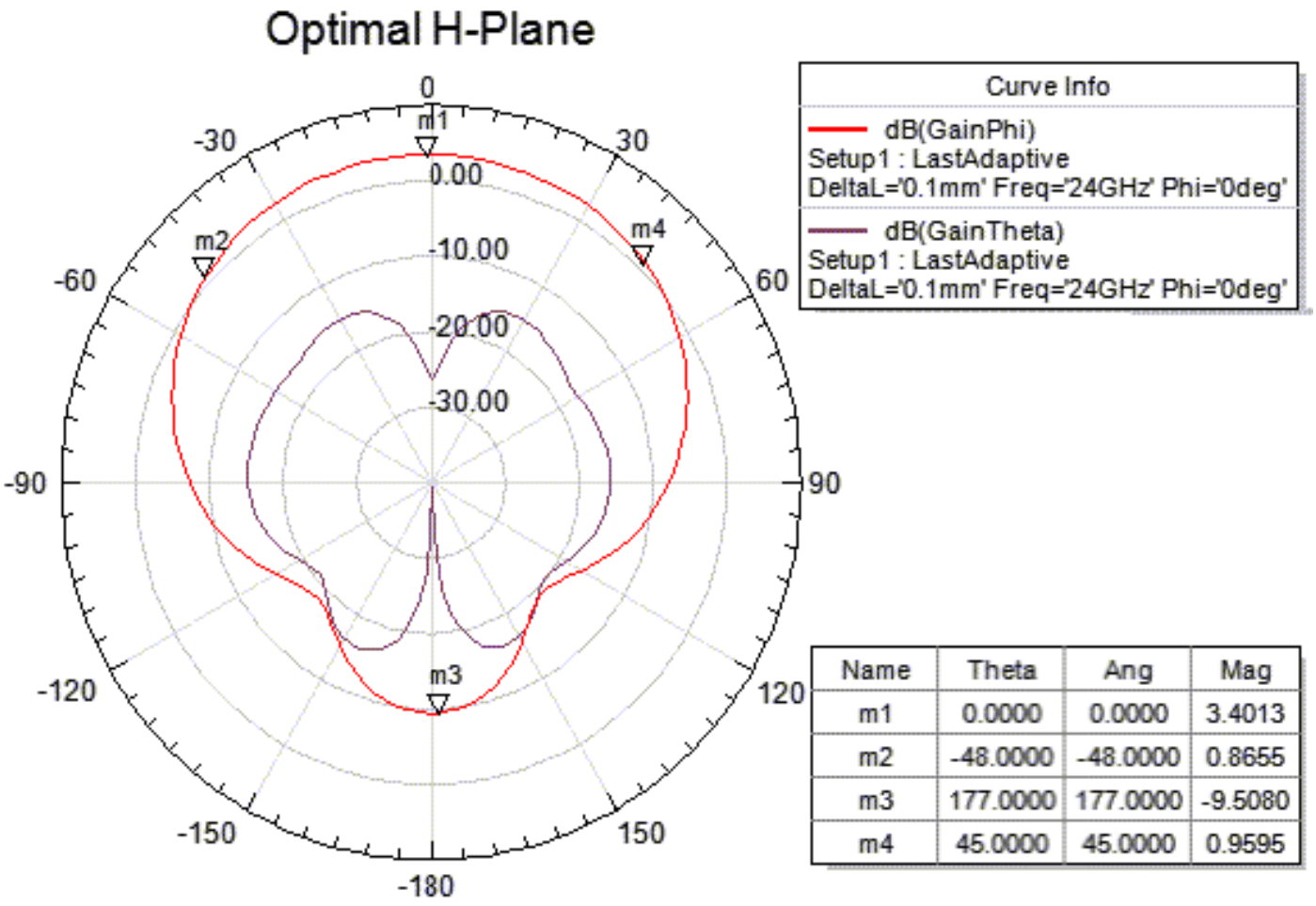

Figure 3.18 2D Radiation plot of the meta-DRA in the H-Plane showing the dB(GainPhi) and dB(GainTheta) curves in HFSS.

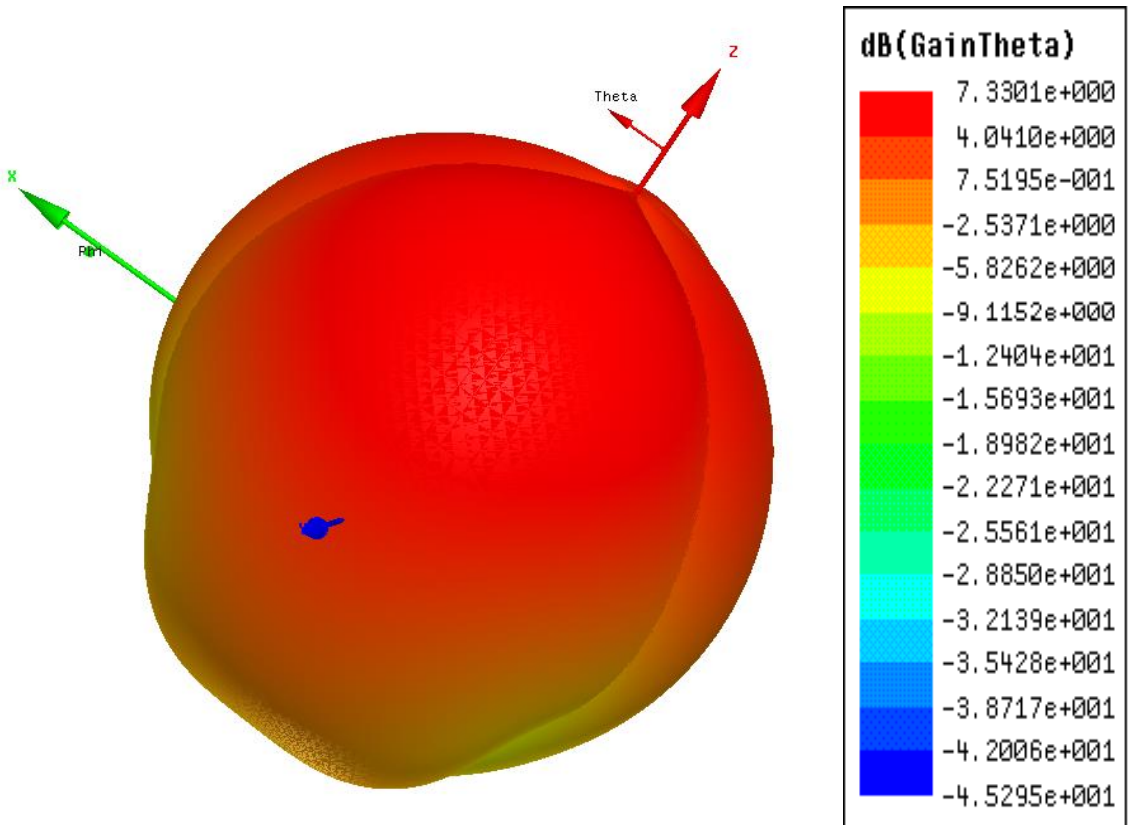

Figure 3.19 3D Radiation plot of the meta-DRA.

3.5.3 Mesh Structure of the meta-DRA

Meshing is a process of forming small geometrical structures with finite vertices that are used to determine the solution to partial differential wave equations by Finite Element Method (FEM). HFSS has a key advantage when it comes to meshing. The mesh structure is automatically defined when geometry, material properties and the desired output is mentioned. This is also known as adaptive meshing technique. This process of meshing uses a highly robust volumetric meshing technique and includes a multi-threading capability that reduces the amount of memory used and speeds up the simulation.

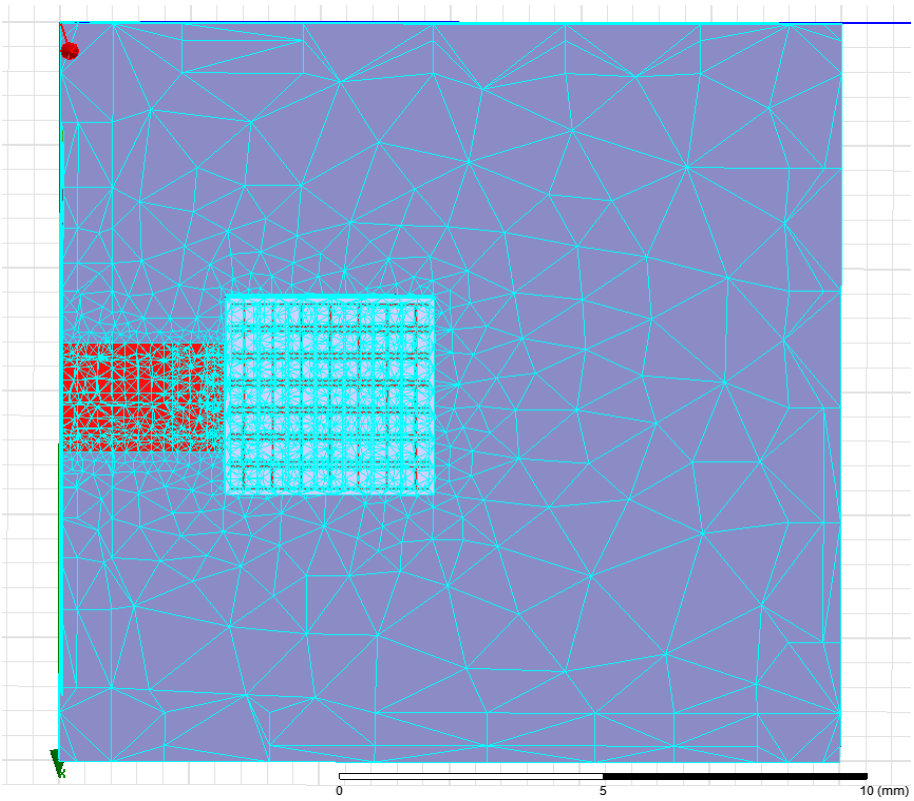

Figure 3.20 Top-view of the meta-DRA under consideration showing the mesh pattern around the structure.

Figure 3.20 shows the top view of the meta-DRA considered as an example in this section with the mesh structure. It can be seen that the density of the mesh elements is higher near the feed line and the meta-DRA where the field computation takes place. The default number of mesh elements defined by HFSS according to the geometry, material and desired resonating frequency is 1000 for this project. Generally the distance between the vertices of a mesh element is λ/10. This varies depending on the size of the structure under consideration. In order to see the effect of an increased number of mesh elements on the design solution, the above meta-DRA example was simulated with 5000 mesh elements instead of 1000. The resonance at ΔL = 0.06mm was compared with the plot at Figure 3.17.

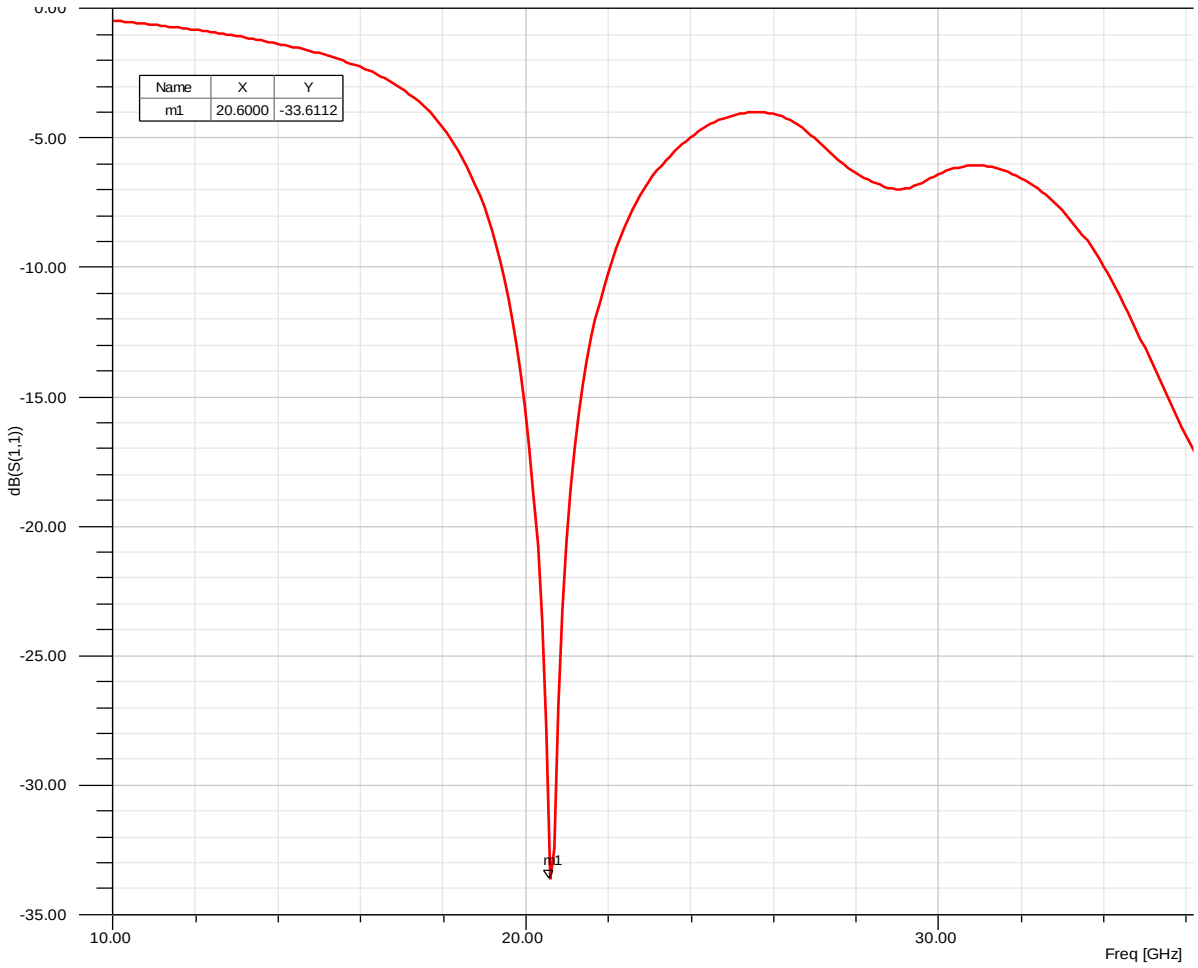

Figure 3.21 dB(S_{11}) vs Frequency at ΔL = 0.06mm for the meta-DRA.

From Figure 3.21 it can be noted that the resonant frequency is 20.6 GHZ whereas it was originally 20.9 GHz with the default meshing technique. This shows that there is not a lot of difference due to the change in the number of mesh elements in terms of the resonant frequency of the design. But the negative dB(S_{11}) value increases to -33.61 from -14.45. However, a meta-DRA with a dB(S_{11}) of -10 or lower is acceptable for transmission. Hence this is not a grave concern as far as the goals of this project are concerned.

3.6 Layout for Fabrication of X-Ray Mask

The next step would be to create a mask for fabrication of the meta-DRAs. This can be done in a layout editing software. ADS (Advance Design System) was used in this case. The design

needs to be exported in .DXF format so that it can be imported in ADS. Before forming the final mask, each design needs to have their corners rounded. The entire process leading to the formation of the final mask is described in the following sub sections.

3.6.1 Rounding the Corners

The corners of the meta-DRA elements have sharp edges. This can cause cracking of the polymer-base of the meta-DRA due to shrinkage in processing. Hence it is important to round these corners of the designs. The radius for rounding the corners should be less than half the width of the metal inclusions. The radii chosen here were 0.009 mm for the 24 GHz and 0.003 mm for the 60 GHz designs. The following section will talk about a nomenclature developed in this thesis to identify each element in the final mask of the meta-DRA.

3.6.2 Nomenclature

With so many different samples of meta-DRA in the final mask, it was very important to be able to identify each sample after the fabrication process for the purpose of testing and comparing. Hence a naming pattern for the meta-DRAs was formed which can be summarized in Figure 3.22. The first meta inclusion of each sample was changed according to the order at which they appear on the final mask. The geometry denoting the order of the samples was designed such that it does not differ to a great extent from the meta inclusions themselves. This ensures that the resonating frequency and other attributes such as field patterns and radiation from the meta-DRA are not altered. For example, the first sample of the 24 GHz *H* designs (H_1) has the same numbering pattern as that of the first sample of the window design. This is because they can be easily distinguished under a microscope due to the difference in geometries. Thus the numbering or naming of the samples is used to distinguish between the same shape inclusions of similar dimensions or resonant frequencies.

Figure 3.22 Structures of the elements used for naming the meta-DRAs.

3.6.3 Forming the Final Mask

The final mask for all the meta designs was formed with the help of ADS and verified in AutoCAD. The dimension for the mask suggested by fabrication engineers at KIT was a disk of 70 mm diameter. But the entire disk could not be filled with designs as it would become too compact and would lead to unsuccessful processing. Thus an area covered by a square of 50 mm sides to insert the meta-DRAs is used. This ensured enough space on the edge of the mask, which had no samples.

Hence even if the corners get damaged, no samples would be lost. There also had to be enough gaps between the elements to ease the cutting process. Hence the entire packaging had to be

done with a lot of care and was a challenge in itself. A lot of combinations were tried to fit in the above dimensions. The goal was simple: to fit as many favorable meta-DRAs as possible. The final mask dimensions and other details are listed as below:

- Size of circular mask: 70 mm diameter.
- Actual mask area: An inscribed square of 50 mm sides.
- Number of elements:

Type of Meta-DRA	Number of Elements
Resonating at 24 GHz	24
Resonating at 60 GHz	38
Arrays of 24 GHz	3
Arrays of 60 GHz	4

Table 3.2 Number of elements for each type of meta-DRA.

- Total number of meta-DRA samples: 69.
- Gap between the 24 GHz designs: 2 mm.
- Gap between the 60 GHz designs: 3 mm.

The following figures depict some example samples of meta-DRA after exporting from HFSS and editing in ADS. Notice that the first metal inclusion in each figure is different from the usual geometry used for designing the meta-DRAs. This helps in identifying the fabricated miniature samples as discussed in Section 3.6.2. Figure 3.30 shows the final mask formed with the above specifications in mind.

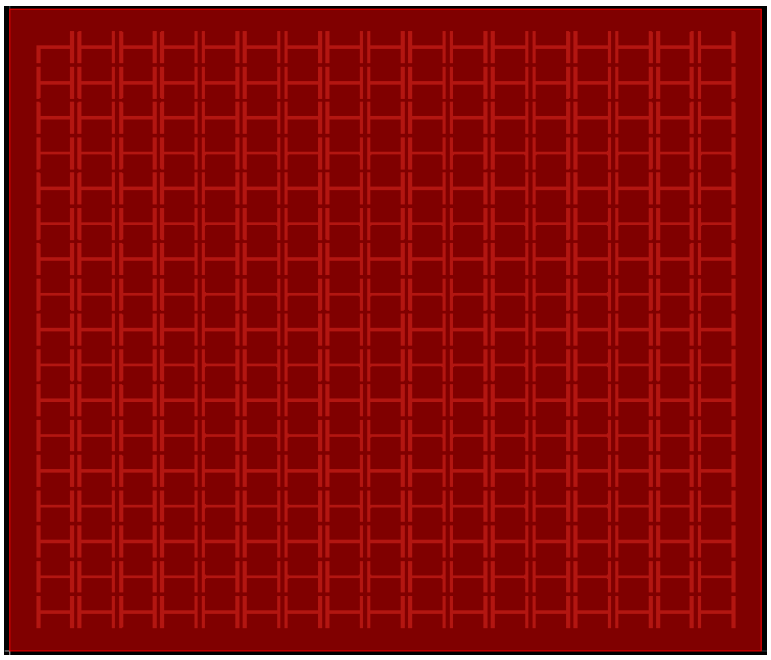

Figure 3.23 H inclusions with element size 200 by 200 μm with a gap of 20 μm and resonating @ 24 GHz.

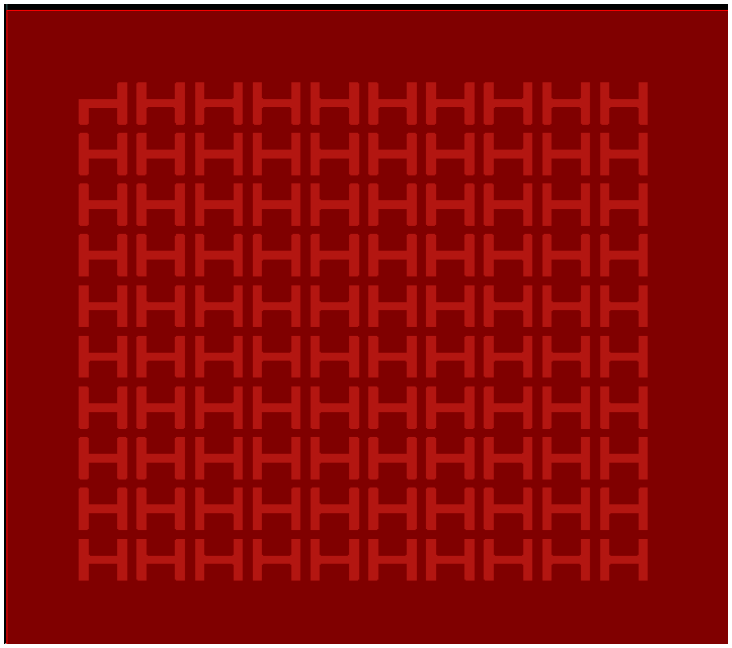

Figure 3.24 H inclusions with element size 100 by 100 μm with a gap of 20 μm and resonating @ 60 GHz.

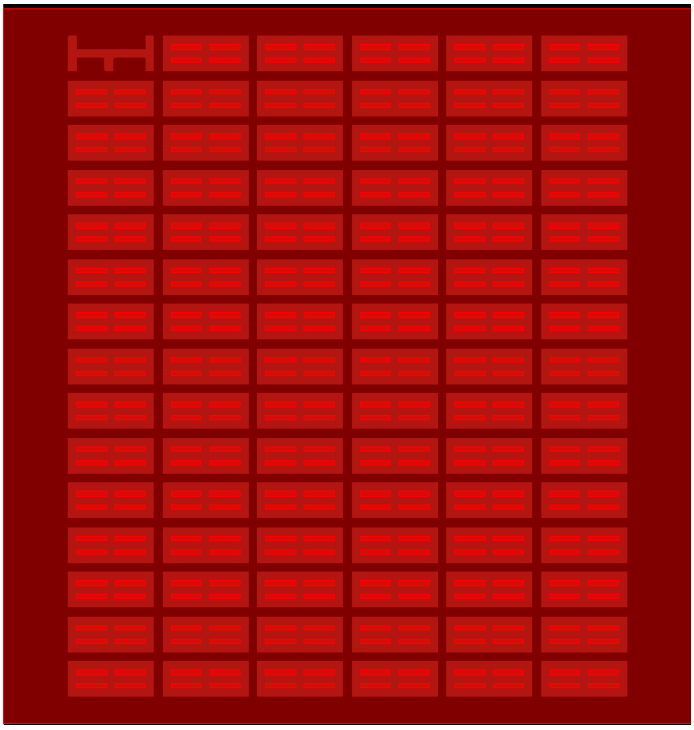

Figure 3.25 Window inclusions with element size 200 by 500 μm with a gap of 50 μm and resonating @ 24 GHz.

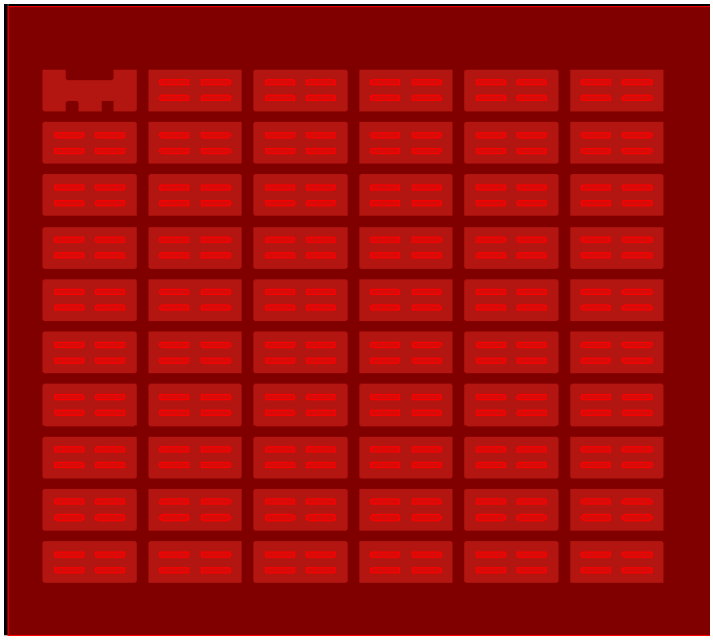

Figure 3.26 Window inclusions with element size 100 by 200 μm with a gap of 25 μm and resonating @ 60 GHz.

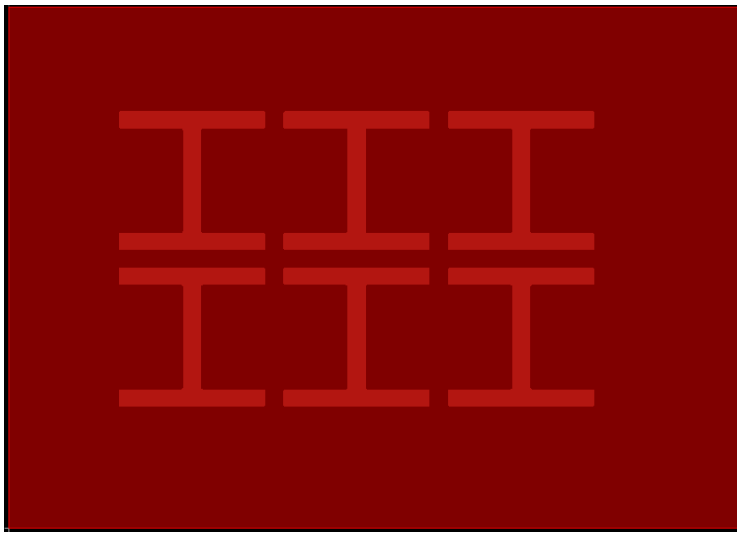

Figure 3.27 H inclusions with element size 400 by 400 μm with a gap of 50 μm and resonating @ 60 GHz.

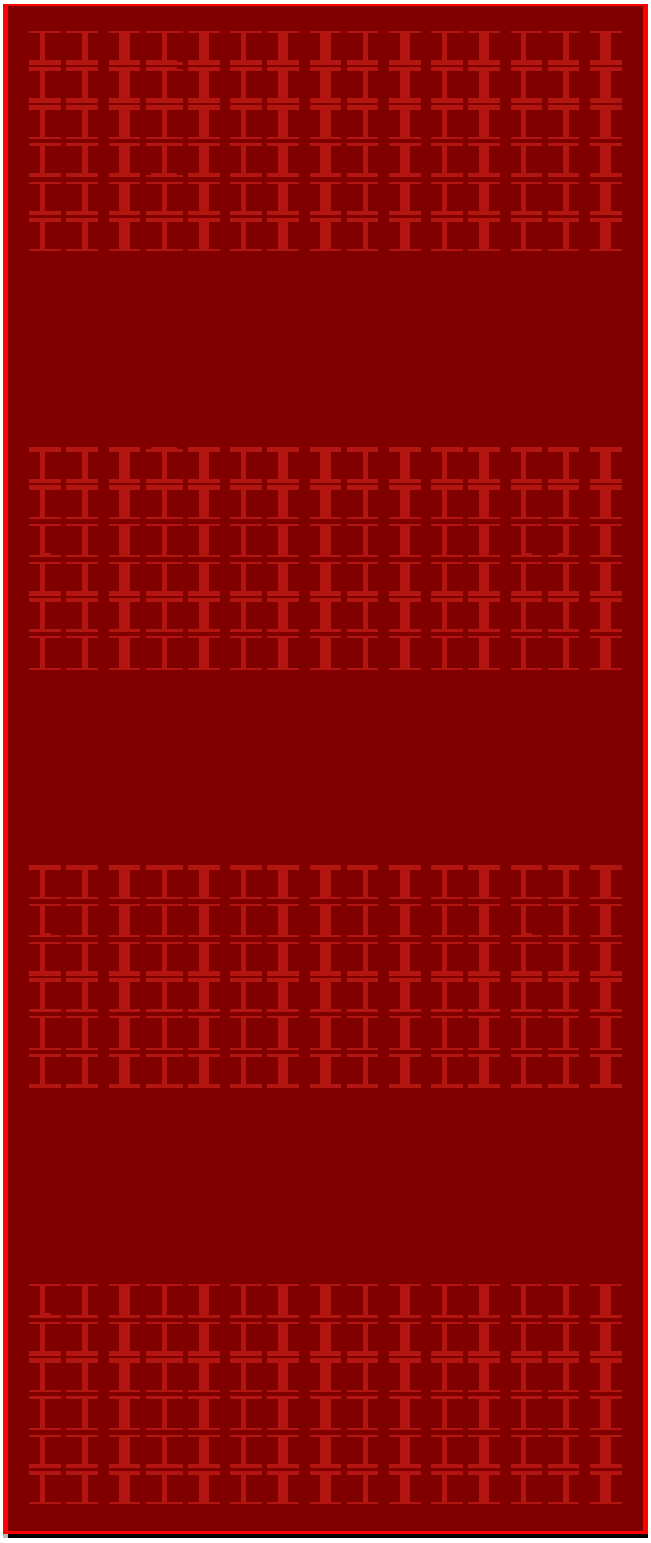

Figure 3.28 Array of H inclusions with element size 200 by 500 μm with a gap of 50 μm and resonating @ 24 GHz.

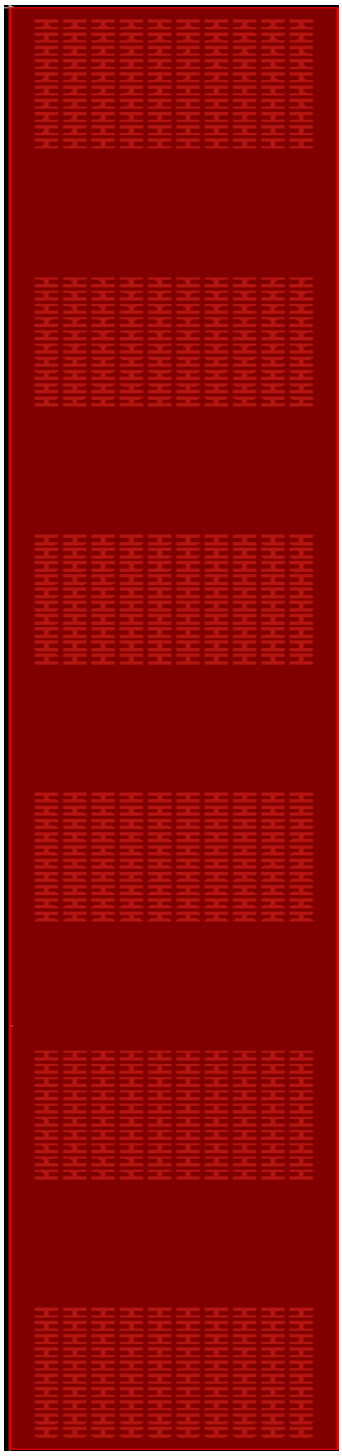

Figure 3.29 Array of H inclusions with element size 100 by 100 μm with a gap of 30 μm and resonating @ 60 GHz.

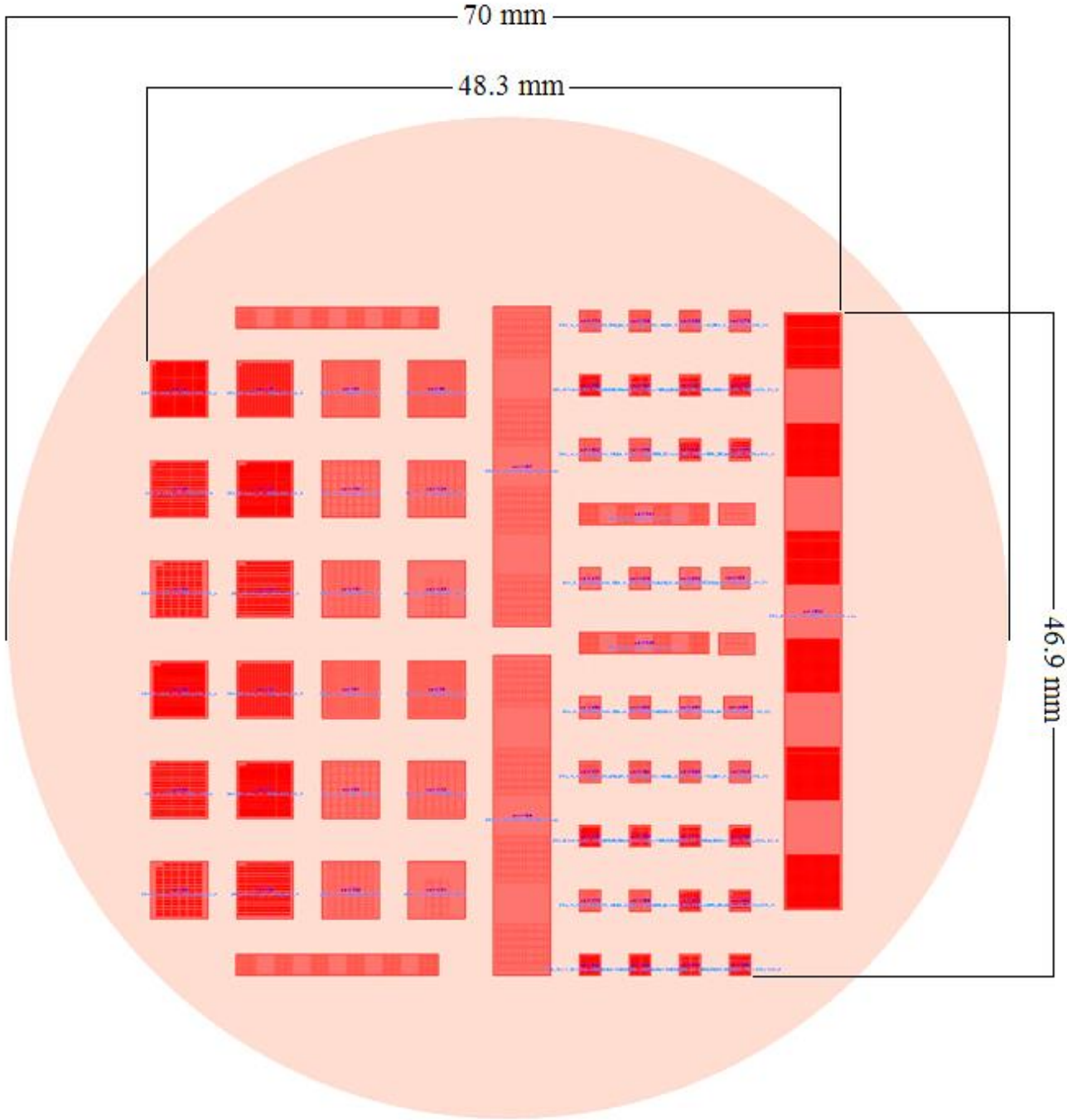

Figure 3.30 The final mask, which was sent to Karlsruhe Institute of Technology, Karlsruhe, Germany.

3.7 Deep X-Ray Lithography (DXRL)

In this section, a brief introduction to DXRL is given. Although the designs were not fabricated in the lab here, the process of X-ray fabrication that has been used to fabricate the meta-DRAs at KIT, Germany, is presented.

X-ray lithography is a process in which a design mask is imprinted or developed in a resist material, PMMA in this case. High-precision designs depend on the beam exposure, the accuracy of the pattern formation on the mask and the purity of the resist. Selective X-ray absorbing or transmitting materials form the mask. The exposed areas in PMMA are etched (Figure 3.31 (b)). The incised parts of the resist are later filled with nickel for the meta-DRA designs. The pattern on the resist determines the shape and dimension of the metal inclusions in the meta-DRA design. Hence the X-ray mask should withstand many exposures without distortion, be sturdy and must be aligned with the sample.

From Figure 3.31 (a), it can be seen that the mask consists of an absorber, a membrane and a frame. The pattern is formed by the design of the absorber, which allows the rays to fall on the hollow spaces, which are metal inclusions in this case. The absorber is formed by a material with high atomic number (Z). A high Z material absorbs X-rays whereas a low Z material transmits X-rays. The frame holds the membrane-absorber assembly and is robust. Due to the depth of the resist, the absorber should be very thick (>10 μm) and the membrane should be highly transparent and thin (2 to 4 μm) in order to achieve better etching [56]. The transparency of the low-Z membrane should be at least 80%. The membrane should contribute to minimal scattering of the X-rays. Beryllium is commonly used as a membrane due to its high transparency and ruggedness. The absorber of a mask has the following attributes: high attenuation (>10 dB), stable under prolonged radiation, ease of patterning and minimal deformation. Some popular materials used as absorbers are gold, tungsten,

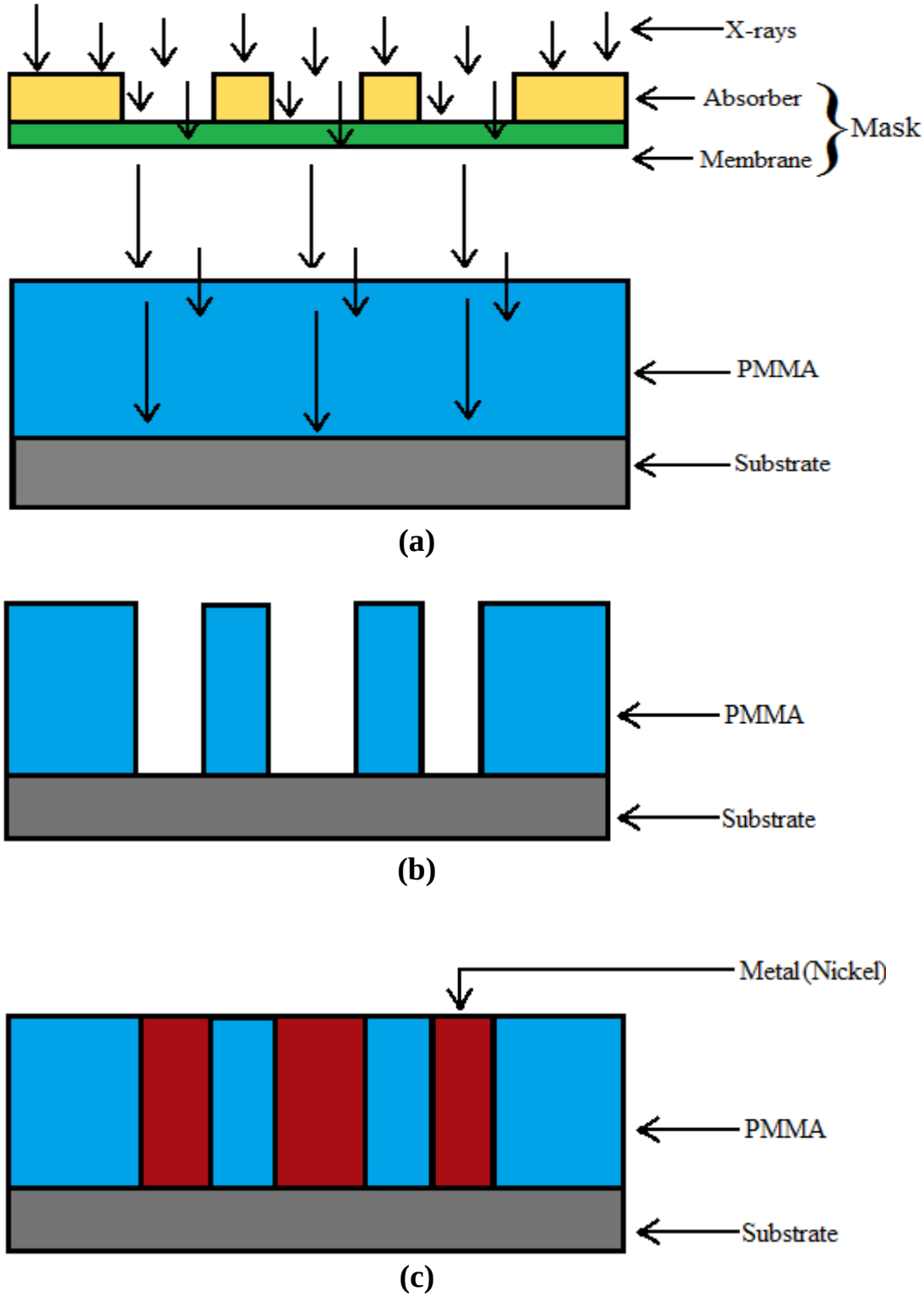

Figure 3.31 Schematic of the DXRL process.

tantalum and alloys. For this research, titanium was used as a membrane with gold absorbers. After the formation of the design, the sacrificial Si wafer is etched in order to release the meta structures.

3.8 Post Fabrication

Some early results from the fabrication of the meta-DRAs (H inclusions) at KIT, carried out by Martin Boerner and his team, were promising and also raised a few questions which could lead towards a new area of research for the meta-DRAs. This will be discussed later in this section. A few sample pictures from the SEM have been given below. The PMMA body of the meta-DRA has been removed to allow imaging.

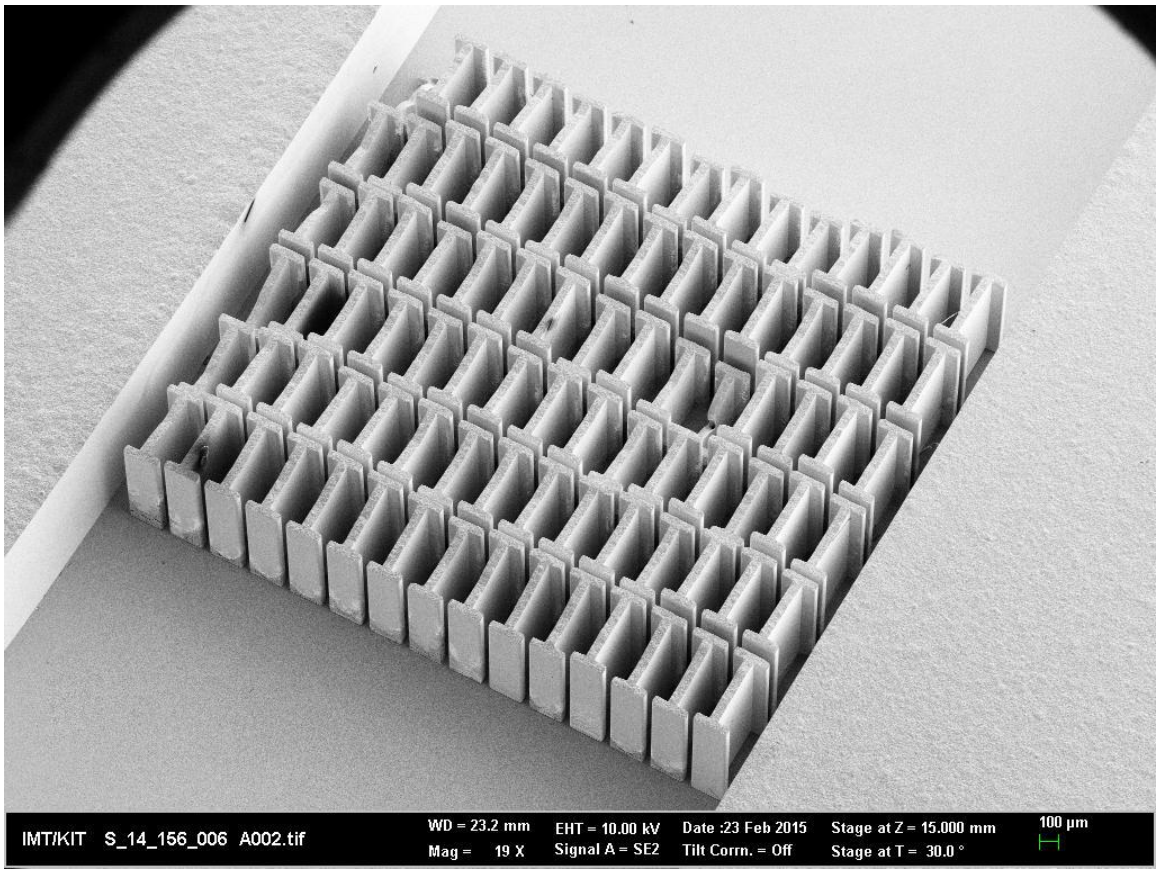

Figure 3.32 SEM image of meta-DRA fabricated at KIT, Germany. The PMMA body has been removed for imaging.

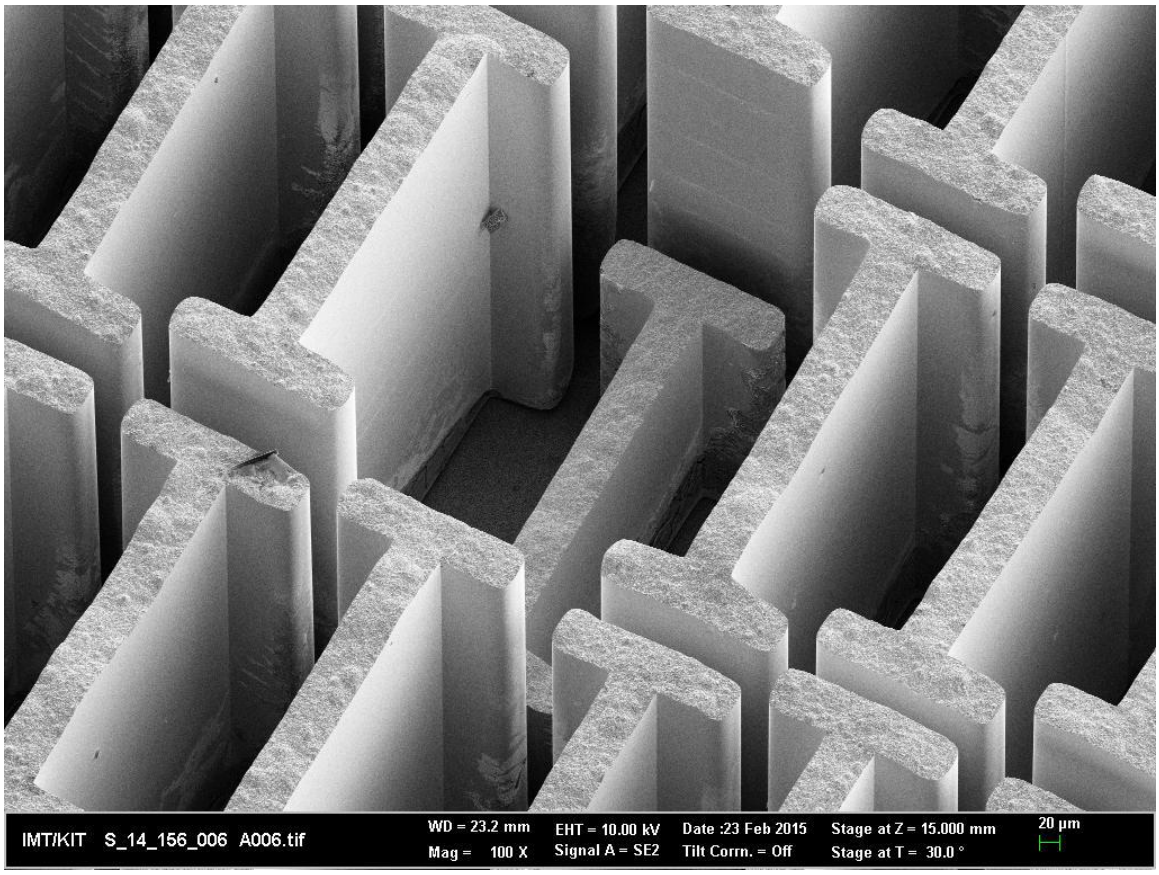

Figure 3.33 SEM image of meta-DRA fabricated at KIT, Germany. The PMMA body has been removed for imaging.

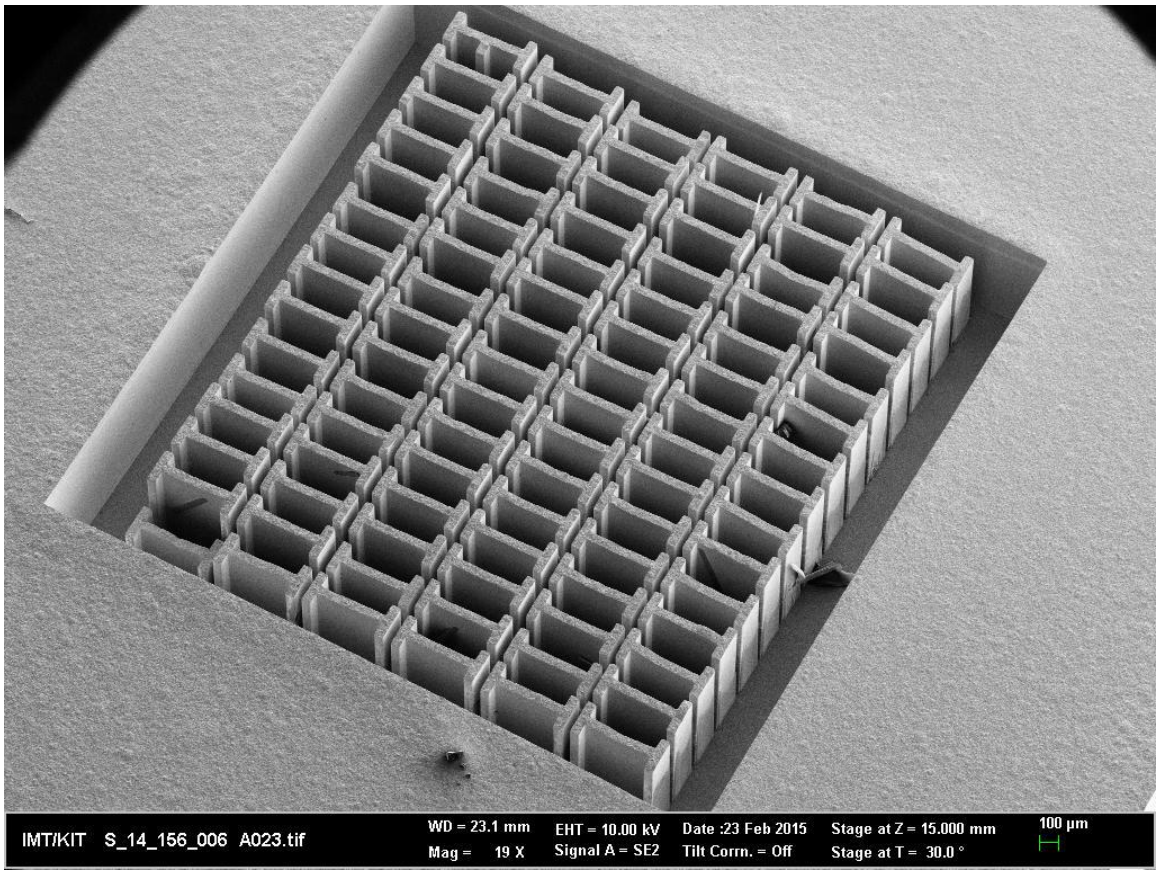

Figure 3.34 SEM image of meta-DRA fabricated at KIT, Germany. The PMMA body has been removed for imaging.

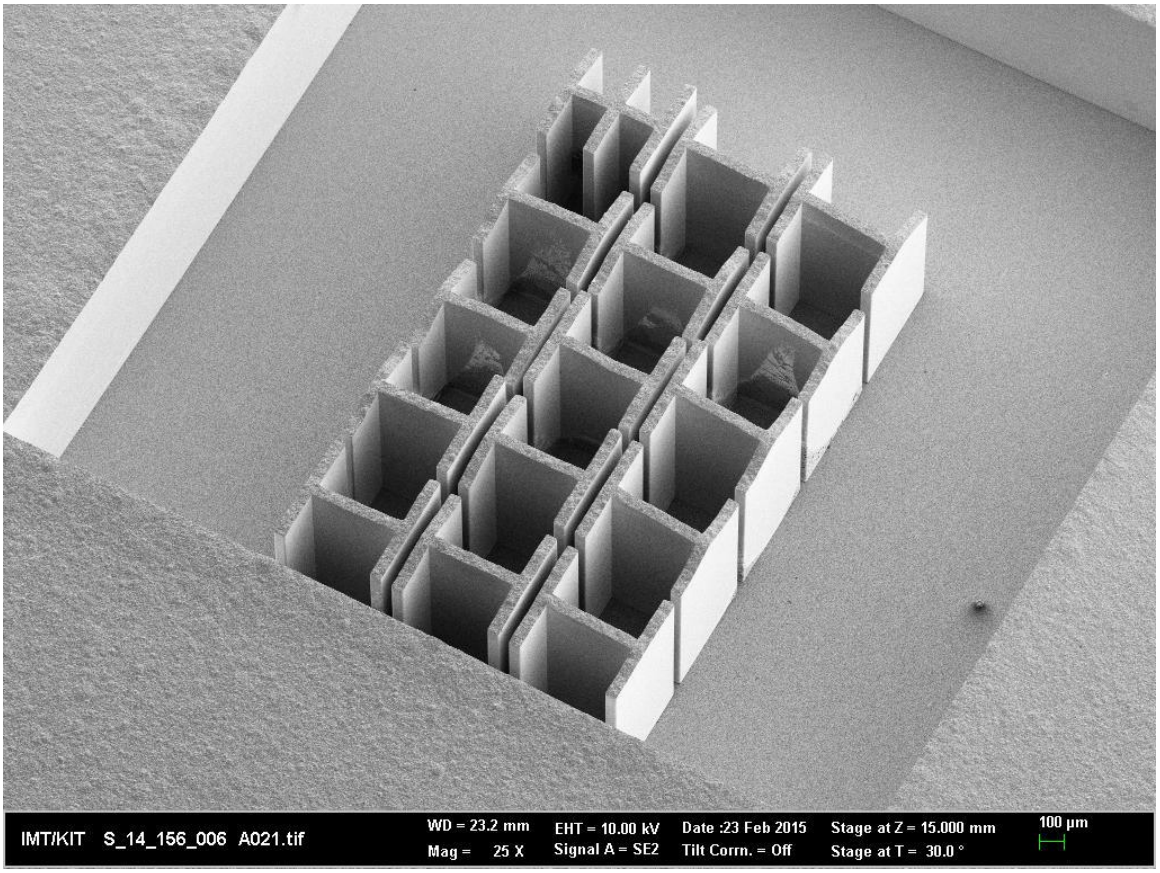

Figure 3.35 SEM image of meta-DRA fabricated at KIT, Germany. The PMMA body has been removed for imaging.

The SEM pictures reveal a generally uniform meta-DRA electroplating. The samples have a nominal height of 800 μm of nickel. Some of the nickel inclusions may have been lost due to the stripping process. It was interesting to note the variation in height of the metal inclusions in the fabricated samples. Does the height variation have any affect on the resonant frequency? In order to try and an answer this question, two patterns of height variation were tried on the meta-DRA design given as an example previously in this chapter (Section 3.5.1). Figures 3.36 and 3.37 show the assumed pattern of variation for the analysis (Type 1 and Type 2). Type 1 is a progression of decreasing height in the direction of the excitation and type 2 is a decreasing series from the periphery of the meta-DRA to its center.

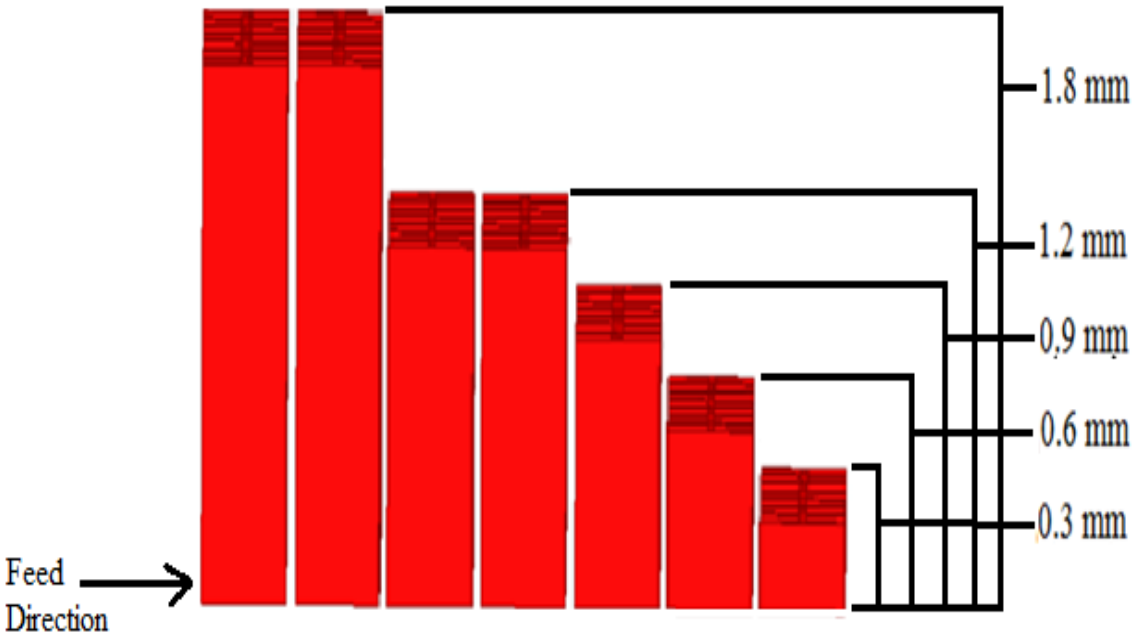

Figure 3.36 Type 1 - Linear variation in the height of meta inclusions (decreasing away from the source of excitation). Only the metal inclusions have been shown.

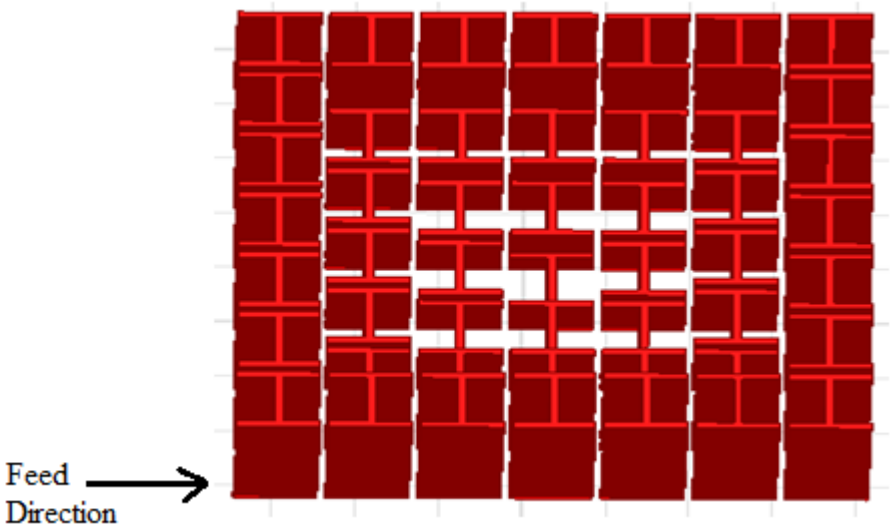

Figure 3.37 Type 2 - Variable height (1.8 mm to 0.3 mm from boundary to center) of meta inclusions from outside to inside. Only the metal inclusions have been shown.

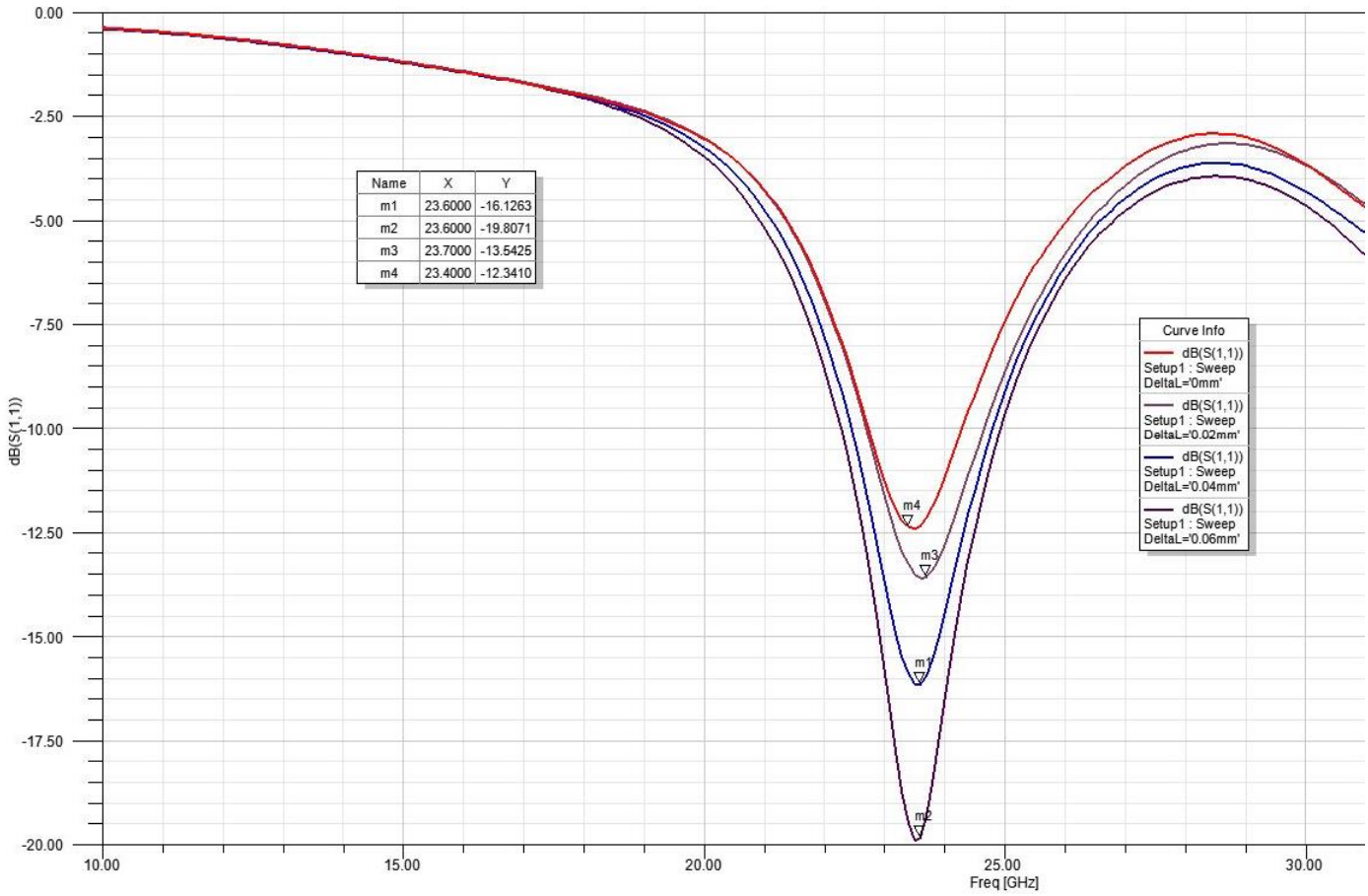

Figure 3.38 dB(S_{11}) vs Frequency for Type-1 meta-DRA.

The dB(S_{11}) vs frequency plot for the meta-DRAs are given in Figures 3.38 and 3.39. The resonances for both the designs have been compared with each other and also the original design in the section 3.5.1. Type -1 meta-DRA resonates at 23.4 GHz with a negative dB(S_{11}) value of -19.8 and type-2 meta-DRA initially resonates around 23.3 GHz. The type-2 design shows a dual resonance pattern and the second resonance occurs at 39.2 GHz. But the resonance obtained varies constantly when optimized with the changing length of the feedline. Comparing these designs to the original design in the previous section, type-2 seems to be closer to the expected resonance pattern. This is because the parent design had a dual resonance at 20.8 GHz and 37 GHz.

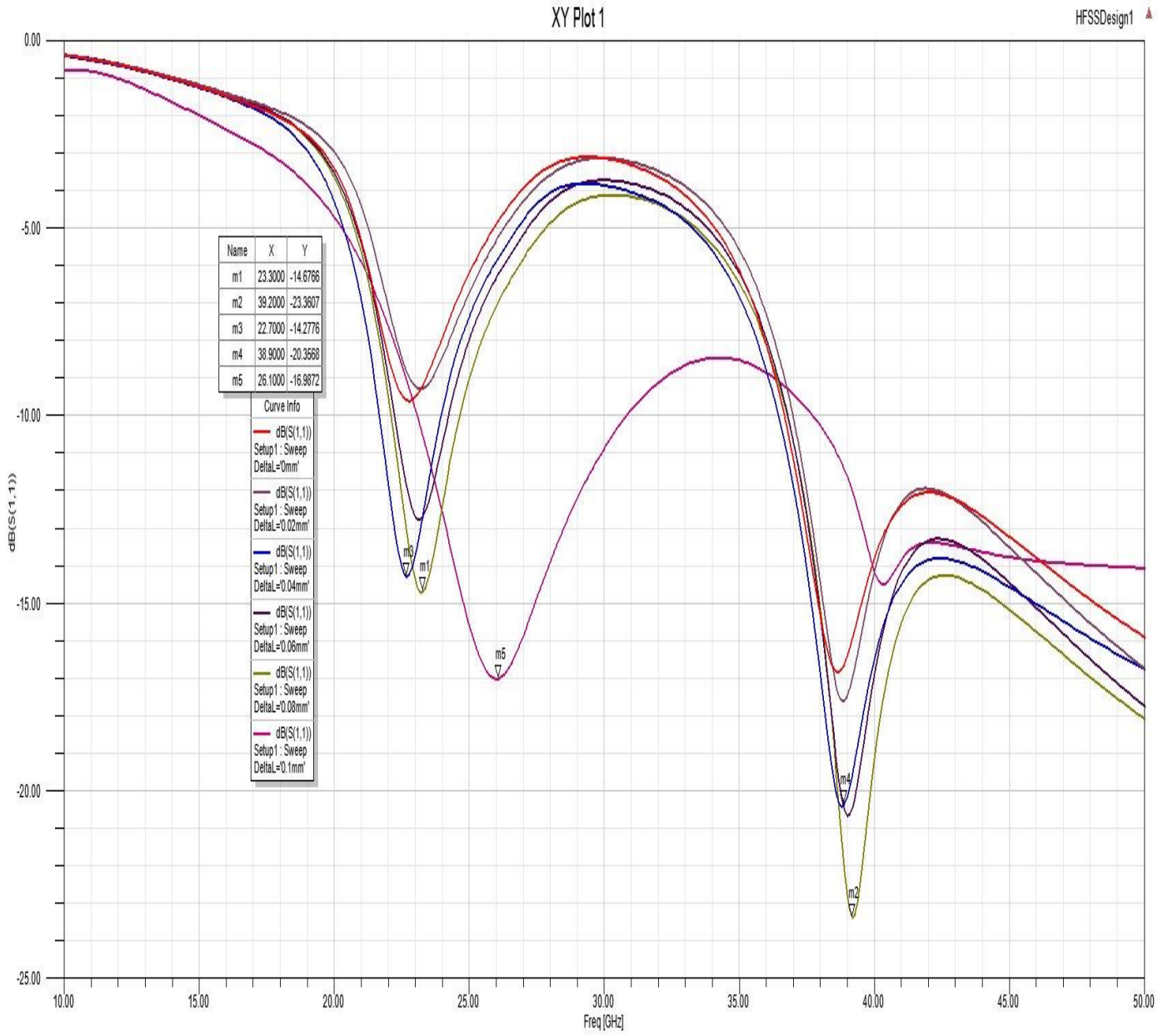

Figure 3.39 dB(S_{11}) vs Frequency for Type-2 meta-DRA.

For some reason, type-1 meta-DRA goes askew after 40 GHz. There is a strange pattern in the plots. Both designs were plotted until 100 GHz. No distinctive changes were found in them after the 50 GHz mark. Although there are some anomalies in the resonances of the designs, these meta-DRAs were designed to resonate close to 24 GHz, which they do. Thus, it can be said that the change

in the height of the metal inclusions in a meta-DRA does affect the resonance. But it cannot be said whether it actually hampers the purpose of the design (resonating at a certain frequency and radiating power). For that, more samples need to be simulated with different variations in height.

Chapter 4

Meta-DRA Design and Simulation Results

4.1 Introduction

In the previous chapters, the motivation, theory and design procedure for the meta-DRAs in the thesis/project have been explained in detail. In this chapter, all the meta-DRA designs and their simulation results are discussed and notable comparisons are drawn. Each kind of metal inclusion has been represented by an example meta-DRA design. All the designs have a good negative dB(S_{11}) which shows that the antenna has a good transmission. Based on the results, other criteria such as shift in resonance with change in metal gap/width and also the suitable length of feedline have been studied which might prove to be useful for future implementations. The detailed structural dimensions of the designs have been included in Appendix A and Appendix B in the thesis.

4.2 H inclusions

4.2.1 Resonating at 24 GHz

The meta-DRAs with H inclusions and resonating at around 24 GHz were discussed in the previous chapter as an example design. The reflection coefficient and radiation plots have been explained in detail as well. In this section, a comparison in the resonances of the meta-DRA due to the change in gap/width of the metal inclusions has been made.

Most of the design parameters like the size of element and the metal gap/width have been determined in multiples of 1, 2, 5 and 10 in order to have a uniform variation for the different shapes of inclusions. Keeping this in mind, the metal inclusion gap/width has been altered from 20 μm to 50 μm in most designs. Some of the samples have variable gap/width in the X and Y-axis. The antenna is excited in the Y direction. So in the same design there is a different width for the individual metal

inclusions and a different gap between each row in the polymer substrate. However, in some designs, only the most suitable gap/width has been chosen keeping the structure in mind. The most common widths used are 20µm, 25µm, 30µm and 50µm. In this section, a meta-DRA with H type of meta inclusions has been chosen for study. The design is shown in Figure 4.1 (a) and (b). The structural details of the individual metal elements are as follows (Appendix A.1, design 5):

Element Size: 200 by 500 µm

Gap: 50 µm

Internal Width: 50 µm

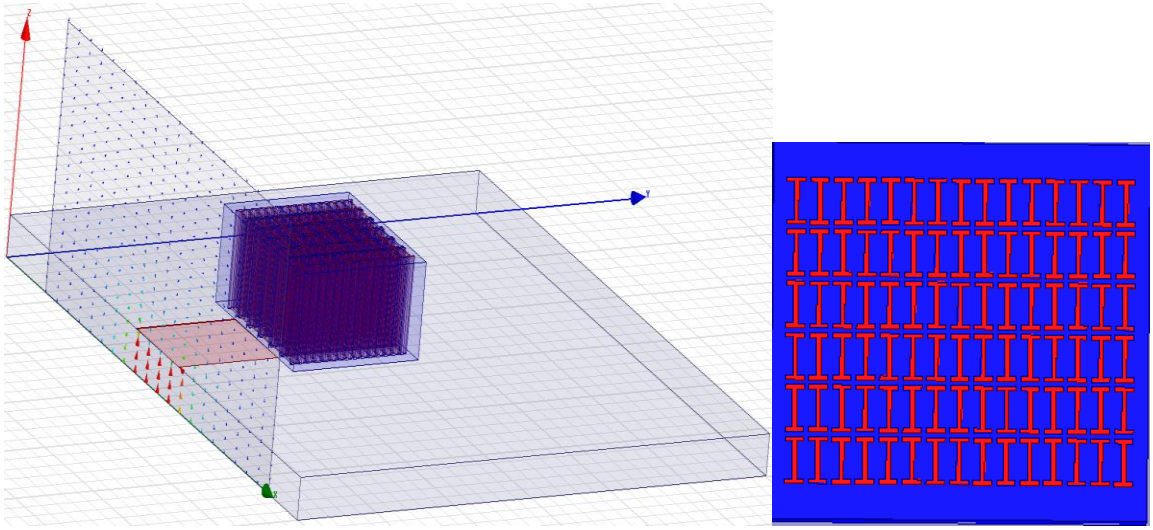

Figure 4.1 (a) Physical structure of the meta-DRA, feed line, substrate and excitation wave-port. **(b)** Top-view of the meta-DRA design.

Figure 4.2 depicts the dB(S_{11}) versus frequency plots for H designs having the same element size of 200 by 500 µm (please refer Appendix A.1 for structural details) but different metal gap/width. The optimized resonance curve with the most negative dB(S_{11}) value has been represented in each segment. The comparison is made in order to find out whether the change in metal width has any affect on the resonance of the antenna. The nominal design with a gap/width of 50 µm resonates at 24.5 GHz. Decreasing the gap/width to 20µm reduces the resonating frequency to 23.6 GHz in this

case. Having a variable gap/width in the metal inclusions (20 μm in X and 50 μm in Y), the resonance shifts to 22.2 GHz.

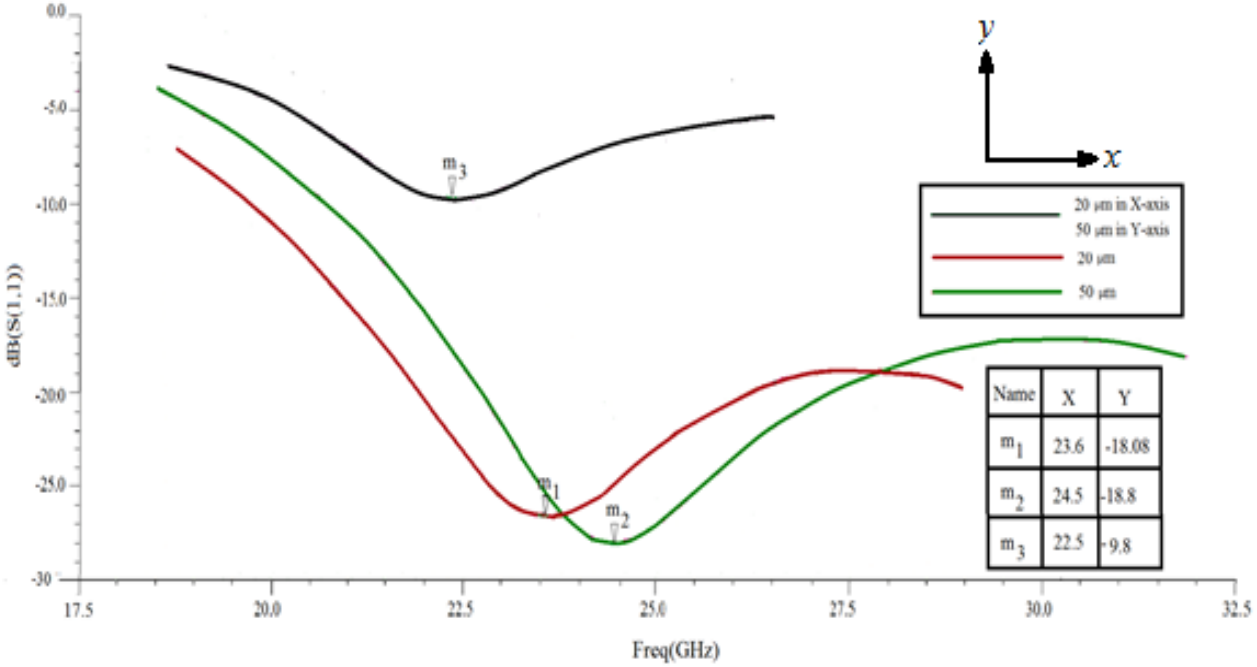

Figure 4.2 200 by 500 μm H designs resonating at 24 GHz.

Metal gap/width (μm)	Meta %	Resonating F (GHz)
20	74.37	23.6
50	56.25	24.5
20-50	65.63	22.2

Table 4.1 Meta percentage and resonant frequency for different gap/width of the metal inclusions.

Varying the gap/width of metal inclusions can alter the resonance of a meta-DRA. Referring to the meta percentage calculations in Table 4.1, it can be seen that the 20 μm design is 74.37% meta compared to the nominal design which is 56.25%. Hence it resonates at a lower

frequency or has a higher permittivity. The higher meta percentage can be resulted from the fact that the 20 µm design has more number of metal inclusions in the array compared to the nominal design. Hence the resonance is affected by factors such as number of metal elements and the area of coupling. The percentage argument doesn't hold good for the non-symmetrical (variable metal gap/width) design. According to the meta percentage of 65.63%, the design is expected to resonate between the two symmetrical designs. This shows that the meta behavior in the non-symmetrical designs is more complicated and doesn't follow any particular pattern.

4.2.2 Resonating at 60 GHz

In this section, the meta-DRAs with H inclusions and resonating at 60 GHz are discussed. An example structure of the meta-DRA is shown in Figure 4.3 (a) and (b). Since these need to resonate at higher frequencies, the size of the meta-DRAs has to be smaller than the ones resonating at 24 GHz as discussed in the previous chapters of the thesis. Hence, miniaturization is required to lower the overall permittivity of the structure compared to that of the 24 GHz designs.

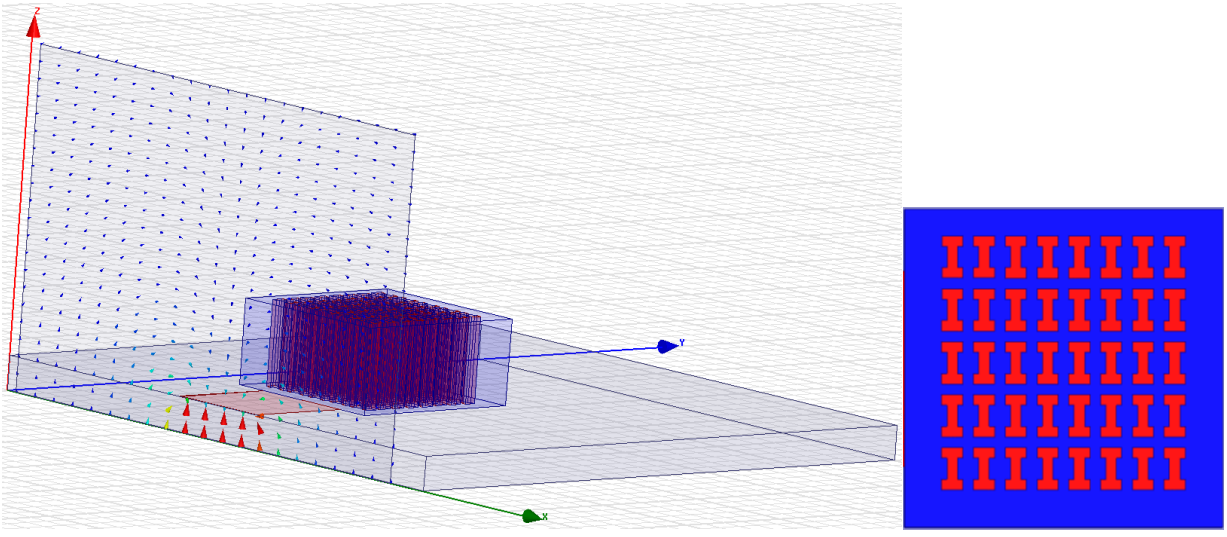

Figure 4.3 (a) Physical structure of the meta-DRA, feed line, substrate and excitation wave-port. **(b)** Top-view of the meta-DRA design.

The structural specification of the metal inclusions in the above figure is (Appendix B.1, design 5):

Element Size: 100 by 200 μm

Gap: 50 μm

Internal Width: 50 μm

As can be seen, the element size is much smaller than the 24 GHz designs. However larger size elements were also tried as an experiment and the results have been compared later in this chapter under *special designs*. In Figure 4.4, the H designs have been compared just as in the previous section in order to see whether the gap/width affects the resonance in any way. Again, all the individual resonance curves were optimized using the feedline underneath the meta-DRA and the curve with the most negative dB(S_{11}) was selected. The nominal design (50μm) resonates at 69 GHz, which is much higher than expected. The designs with gap/widths of 20μm and 30μm resonate at 61.5 and 61.7 GHz respectively. These designs with less change in the metal gap/width have similar resonances. When the width is more than double as in the case of 50 μm, there is a considerable shift in resonance. The meta-DRA with variable gap/width of 20 μm and 50 μm has a resonance at 60.8 GHz.

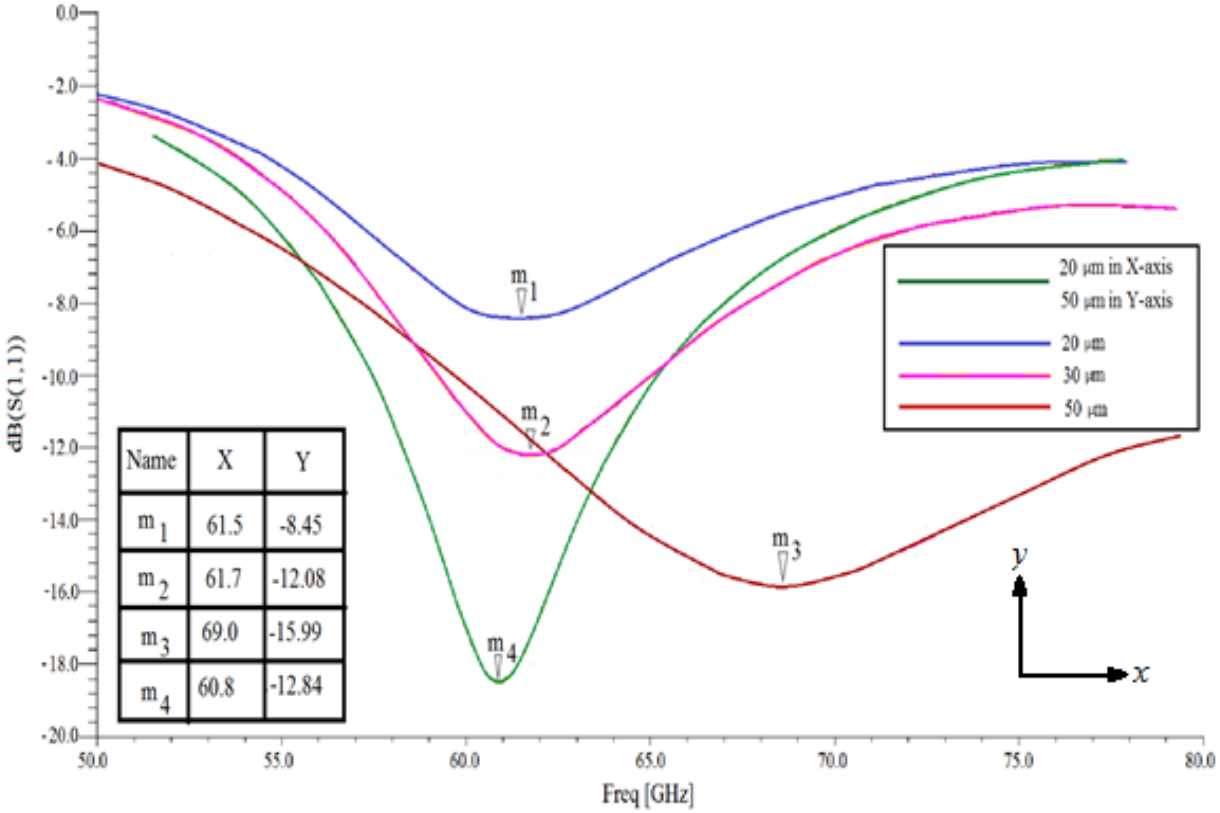

Figure 4.4 100 by 200 µm H designs resonating at 60 GHz.

Metal gap/width (µm)	Meta %	Resonating F (GHz)
20	53.33	61.5
30	44.44	61.7
50	35.56	69
20-50	48.89	60.8

Table 4.2 Meta percentage and resonant frequency for different gap/width of the metal inclusions.

From Table 4.2 it can be seen that when the metal gap/width is varied uniformly in *x* or *y* direction, the design with the highest meta percentage resonates at the lowest frequency. This is

expected as the relative permittivity is higher for an increasingly meta design. When the low permittivity polymer is higher in volume as in the case of the 50 μm design (meta percentage 35.56%), the design resonates at a much higher frequency of 69GHz. Thus the resonance of a meta-DRA having metal inclusions with equal dimensions does not occur at the same frequency and it varies with the metal gap/width.

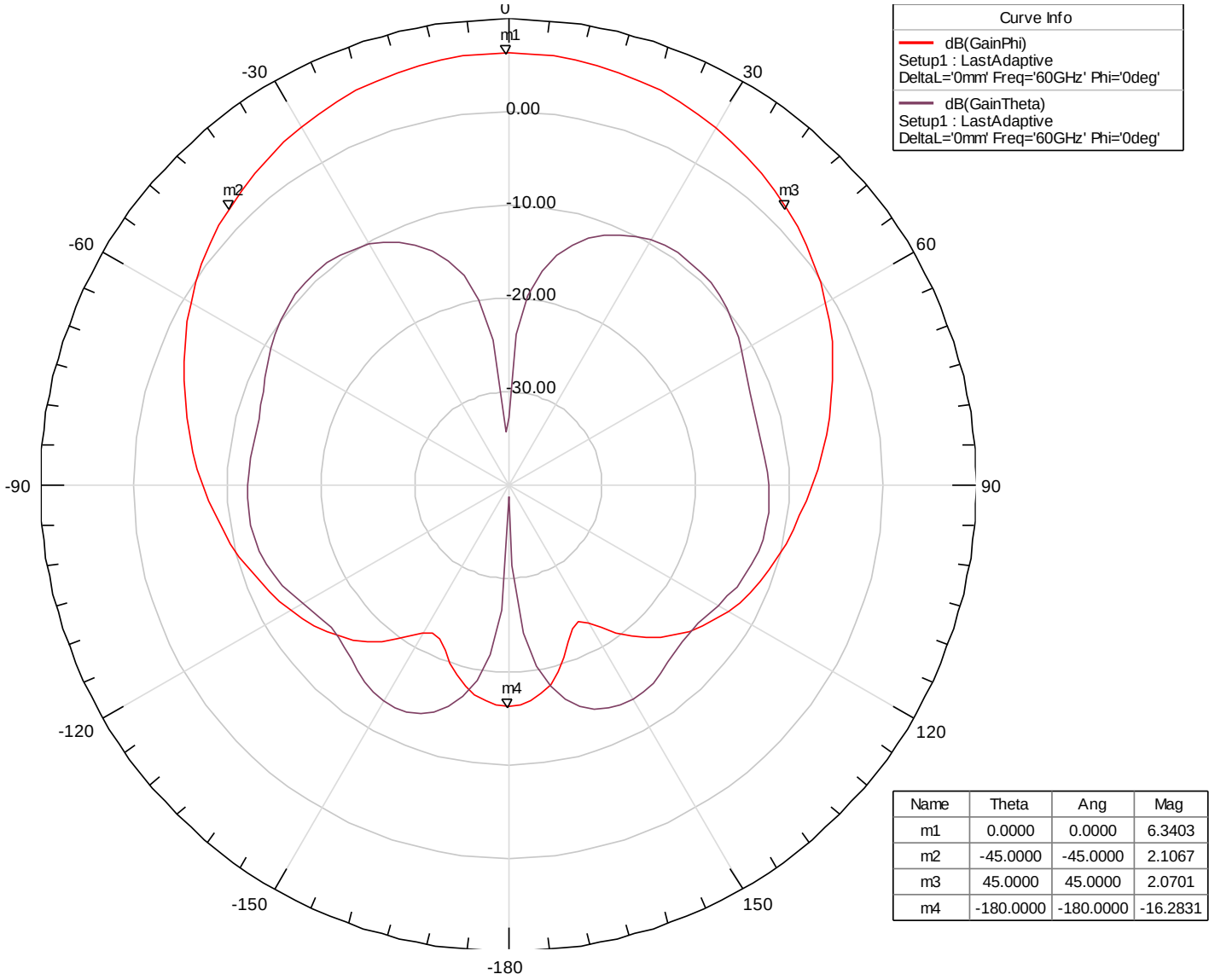

4.5 2D Radiation plot of the meta-DRA in the H-Plane showing the dB(GainPhi) and dB(GainTheta) curves in HFSS.

The radiation plot in the H-plane for the nominal design is provided below in Figure 4.5. Here it can be observed that the antenna has a good realized gain of 6.3 dB (a rectangular DRA with similar ε_r would typically have a gain of 5 dB). Hence these batches of antennas prove to radiate well above expectations. The 3-D representation of the radiation plot is given in Figure 4.6.

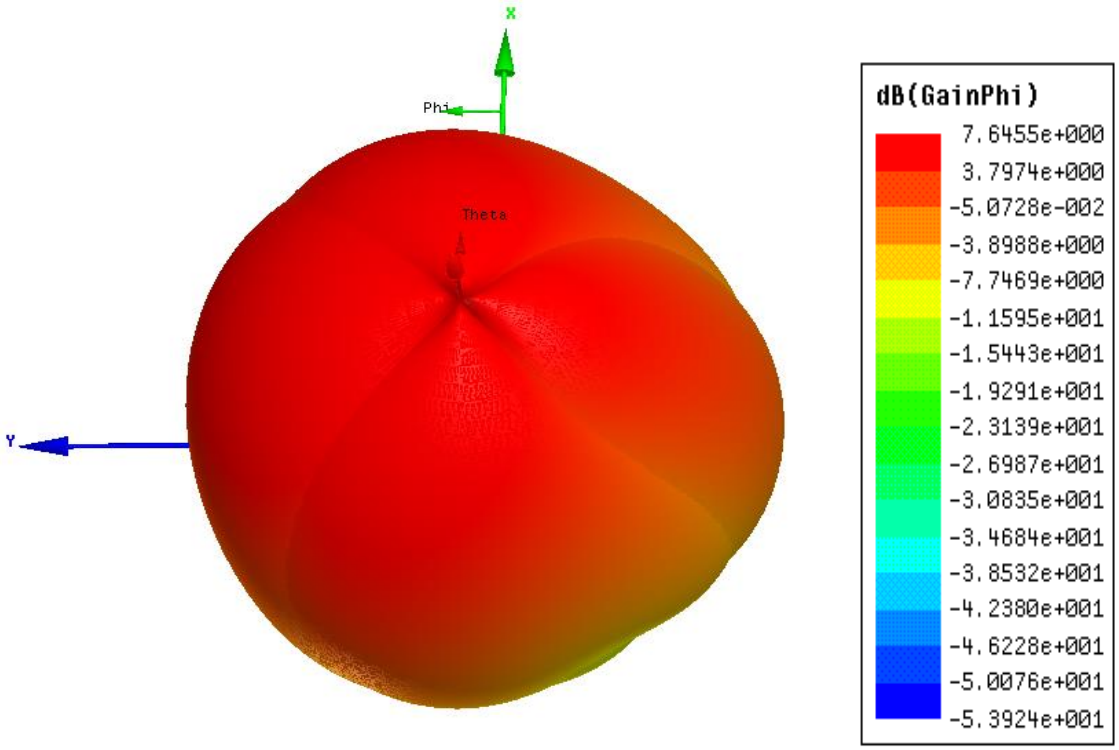

4.6 3-D Radiation plot.

4.3 Window (W) Inclusions

In this section, the metal inclusions in the shape of windows resonating around 24 GHz will be discussed. The shape of the inclusions has already been described in Section 3.4. Figure 4.7 shows the structure of an example meta-DRA with window inclusions and resonating at 20 GHz. Structural attributes of the metal inclusions are as follows (Appendix A.2, design W_2):

Element Size: 200 by 200 μm

Gap: 30 μm

Internal Width: 30 μm

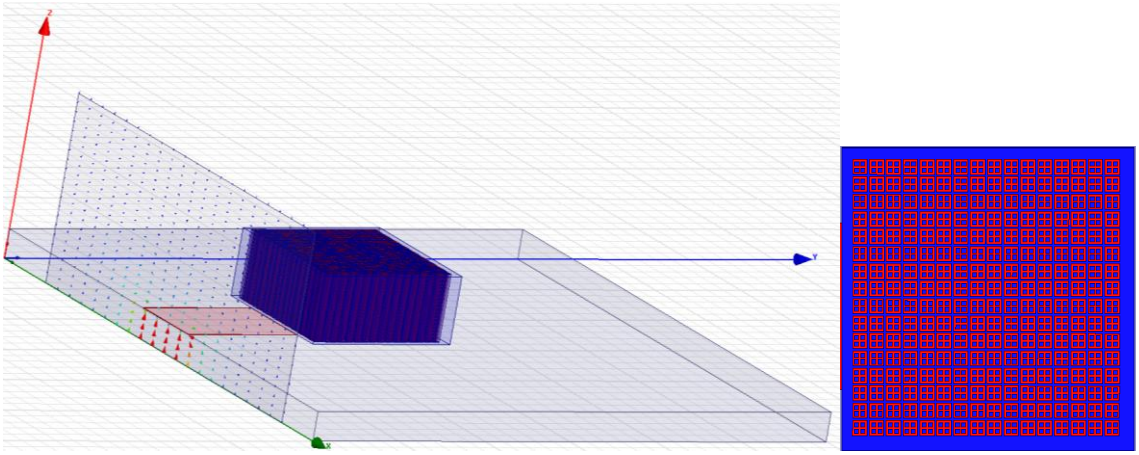

Figure 4.7 (a) Physical structure of the meta-DRA, feed line, substrate and excitation wave-port.

(b) Top-view of the meta-DRA design.

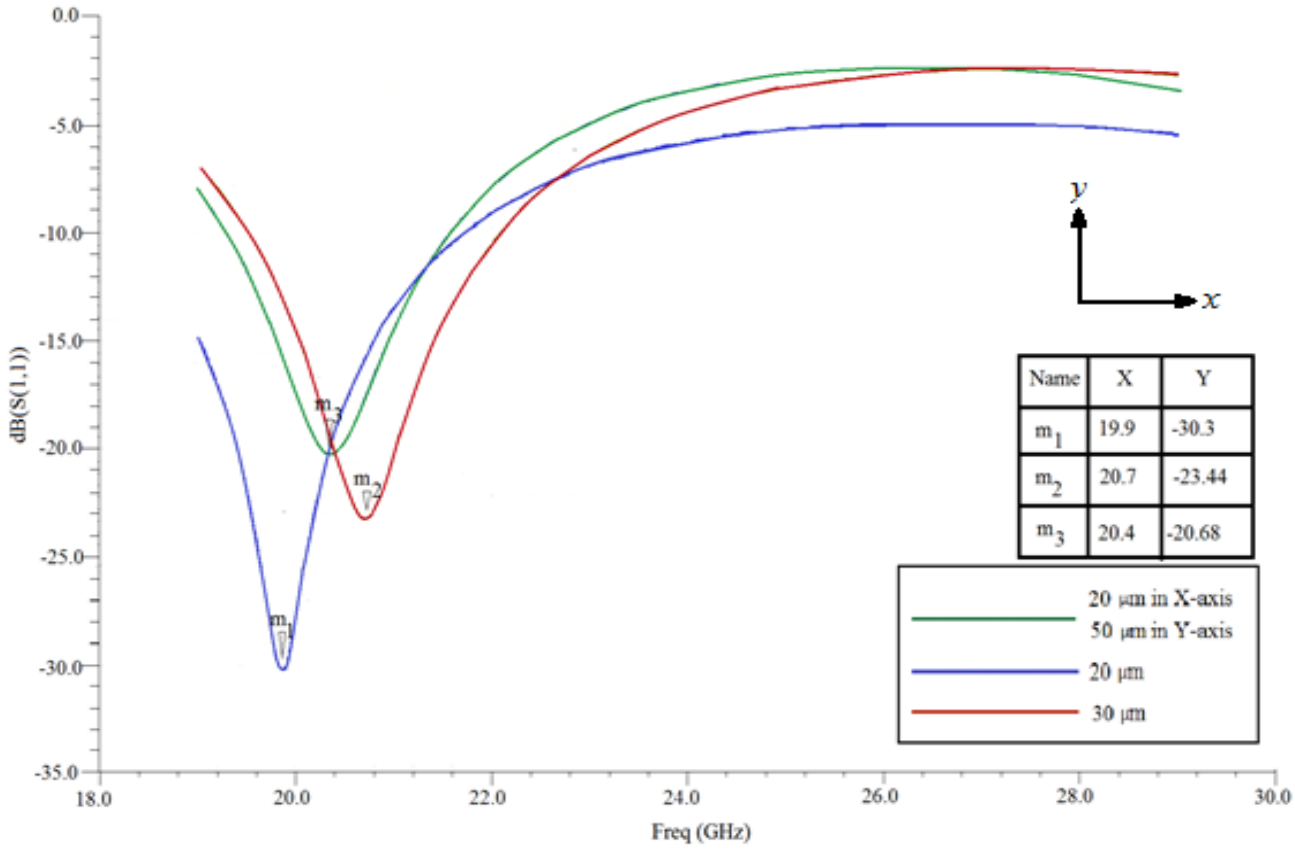

Figure 4.8 200 by 200 µm Window designs resonating @ 24 GHz.

In this case, the nominal design has a gap/width of 30 µm and resonates at 20.7 GHz as shown in Figure 4.8. Upon decreasing the gap to 20 µm, the meta-DRA resonates at 19.9 GHz which is lower than the nominal design. The sample with variable widths (20 µm in X-axis and 50 µm in Y-axis) resonates at 20.4 GHz, fairly close to the nominal design.

Metal gap/width (µm)	Meta %	Resonating F (GHz)
20	72.25	19.9
30	64	20.7
20-50	63.75	20.4

Table 4.3 Meta percentage and resonant frequency for different gap/width of the metal inclusions.

Again, the designs do not resonate at the exact same frequency. This actually shows the change in the relative permittivity of the meta-DRA with the change in the metal gap/width. The higher the ε_r of the antenna, the lower is the resonant frequency (refer to Section 2.1). This can be seen from Table 4.3 where the design with the highest meta percentage (higher ε_r) resonates at the lowest frequency. The magnetic coupling varies with the metal width and gap. This change in the coupling of the field affects the resonance of the LC circuit in the antenna.

The gain of the nominal meta-DRA design can be seen in the radiation plot in Figure 4.9. The frontal lobe denotes that a power signal is transmitted with a gain of 2.29 dB. This is lower than a typical rectangular DRA gain of 5 dB. The design can be further optimized to achieve better gain. The three-dimensional image of the radiation from the antenna has been given in Figure 4.10.

The window meta-DRAs were also designed to resonate at 60 GHz and were part of the final mask. But they have not been included in this chapter. Instead half-window meta-DRAs resonating at 60 GHz have been dealt with in the next section in order to include as many metal inclusion geometries as possible. A detailed description of the structural arrangement of these designs can be found in the Appendix B, Section B.2.

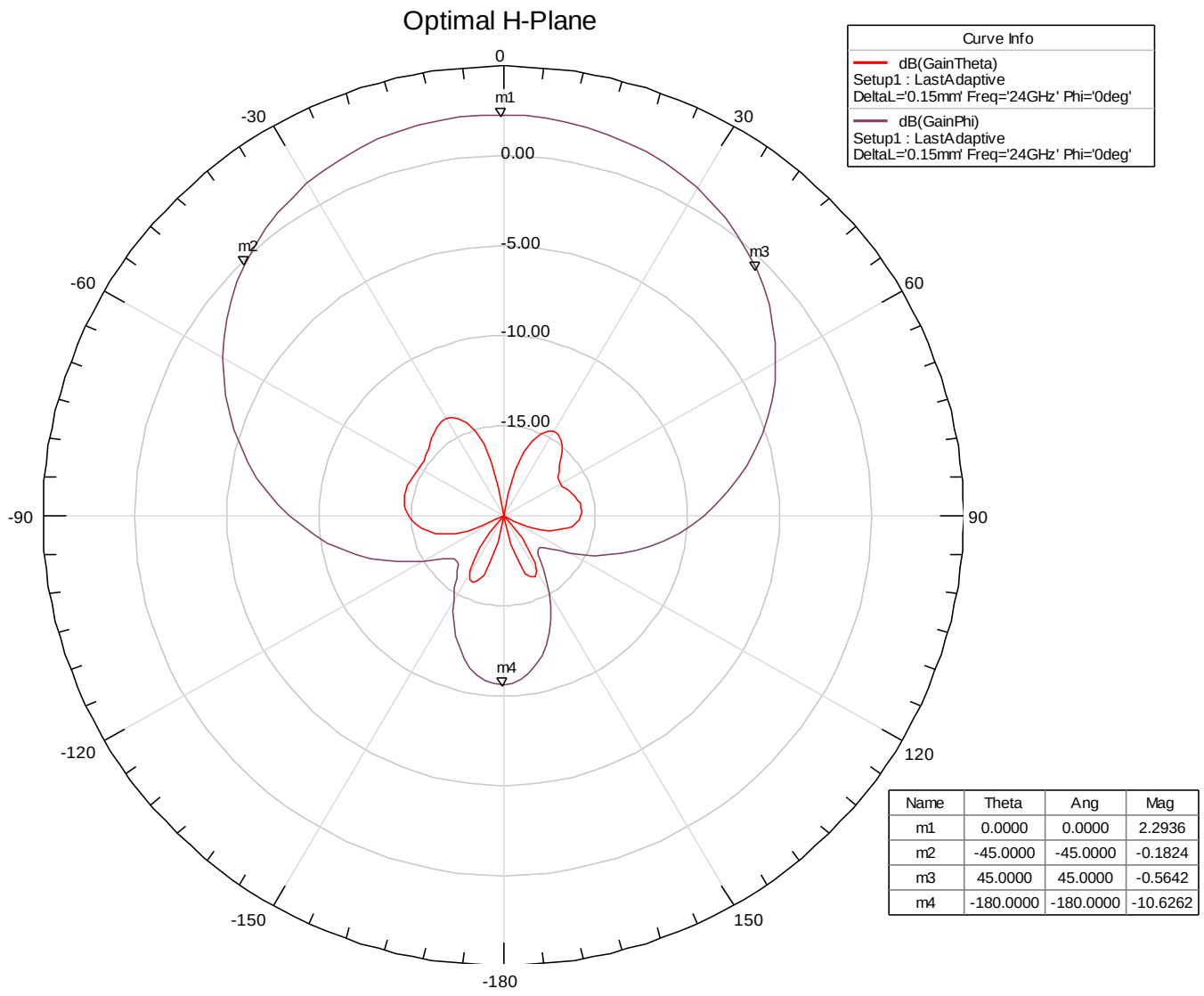

4.9 2D Radiation plot of the meta-DRA in the H-Plane showing the dB(GainPhi) and dB(GainTheta) curves in HFSS.

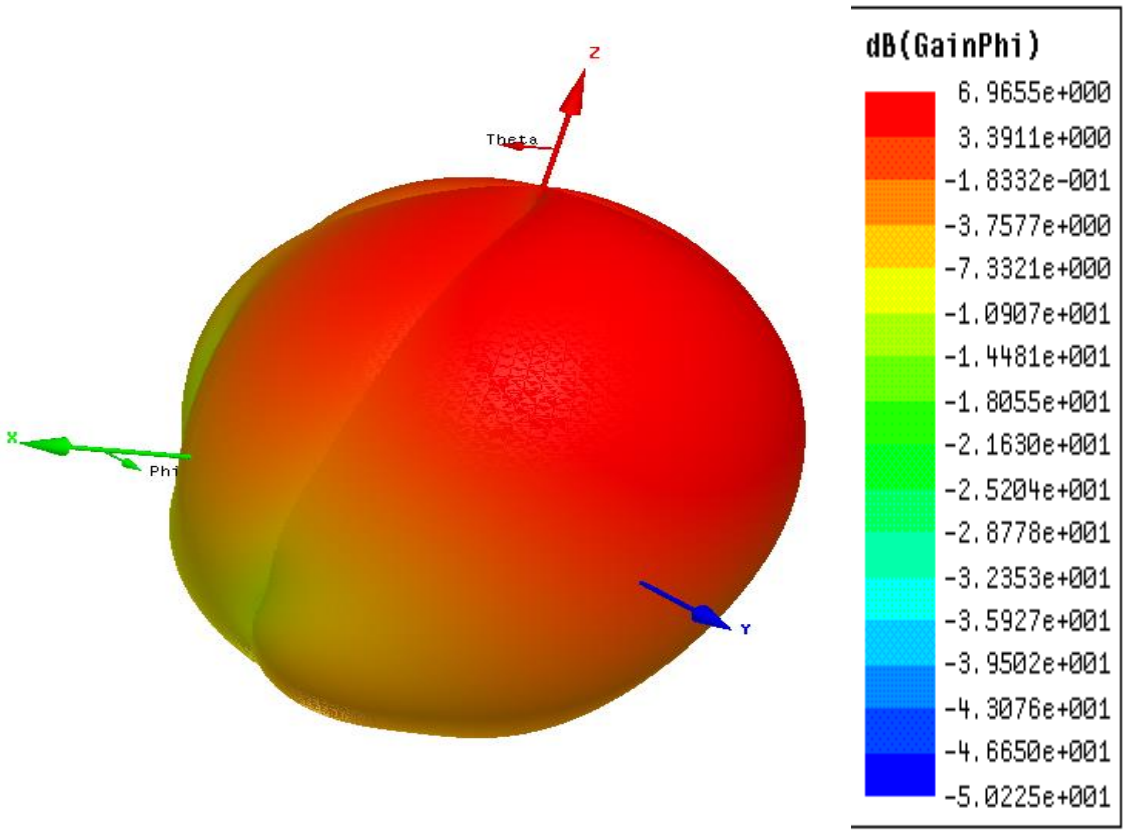

4.10 3-D Radiation plot

4.4 Half-Window Inclusions

As stated in the previous section, an example design of a meta-DRA with half-window metal inclusions resonating at 60 GHz has been presented here. The geometrical shape of a half-window inclusion has been shown in the previous chapter. Figure 4.11 (a) and (b) show the structure of the resonator.

The details of the size of the element and metal gap/width are given as follows:

Element Size: 100 by 100 μm

Gap: 20 μm

Internal Width: 20 μm

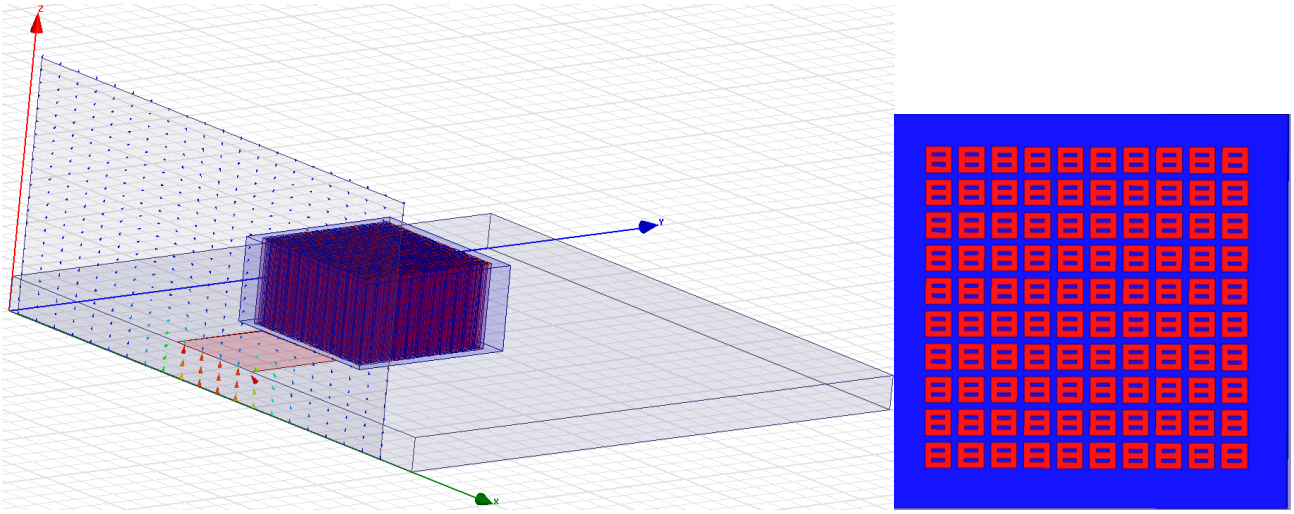

Figure 4.11 (a) Physical structure of the meta-DRA, feed line, substrate and excitation wave-port. (on the left) **(b)** Top-view of the meta-DRA design. (on the right)

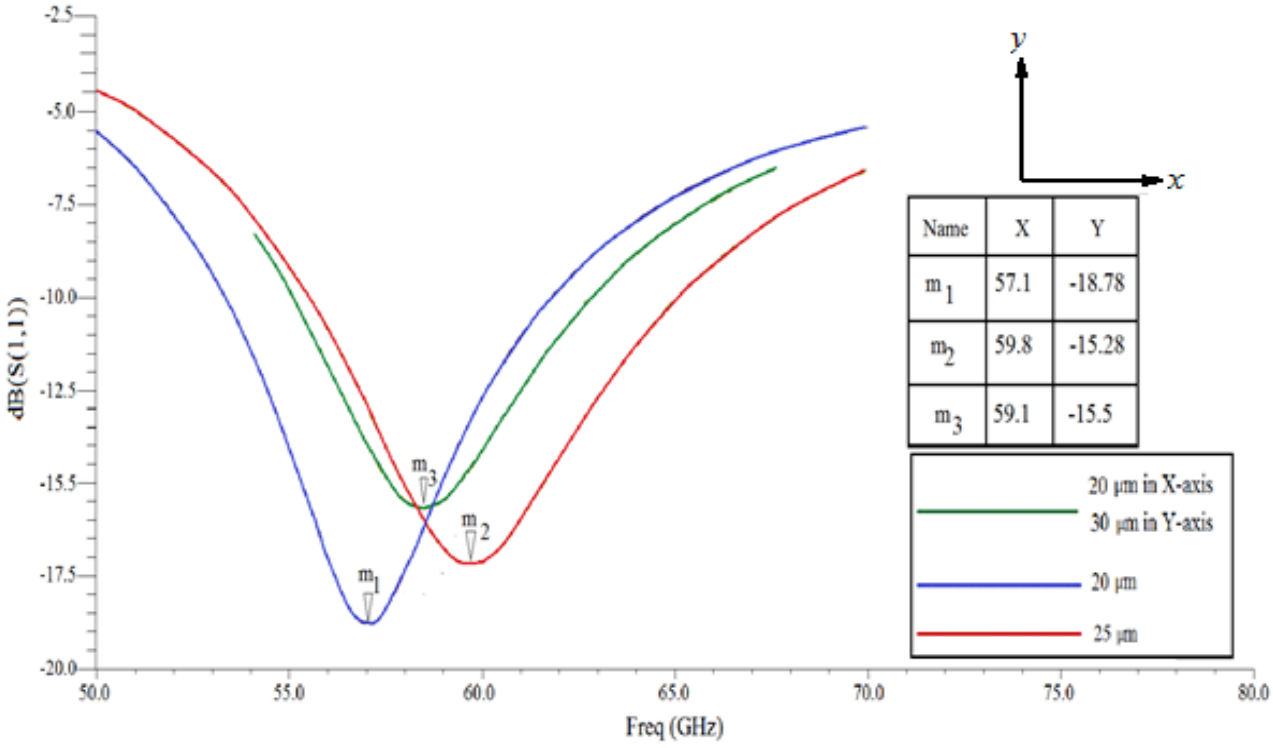

Figure 4.12 100 by100 µm Half-Window designs resonating @ 60 GHz.

Metal gap/width (μm)	Meta %	Resonating F (GHz)
20	53.78	57.1
25	44.44	59.8
20-30	48.88	59.1

Table 4.4 Meta percentage and resonant frequency for different gap/width of the metal inclusions.

Figure 4.12 depicts the dB(S_{11}) vs Frequency plot for the half-window designs with varying widths/gaps. The nominal design has a gap/width of 25 μm and resonates at 59.8 GHz. This design resonates closest to 60 GHz. Decreasing the metal gap/width to 20 μm reduces the resonating frequency to 57.1 GHz, which also means a greater relative permittivity. The design with variable gap/width, which is 20 μm in X-axis and 30 μm in Y-axis in this case, has a resonance at 59.1 GHz. This is closer to the nominal meta-DRA.

Also, from Table 4.4, the meta percentage of the nominal design is the lowest (44.44%). Hence it has a lower relative permittivity and resonates higher than the other designs. By now it is certain that by altering the metal gap/width even by a few microns one can affect the overall permittivity and hence the resonance of the meta-DRAs.

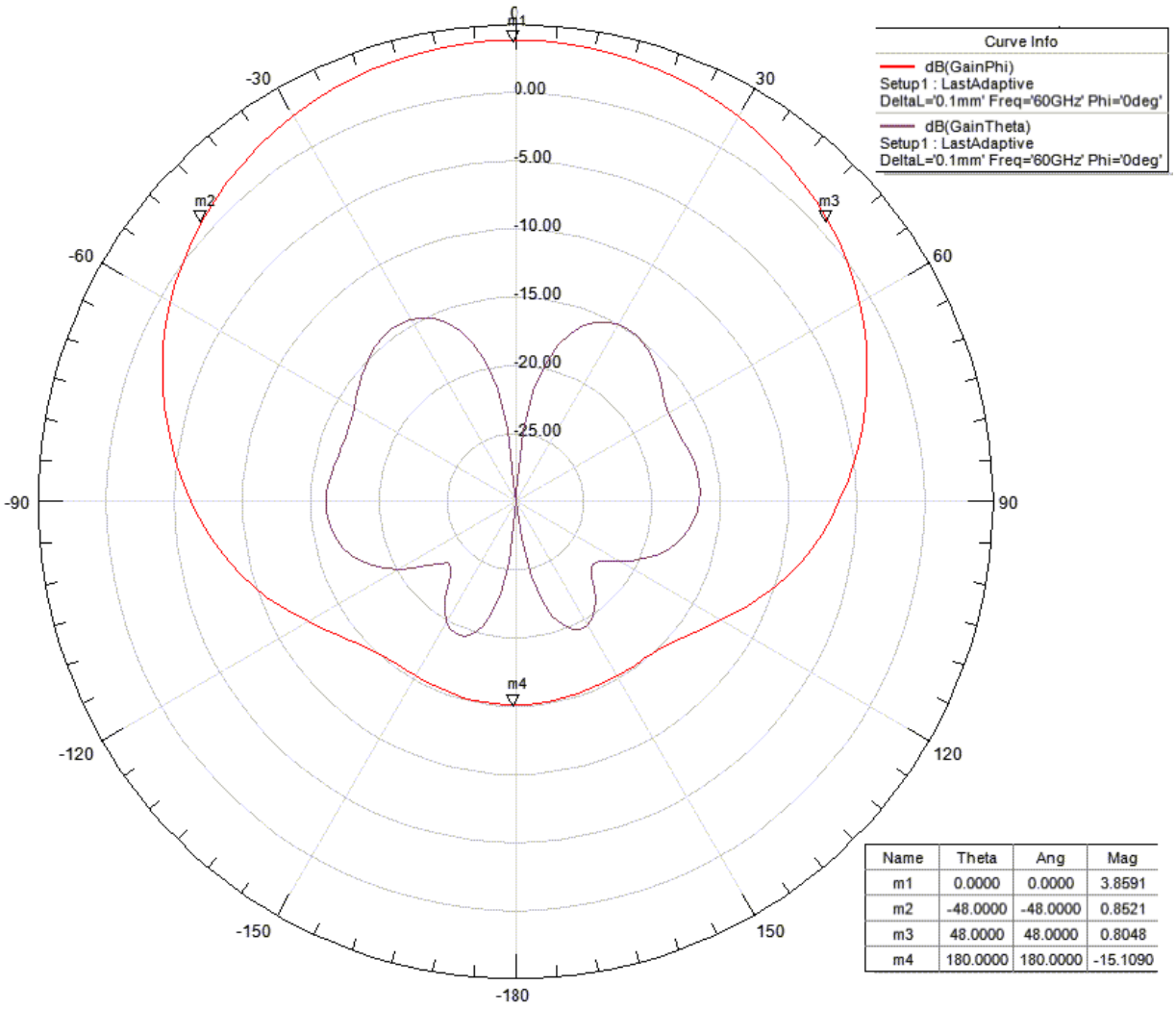

Figure 4.13 2D Radiation plot of the meta-DRA in the H-Plane showing the dB(GainPhi) and dB(GainTheta) curves in HFSS.

Figure 4.13 shows the radiation pattern in the H-plane for the design under consideration. A realized gain of 3.86 dB has been achieved which is slightly lesser than the gain of 5 dB for a similar permittivity material rectangular DRA. The 3-D pattern is shown in Figure 4.14.

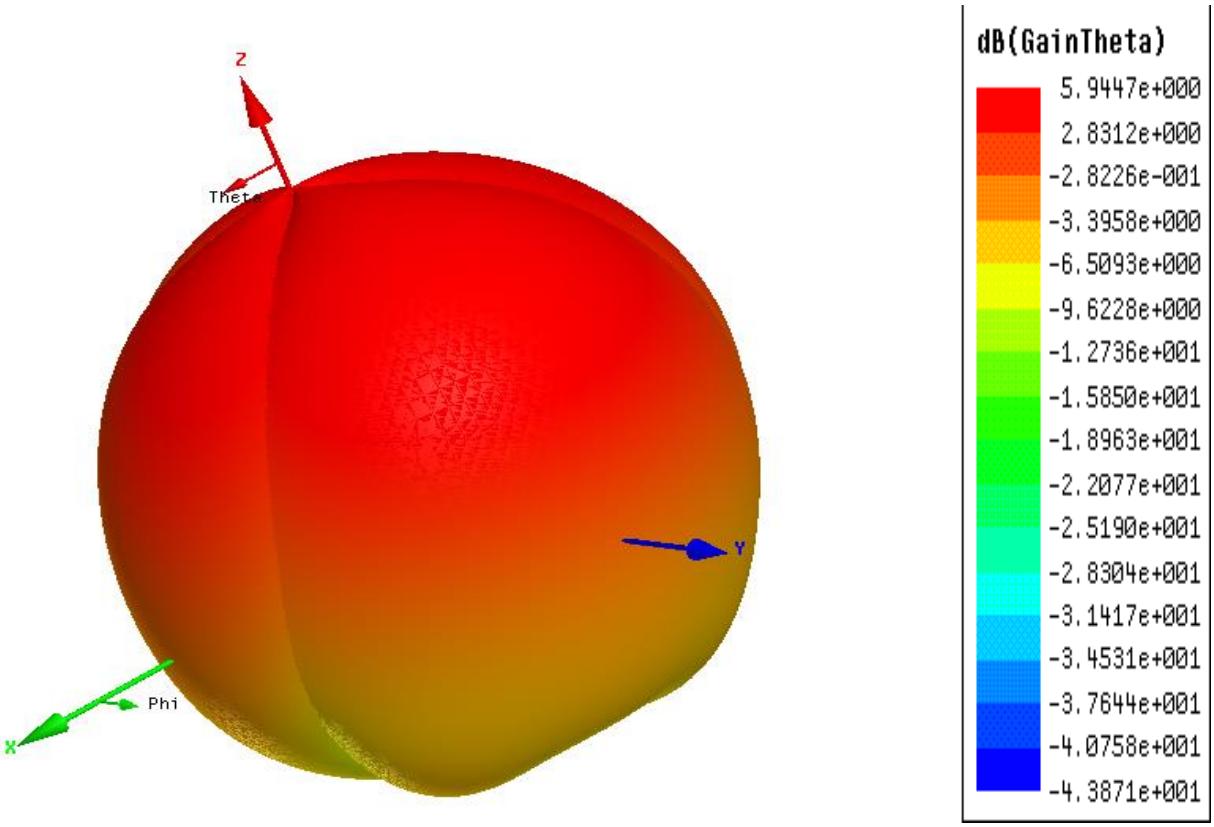

Figure 4.14 3-D Radiation plot.

4.5 Special Designs

As discussed in Chapter 3, there were sets of designs which did not belong to a particular pattern but were considered as an experimental study. The most common alterations carried out were halving the inclusions in a particular sample (H and Window) and extending the base of the polymer of the DRA in the direction of the excitation (positive Y-axis). The effect of these changes on the resonance and dB(S_{11}) of the DRA have been recorded.

In this section, a meta-DRA with a larger polymer base and a meta-DRA with larger metal inclusion size are compared to the performance of a regular meta-DRA resonating around 60 GHz. As discussed earlier, miniaturization of the design is important in order to make it resonate at very high frequencies. Hence the size of the elements has been reduced to the range of 100 μm and 200 μm in order to maintain aspect ratio. As an experiment, larger inclusions were used to form these

meta-DRAs resonating at 60 GHz. Their size was considerably increased from the standard range of 100-200 μm to 400 μm. As a result, there were less number of inclusions but the surface area covered by the individual elements was increased considerably. Figure 4.15 depicts the top-views of the meta-DRAs having an element size of 100 by 200 μm, 400 by 400 μm and the extended polymer design with an element size of 400 by 400 μm. The rectangular polymer surface of the design in Figure 4.15 (c) is visibly larger and different from the other samples. All the designs have the same gap/width of 50 μm.

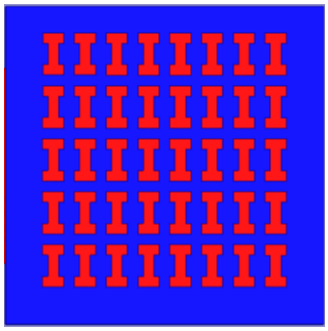

(a)

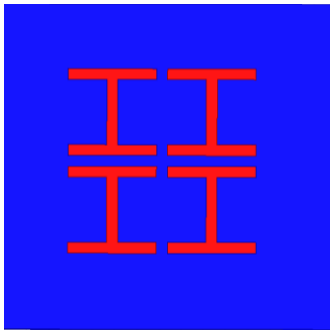

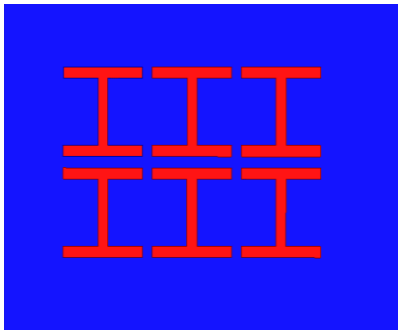

(b) **(c)**

Figure 4.15 (a) H inclusions 100 by 200 μm **(b)** H inclusions 400 by 400 μm **(c)** H inclusions 400 by 400 μm with an extended polymer base.

The polymer-base of a DRA resonating at a very high frequency of 60 GHz has dimensions of 1.5 by 1.5 by 0.7 μm (XYZ coordinate) as explained in the previous chapter. In this case, the size of the polymer is increased to 1.5 by 2 by 0.7 μm. It is known that increasing or decreasing the height of the DRA affects the resonating frequency. But the heights of the DRAs are uniform and hence none of the changes in the resonance in the following results could be attributed to the height of the design.

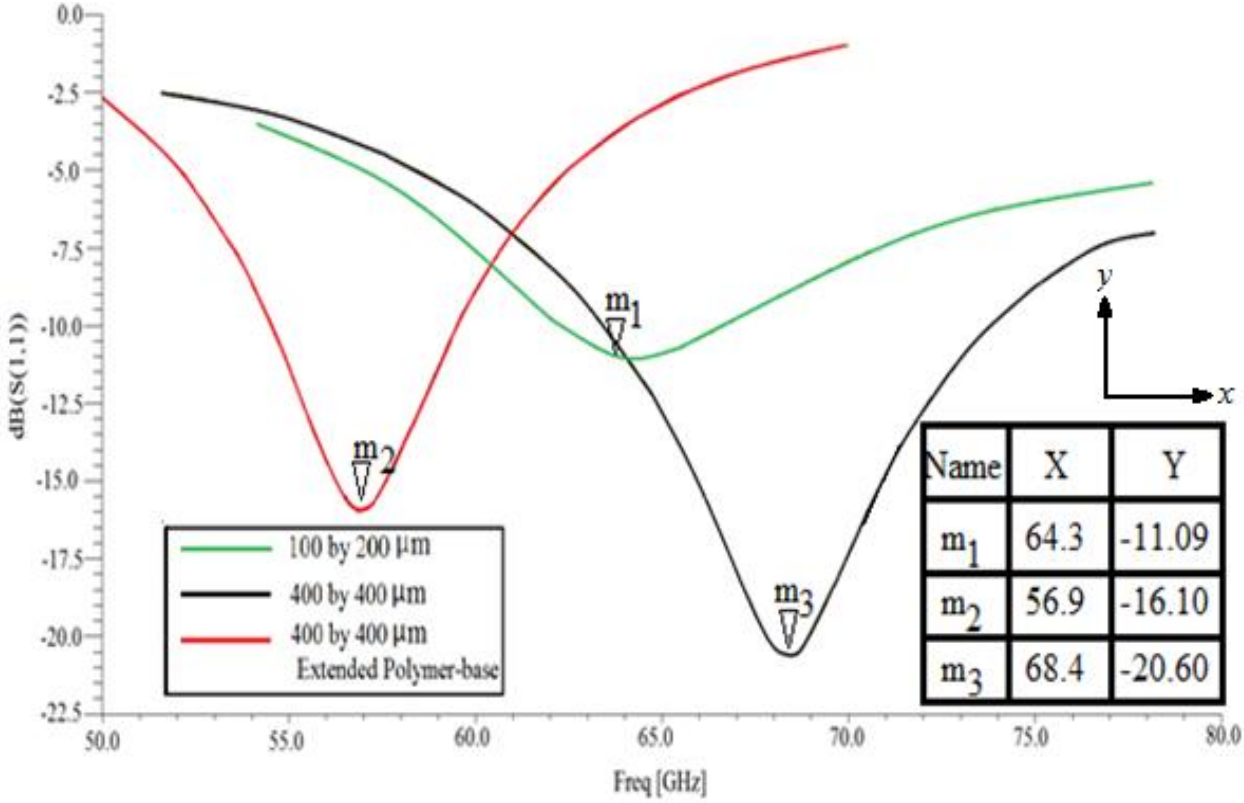

Figure 4.16 Meta-DRAs having the same width/gap of 50μm.

The above figure shows the dB(S_{11}) for the meta-DRAs versus frequency. It can be seen that none of the designs resonate exactly at 60 GHz. While the design with 'regular' polymer dimension has a resonance at 64.3 GHz (m_1), the one with extended polymer resonates at a much lower frequency of 56.9 GHz (m_2). The resonance increases drastically to 68.4 GHz (m_3) for the

same design (400 by 400 μm) but with a standard sized polymer-base. Thus the extended polymer reduces the resonant frequency compared to the nominal designs. But by increasing the element size by four, a much higher resonant frequency is obtained compared to the other meta designs resonating at 60 GHz.

Design	**Meta %**	**Resonating F (GHz)**
a	42.66	64.3
b	32.11	68.4
c	36.83	56.9

Table 4.5 Meta percentage and resonant frequency for different gap/width of the metal inclusions.

Table 4.5 shows the meta percentage for each of the designs under consideration. Although the design *c* has an extended polymer-base, it has a higher meta percentage of 36.83% compared to the meta percentage of the regular polymer design (*b*). Hence it resonates at a lower frequency. This goes to show that irrespective of the polymer size, the meta percentage alone determines the resonance of the meta-DRAs.

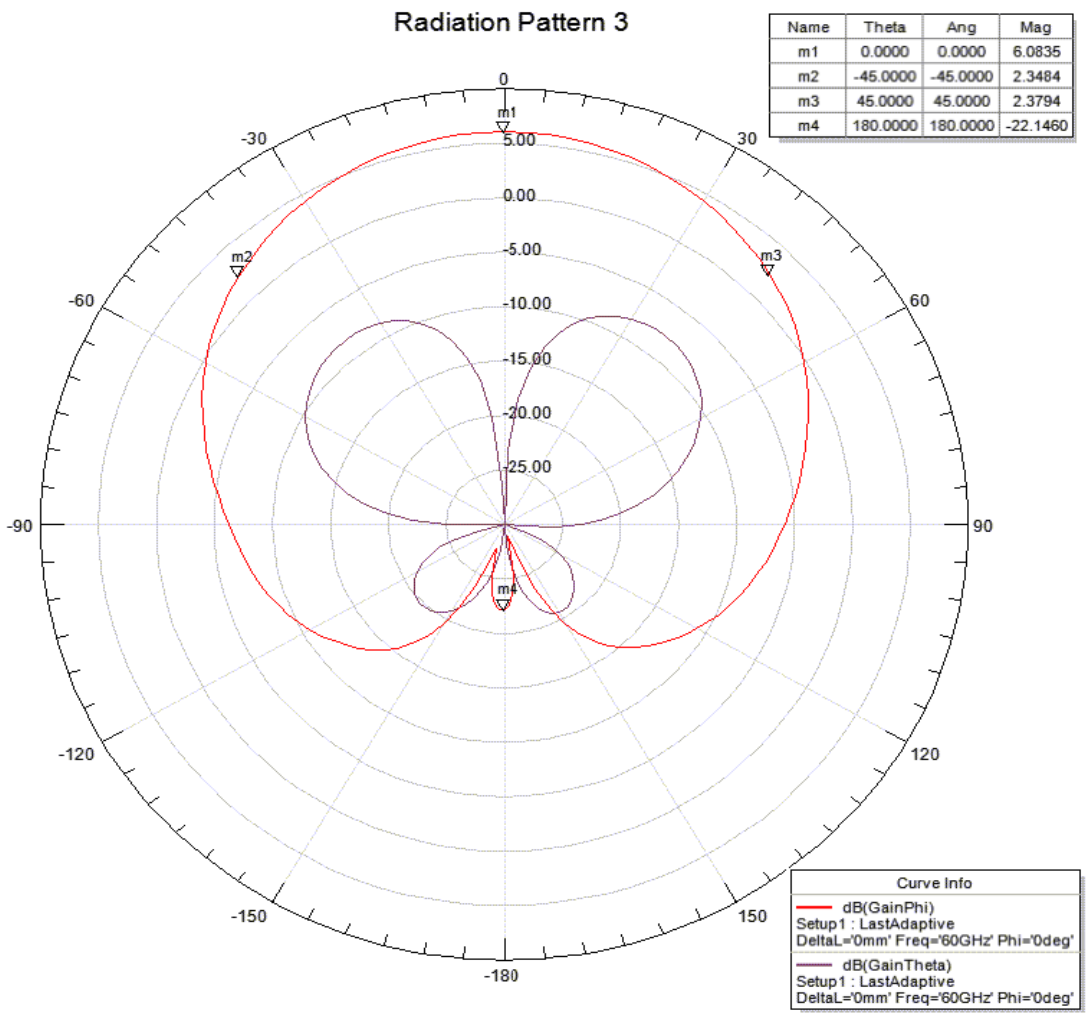

Figure 4.17 Radiation plot in the H-plane of a meta-DRA with 400 by 400 μm H inclusions.

For the radiation comparison, inclusions with same dimensions (400 by 400 μm in this case) but different sized polymer-base have been considered. The radiation plots for the designs are given in Figures 4.17 and 4.18. It can be observed that the dB gain for the regular sized polymer-base DRA is 6.08 dB. For the extended DRA, the gain reduces to 3.65 dB. This is a considerable change considering the fact that both the designs have exact same specifications apart from the dimension of the polymer. This study indicates that, there needs to be a minimum amount of metal area in a meta-

DRA for it to radiate and transmit at a certain frequency. Designs with lower metal density do not perform as desired.

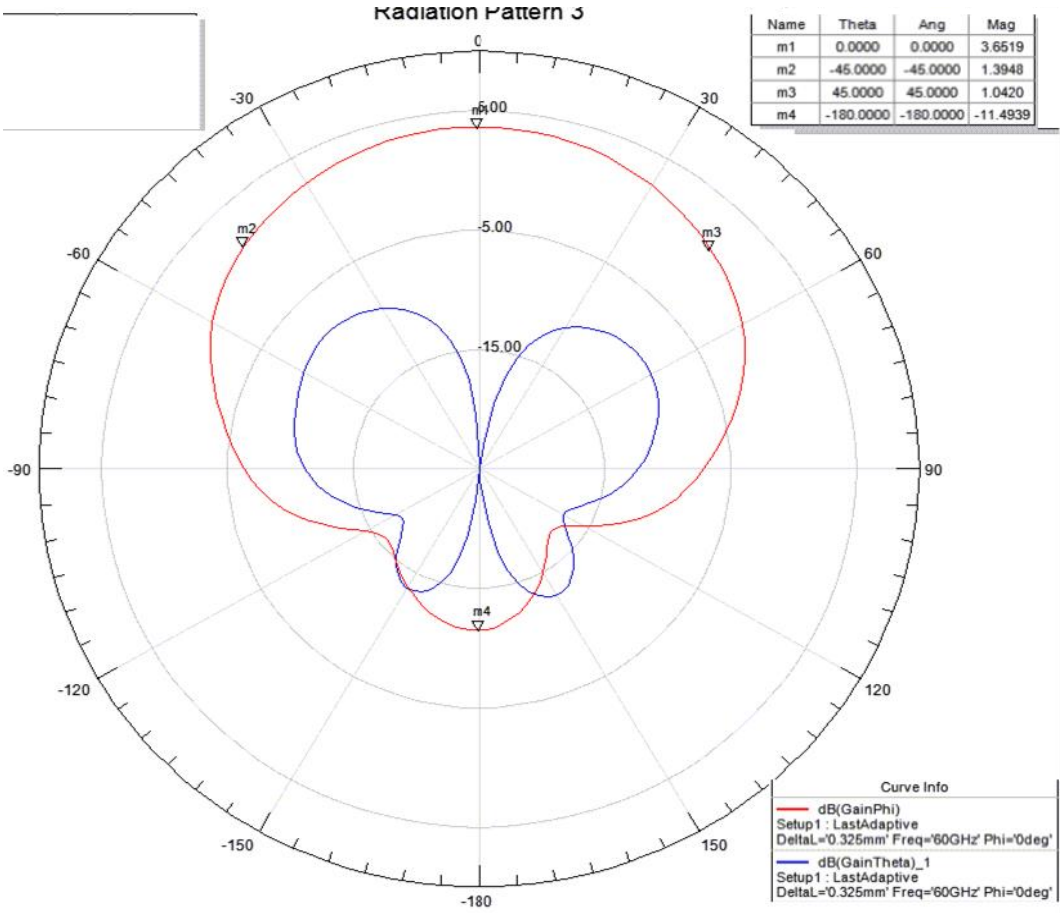

Figure 4.18 Radiation plot in the H-plane of a meta-DRA with 400 by 400μm H inclusions with an extended polymer-base.

4.6 ΔL vs dB(S_{11})

During simulation of the designs, the microstrip feed line was extended beneath the meta-DRA surface as stated in Chapter 3. The variation in the length of the feed line was defined as a variable (ΔL) in HFSS. The length extended from the wall of the meta-DRA to the wall of the first row of metal inclusions. It has to be ensured that the feed line does not touch or extend underneath the metal inclusions. ΔL was added as a parametric study for all the meta-DRAs in HFSS. This parameter was used to optimize the dB(S_{11}) of the meta-DRA. The length of the feedline at which the dB(S_{11}) value of the meta-DRA was most negative was recorded and plotted against their corresponding dB(S_{11}) values. This was an attempt to find out the most suitable length of the feedline beneath the meta-DRA that gives the best transmission of power or signal. Figure 4.19 shows the plot obtained.

From the plot, it can be seen that most of the designs have a good negative dB reflection coefficient around 0.1 mm. However, the best results were obtained at 0.12 mm. Hence it can be deduced that the feed line should ideally be between 0.9-0.15 mm underneath the meta-DRA for the design specifications in this thesis.

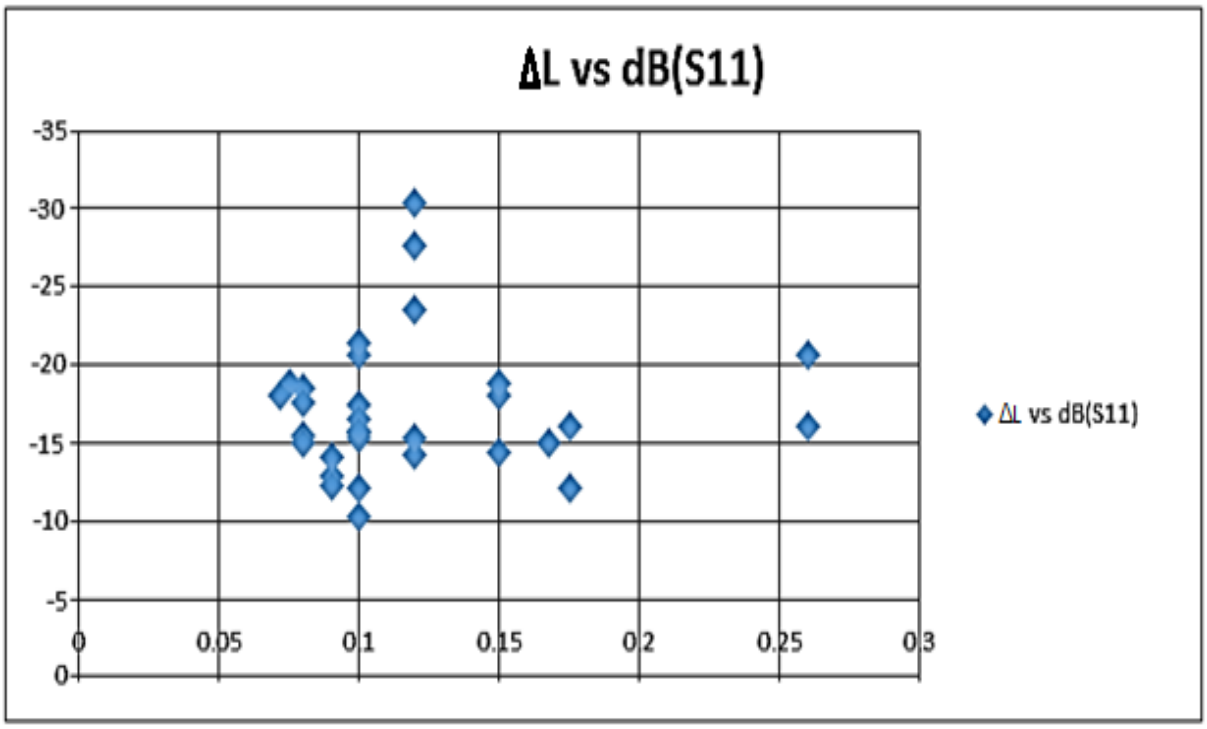

Figure 4.19 ΔL vs dB(S_{11}) for meta-DRAs**.**

4.7 Summary of the Meta Designs

In this section, an account of the meta-DRAs has been presented in a tabular format. All the designs have been summarized as shown in Table 4.6. After observing the data, it can be seen that most of the antennas operate close to the desired resonating frequencies of either 24 GHz or 60 GHz. The reflection coefficient also has a considerable high negative value. This suggests most of the meta-DRAs are well matched. The ideal ΔL values show the importance of the feedline below the DRA.

S.N.	SHAPE	ELEMENT SIZE (µm)	METAL & GAP WIDTH (µm)	SIZE OF DRA (mm)	OPERATING F (GHz)	dB S11	ΔL (mm)
1	H	200 by 200	20	4*4	23.2	-10.3	0.1
2	H	200 by 200	50	4*4	21.7	-17.28	0.15
3	H	200 by 200	20 in X & 50 in Y	4*4	23.6	-14.33	0.15
4	H	200 by 500	20	4*4	23.6	-10.13	0.12
5	H	200 by 500	50	4*4	24.5	-18.8	0.15
6	H	200 by 500	20 in X & 50 in Y	4*4	22.5	-10.08	0.15
7	W	200 by 200	20	4*4	19.9	-30.3	0.12
8	W	200 by 200	30	4*4	20.7	-23.44	0.12
9	W	200 by 200	20 in X & 50 in Y	4*4	20.4	-20.68	0.1
10	W	200 by 500	20	4*4	19.8	-27.7	0.12
11	W	200 by 500	50	4*4	20.2	-21.38	0.1
12	W	200 by 500	20 in X & 50 in Y	4*4	20.3	-15.6	0.1
13	H	100 by 100	20	1.5*1.5	59.9	-14.28	0.1
14	H	100 by 100	30	1.5*1.5	59.3	-17.38	0.1
15	H	100 by 100	20 in X & 50 in Y	1.5*1.5	66.9	-16.5	0.075
16	H	100 by 200	20	1.5*1.5	61.5	-8.45	0.1
17	H	100 by 200	30	1.5*1.5	61.7	-12.08	0.1
18	H	100 by 200	20 in X & 50 in Y	1.5*1.5	60.8	-12.84	0.09
19	HW	100 by 100	20	1.5*1.5	57.1	-18.78	0.075
20	HW	100 by 100	25	1.5*1.5	59.8	-15.28	0.1
21	HW	100 by 100	20 in X & 30 in Y	1.5*1.5	59.1	-15.5	0.08
22	W	100 by 100	20	1.5*1.5	56.7	-18.04	0.072
23	W	100 by 100	25	1.5*1.5	59.6	-15.77	0.1
24	W	100 by 100	20 in X & 30 in Y	1.5*1.5	59.2	-15.04	0.08
25	W	100 by 200	20	1.5*1.5	59.3	-10.5	0.09
26	W	100 by 200	25	1.5*1.5	59.5	-12.17	0.09
27	W	100 by 200	20 in X & 50 in Y	1.5*1.5	60.1	-14.01	0.09

Table 4.6 Summary of the meta-DRA designs.

Chapter 5

Summary and Conclusion

5.1 Summary

The prime objective of this thesis was to try and design meta-DRAs that could radiate power similar to that of DRAs made of high permittivity materials. The objectives set out to achieve in Chapter 1 are listed as below:

1. Select the shape/geometry of the metal inclusion to form the meta-DRAs and develop a set of parameters to vary for the parametric performance study.
2. Design and simulate the meta-DRAs in a three dimensional (3D) full-wave electromagnetic simulator. Define various parameters needed for design and obtain the dB reflection coefficient of the antenna.
3. Evaluate resonant frequency, radiation patterns, and absolute gain obtained from the antennas to assess the effects of inclusion geometries.
4. Compare the results obtained and choose best samples for developing a layout.
5. Have structural demonstrator devices fabricated using D-XRL technology to demonstrate the fabrication feasability.

The theory of DRAs was dealt with in Chapter 2. Modes of RDRAs were studied thoroughly with the help of equations and electrical and magnetic field patterns. The microstrip feedline used to excite the meta-DRAs in this thesis were presented. In the same chapter, a detailed study was presented on the discovery and applications of metamaterials. An example meta-DRA simulation was also compared with a high permittivity DRA. The comparison exhibited the fact that,

metal inclusions in a polymer can increase the relative permittivity of the polymer-base antenna from 2.5 and it makes it radiate like a high permittivity material antenna.

A complete account of the steps involved in the design of a meta-DRA using HFSS was explained in Chapter 3. All the boundary conditions were defined. The structure of the DRA, substrate and feedline were discussed thoroughly. The geometries of the metal inclusions were also justified in this chapter. A brief explanation was given on S-parameters and multi-port network. Furthermore, the concept of variable feedline used to optimize the dB(S_{11}) of the meta-DRA was introduced. The radiation of an antenna was explained subsequently. After establishing the parameters for the design, an example meta-DRA design resonating at ~20GHz was presented including the results obtained. The dB(S_{11}) and resonance were studied. The radiation plot in H-plane was discussed with an aim of 5dB power transmission. Later in the same chapter, the steps leading to the formation and editing of the layout using ADS was introduced. Some example meta-DRA layouts were also provided. Then a brief introduction to DXRL, used to fabricate the meta-DRAs at KIT, Germany was presented. Some designs, which were already fabricated, have been discussed in the next section. Judging from the SEM images, there was an irregularity in the metal inclusion in some of the designs. Wondering whether this could affect the performance of the meta-DRA, two samples having varying height (different pattern of variation) were designed and simulated. Both the designs were meant to resonate around 24 GHz. Only one of the height variations seemed to cause an askew pattern, but after 40 GHz.

Having established the motive, theory and implementation of the research, comparisons between various meta-DRA designs were made in Chapter 4. The major factor for comparison was to find whether the change in the metal gap/width (for the same size of the element) in the meta-DRA affects the resonance in any way. H, window and half-window inclusions were compared, some

resonating at 24 GHz and others at 60 GHz. The most common gaps/widths were 20 µm, 25 µm, 30 µm and 50 µm, with 50 µm designs considered to be nominal. Some meta-DRAs had dual gaps/widths across X and Y-axis. Almost all the designs varied their resonance with the metal gap/width. This could be due to the change in overall permittivity of the meta-DRA, which shifts the resonance. The ΔL variable used to optimize the reflection coefficient was plotted against the optimized dB(S_{11}) values in order to find out the best length for the microstrip feedline underneath the polymer-base of the meta-DRA. The length was found to be between 0.9 mm and 0.15 mm. The chapter was concluded with a tabular summary of all the meta-DRAs designed, simulated and included in the layout that was sent to KIT, Germany, for fabrication.

5.2 Conclusion

The experiments carried out in this thesis go a long way in assuring the use of antennas made of metamaterials. The results obtained from these meta-DRAs were promising. They have resonances at desired frequencies of 24 GHz and 60 GHz, which verifies the expected increase in the relative permittivity of the polymer-base DRA. Also, the power gain from these meta-DRAs was around 5 dB. This is comparable to a high permittivity RDRA. Hence it was verified that with low permittivity polymer-base, meta-DRAs can provide similar performance as that of a high permittivity DRA and also they are easier to fabricate. The shift in the resonance with metal gap/width goes to show the scope of this research. The meta percentage calculated for all the design focuses on the effect of metal inclusions in the polymer-base. Any sized polymer can be made to resonate by having a certain amount of meta in them. However, the non-symmetric designs (variable metal gap/width) have a complicated behavior that cannot be assessed by the meta percentage calculation. Another interesting observation that was obtained during the project was the effect of the variation of the metal inclusion height. This certainly affects the resonance of the meta-DRA structures but not so

much the motive of resonating the antennas at 24 GHz and 60 GHz. Several errors could affect the performance of the meta-DRAs such as fabrication tolerances, material property differences, numerical errors (discretization, meshing) and measurement errors in a network analyzer. These errors are important and might effect the simulation results. However this is not critical to the present project related to the effect of varying geometries in meta-DRA performance.

5.3 Scope for Research in Future

Recommended future research scope for this project are:

1. Preliminary fabrication of meta-DRAs have been done at KIT, Germany, to demonstrate feasibility. These designs should be physically teasted using a network analyzer after completion of the final meta-DRAs.

2. Only a few types of geometries could be tried out for the metal inclusions in this project. There could be other patterns or shapes that give better results.

3. After obtaining SEM images of a few fabricated meta-DRAs (H inclusions) from KIT, it might be interesting to vary the height of meta inclusions and observe the effect on the resonace of the meta-DRAs.

List of References

1. M. T. Aligodarz, D. M. Klymyshyn, A. Rashidian, M.Boerner, L. Shafai and J.Mohr (2015). Photoresist-based Artificial Dielectrics with Tall Embedded Metal Grids and Resontor Antenna Application, *IEEE Trans. Antennas & Propagation* (in revision).

2. M. T. Aligodarz, A. Rashidian, D. M. Klymyshyn and L. Shafai (2014). A Fast and Efficient Permittivity Estimation Method for Artificially Engineered Microwave Materials, *Proc. 17th International Symposium of Antenna Technology and applied ElectroMagnetics (ANTEM 2014)*, Victoria, Canada.
3. V. G. Veselago (1968). The electrodynamics of substances with simultaneously negative values of magnetic and electrical permittivity. *Soviet Phys.* , 509-514.
4. A. Sajuyigbe (2010). *Electromagnetic Metamaterials for Antenna.* Durham, North Carolina.: Department of Electrical and Computer Engineering, Duke University.
5. D. M. Pozar (1989). *Microwave Engineering* (Third ed.). Amherst: University of Massachsetts.
6. A. Rashidian, D. M. Klymyshyn, M. Tayfeh Aligodarz, M. Boerner and J. Mohr (2010). Development of Polymer based DRAs for Millimeter-Wave Applications. *Progress In Electromagntics Research C, 13*, 203-216.
7. A. Rashidian (2011). Photoresist-based Polymer Resonator Antennas (PRAs) with Lithographic Fabrication and Dielectric Resonator Antennas (DRAs) with Improved Performance, MSc. Thesis, University of Saskatchewan.
8. S. Kouloudris, G. Kiziltas, Y. Zhou, D. J. Hansford, and J. L. Volakis (2006). Polymer-Ceramic Composites for Microwave Applications: Fabrication and

Performance Assessment. *IEEE Transactions on Microwave Theory and Techniques, 54* (12), 4202-4207.

9. J. A. Rogers, Z. Bao, K. Baldwin, A. Dodabalpur, B. Crone, V. R. Raju, V. Kuck, H. Katz, K. Amundson, J. Ewing and P. Drzaic (2001). Paper like electronic displays: Large area, rubber stamped plastic sheets of electronics and electrophoretic inks. *Proc. Nat. Acad. Sci., 98*, 4835-4840.
10. D.H. Hwang, S.T. Kim, X.C. Li, B.S. Chuah, J.C. DeMello, R.H. Friend, S.C. Moratti and A.B. Holmes (1998). New luminescent polymers for LEDs and LECs. *Proc. Macromolecular Symp., 125*, 111-120.
11. A. Matsuzawa (2002). RF-SoC: Expectations and required conditions. *IEEE Trans. Microw. Theory Tech., 50,* 245-253.
12. J. W. Modelski, and Y. Yashchyshyn (2005). Rigorous analysis and investigations of the scan antennas on a ferroelectric substrate. *IEEE Trans. Microwave Theory Technology, 53*, 427-438.
13. S. Ramesh, B. A. Shutzberg, C. Huang, J. Gao, and E. P. Giannelis (2003). Dielectric nanocomposites for integral thin capacitors: Materials design, fabrication and integration issues. *IEEE Trans. Adv. Packag., 26*, 17-24.
14. A Petosa, A. Ittipiboon, Y.M. M. Antar, D. Rossoe and M. Cuhaci (1998). Recent advances in dielectric resonator antenna technology. *IEEE Antennas Propagat. Mag., 40*, 35-48.
15. Z. Fan, and Y. M. M. Antar (1996). Theoretical investigations of aperture coupled rectangular dielectric resonator antenna. *Proc.Inst. Elect. Eng., Part H, 143*, 113-118.

16. S. A. Long, M. McAllister, and L. C. Shen (1983, May). The resonant cylindrical cavity antenna. *IEEE Trans. Antennas Propagat. ,* 406-412.
17. M. McAllister, S. A. Long and G. L. Conway (1983). Rectangular dielectric resonator antenna. *Electron. Lett., 19*, 219-220.
18. S. A. Long, and M. McAllister (1984). Resonant hemispherical dielectric antenna. *Electron. Lett., 20*, 657-659.
19. R. K. Mongia and A. Ittipiboon. (1997). Theoretical and experimental investigations on rectangular dielectric resonator antennas. *IEEE Trans. Antennas Propagation*, 1348-1356.
20. A. A. Kishk, H. A. Auda, and B. C. Ahn (1989, Feb). Radiation characteristics of cylindrical resonant antennas with new applications. *IEEE Antennas Propagat. Soc. Newslett. ,* 7-16.
21. R. K. Mongia (1989). Half-split dielectric resonator placed on a metallic plane for antenna applications. *Electron. Lett. , 25*, 462-464.
22. K. W. Leung, and K. M. Luk (1993, October). Theory and experiment of a coaxial probe fed hemispherical dielectric resonator antenna. *IEEE Trans. Antennas Propagat.*, 1390-1398.
23. R. K. Mongia, A. Ittipiboon, P. Bhartia, and M. Cuhaci (1994, June). Radiation Q-factor of rectangular dielectric resonator antennas—Theory and experiment. *Int. IEEE APS Symp.*, 764-767.
24. A. Ittipiboon, R. K. Mongia, Y. M. M. Antar, P. Bhartia and M. Cuhaci (1993). Aperture fed rectangular and triangular dielectric resonators for use as magnetic dipole antennas. *Electron. Lett., 29*, 2001-2002.

25. R. K. Mongia, A. Ittipiboon, M. Cuhaci, and D. Roscoe (1993). Electric monopole antenna using a dielectric ring resonator. *Electron. Lett., 29*, 1530-1531.

26. M. Gastine, L. Courtois and J. J. Dormann (1967, December). Electromagnetic resonances of free dielectric spheres. *IEEE Trans. Microwave Theory Tech.*, 694-700.

27. D. Kajfez and P. Guillon (Eds.), (1986). *Dielectric Resonators.* Norwood: Artech House.

28. A. Petosa, (2007). *Dielectric Resonator Antenna Handbook* . Artech House Publishers.

29. G. Bit-Babik, C. Di Nallo, and A. Faraone (2004). Multimode Dielectric Resonator Antenna of Very High Permittivity. *2*, pp. 1383-1386. Monterey, CA: IEEE Antennas & Propagation Symposium Digest AP-S.

30. K. M. Luk and K. W. Leung. (2002). *Dielectric Resonator Antennas.* Hertfordshire, U.K.: Research Studies Press Ltd.

31. *Metamaterials*. (n.d.). Retrieved December 21, 2014, from Wikipedia: http://en.wikipedia.org/wiki/Metamaterial

32. T. J. Cui, D Smith and R Liu (2009). *Metamaterials: Theory, Design and Applications.* Springer Science and Business Media.

33. J. B. Pendry. (2000, October). Negative Refraction Makes a Perfect Lens. *Physics Review Letters* .

34. D. R. Smith and N. Kroll. (2000). Negative refractive index in left-handed materials. *Physics Review Letters* , 2933-2966.

35. D. R. Smith, W. J. Padilla, D. C. Vier et al., (2000). A composite medium with simultaneous negative permittivity and permeability. *Physical Review Letters* , 4184-4187.

36. V. M. Shalaev (2008). "Metamaterials, Part 1: Electrical and Magnetic Metamaterials," http://nanohub.org/resources/4263.

37. L. Mandelshtam. (1945). Zhurnal Eksperimentalnoi i Teoreticheskoi Fiziki in Russian translated in English and published by *Journal of Experimental and Theoretical Physics*.

38. H. C. Pocklington. (1905). Growth of a Wave-group when the Group-velocity is Negative. *Nature* , 607-608.

39. L. I. Mandelshtam. (1950). Lectures on some problems of the theory of oscillations. *Complete Collection of Works, 5*, 428-467.

40. M. Notomi. (2000, October). Theory of light propagation in strongly modulated photonic crystals: Refractionlike behavior in the vicinity of the photonic band gap. *Physical Review B*. DOI: http://dx.doi.org/10.1103/PhysRevB.62.10696

41. L. Brillouin. (1946). *Wave Propagation in Periodic Structures.* New York: McGraw-Hill.

42. J. R. Pierce. (1950). *Traveling-Wave Tubes.* New York: Van Nostrand.

43. G. D.Malyuzhinets. (1951). Zhurnal Technicheskoi Fiziki. *English translation in Sov. Phys. Tech. Phys.*, 940-42.

44. A. Grbic and G. Eleftheriades. (2003). Periodic analysis of a 2-D negative refractive index transmission line structure. *Antennas and Propagation, IEEE Transactions* , 2604-2611.

45. A. Lai, C. Caloz, and T. Itoh, (2004). Composite right/left-handed transmission line metamaterials. *Microwave Magazine, IEEE , 5*, 34-50.

46. D. V. Sivukhin. (1957). The energy of electromagnetic waves in dispersive media. *Opt. Spektroscopy*, 308-312.

47. R. G. E. Hutter. (1960). *Beam and Wave Electronics in Microwave Tubes.* Princeton, NJ: Van Nostrand.

48. R. A. Silin. (1959). Electromagnetic waves in artificial periodic structures. *Voprosy Radioelektroniki, Elektronika*.

49. W. E. Kock. (1948). Metallic Delay Lenses., *Bell System Technical J., 27*, 58-82.

50. Lord Rayleigh. (1892). *Philosophy Magazine Series 5*, Vol. 34.

51. F. Capolino (October 5, 2009). *Theory and Phenomena of Metamaterials.* CRC Press.

52. A. H. Sihvola. (1999). *Electromagnetic Mixing Formulas and Applications.* London: IET Publishers.

53. S. Torquato, T. M. Truskett, and P. G. Debenedetti (2000). Is Random Close Packing of Spheres Well Defined? *Physics Review Letters*. DOI: http://dx.doi.org/10.1103/PhysRevLett.84.2064

54. S. Chapman and T. G. Cowling (1953). *The Mathetical Theory of Non-uniform* Gases. Cambridge: Cambridge University Press.

55. A. P. Vinogradov. (2001). *Electrodynamics of Composite Materials.* Moscow: URSS Publishers.

56. M. J. Jackson (2007). *Micro and Nanomanufacturing*. Springer Science and Business Media.

Appendix A

Design Specifications of H and Window meta-DRAs resonating around 24 GHz

A.1 H Inclusions

The first kind of metal (nickel) inclusions tested were of the shape *H*. The DRA made of a material with permittivity of 2.5, was filled with these *H* inclusions. The following sub sections define the designs in terms of the parameters mentioned in Section 3.2.

Design 1 (H_1):

Element Size: 200 by 200μm

Gap: 20μm

Internal Width: 20μm

Dimension of DRA: 4mm by 4mm by 1.8mm

Dimension of Substrate: 15mm by 15mm by 0.781mm

Feed Dimension: 2.2mm by (3.16 + Δl) mm by 0.003mm

ΔL for Feedline: 0mm to 0.15mm, step of 0.05mm.

Number of Inclusions: 17 by 17

Waveport Dimension: Position [2,0,0]; Size => X=11.5mm Z=5mm.

Air box Dimension: Position [-1,0,-1]; Size => 17mm by 16mm by 8mm.

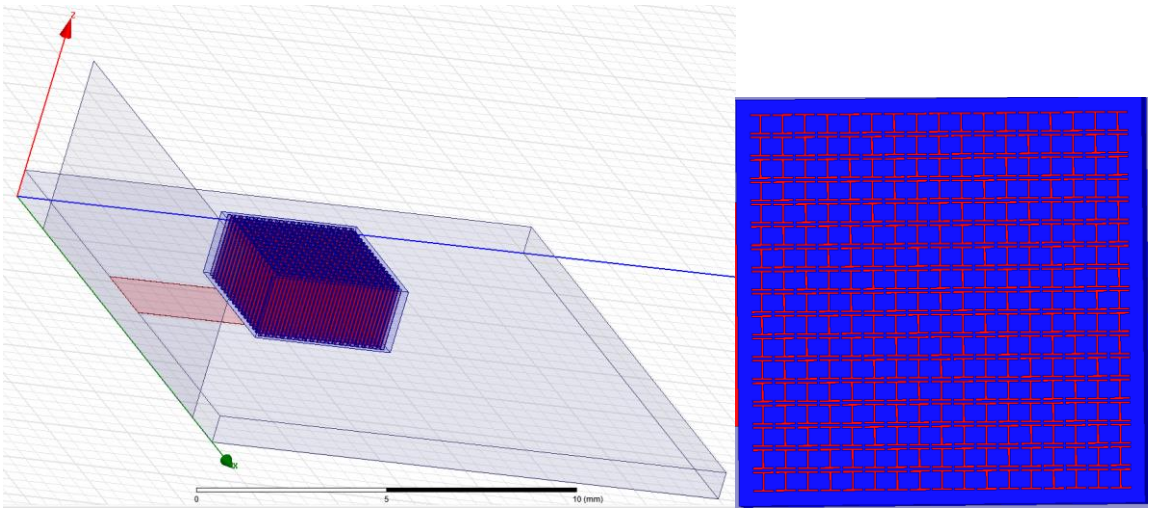

Figure A.1 The meta-DRA design and top-view of H_1.

Design 2 (H_2):

Element Size: 200 by 200μm

Gap: 50μm

Internal Width: 50μm

Dimension of DRA: 4mm by 4mm by 1.8mm

Dimension of Substrate: 15mm by 15mm by 0.781mm

Feed Dimension: 2.2mm by (3.16 + Δl) mm by 0.003mm

ΔL for Feedline: 0mm to 0.15mm, step of 0.05mm.

Number of Inclusions: 15 by 15

Waveport Dimension: Position [2,0,0]; Size => X=11.5mm Z=5mm.

Air box Dimension: Position [-1,0,-1]; Size => 17mm by 16mm by 8mm.

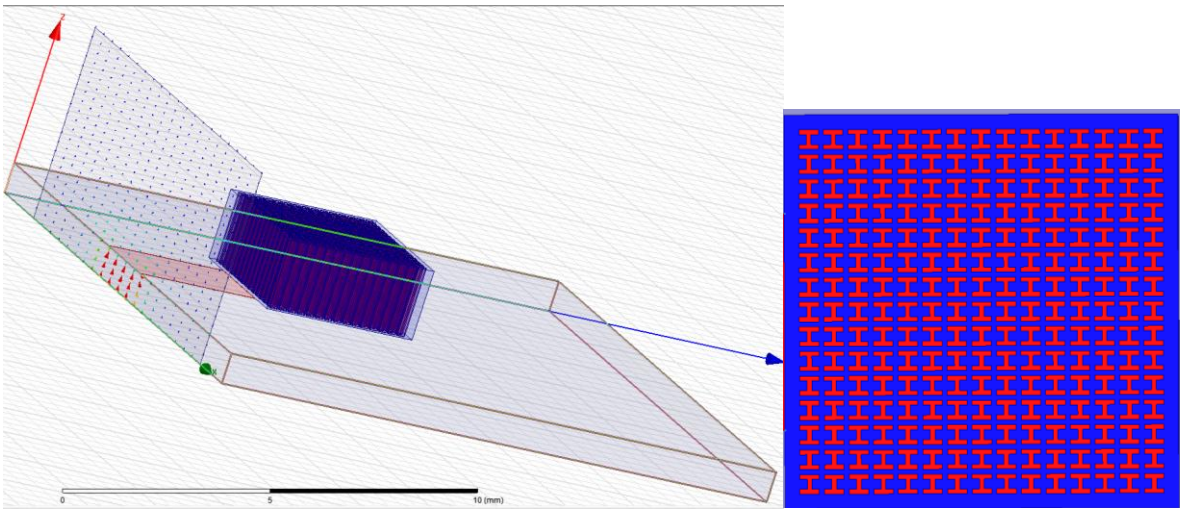

Figure A.2 The meta-DRA design and top-view of H_2.

Design 3 (H_3):

Element Size: 500 by 500µm

Gap: 50µm

Internal Width: 50µm

Dimension of DRA: 4mm by 4mm by 1.8mm

Dimension of Substrate: 15mm by 15mm by 0.781mm

Feed Dimension: 2.2mm by (3.16 + Δl) mm by 0.003mm

ΔL for Feedline: 0mm to 0.1mm, step of 0.02mm.

Number of Inclusions: 7 by 7

Waveport Dimension: Position [2,0,0]; Size => X=11.5mm Z=5mm.

Air box Dimension: Position [-1,0,-1]; Size => 17mm by 16mm by 8mm.

Design 4 (H_4):

Element Size: 200 by 500µm

Gap: 20µm

Internal Width: 20µm

Dimension of DRA: 4mm by 4mm by 1.8mm

Dimension of Substrate: 15mm by 15mm by 0.781mm

Feed Dimension: 2.2mm by (3.16 + Δl) mm by 0.003mm

ΔL for Feedline: 0mm to 0.15mm, step of 0.03mm.

Number of Inclusions: 7 by 17

Waveport Dimension: Position [2,0,0]; Size => X=11.5mm Z=5mm.

Air box Dimension: Position [-1,0,-1]; Size => 17mm by 16mm by 8mm.

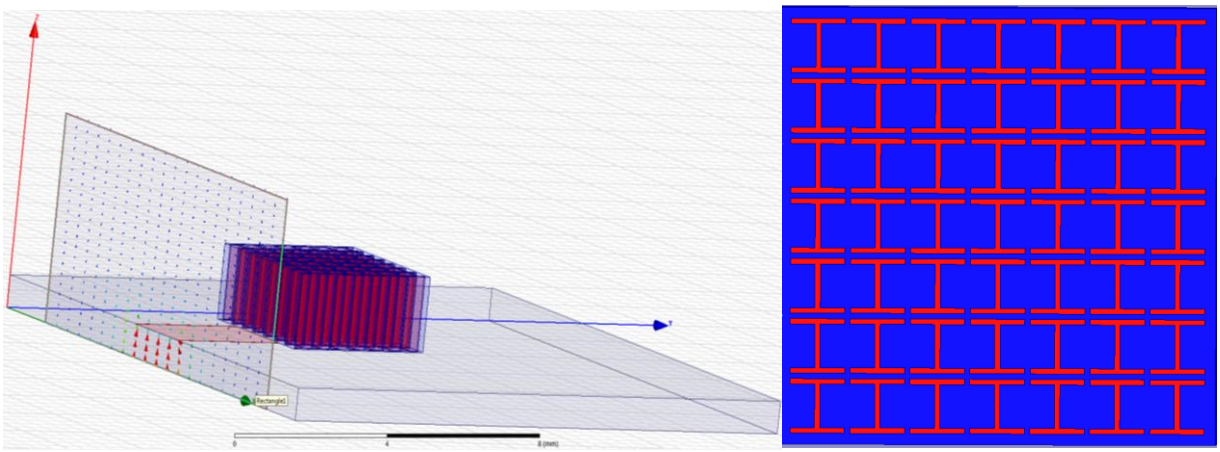

Figure A.3 The meta-DRA design and top-view of H_3.

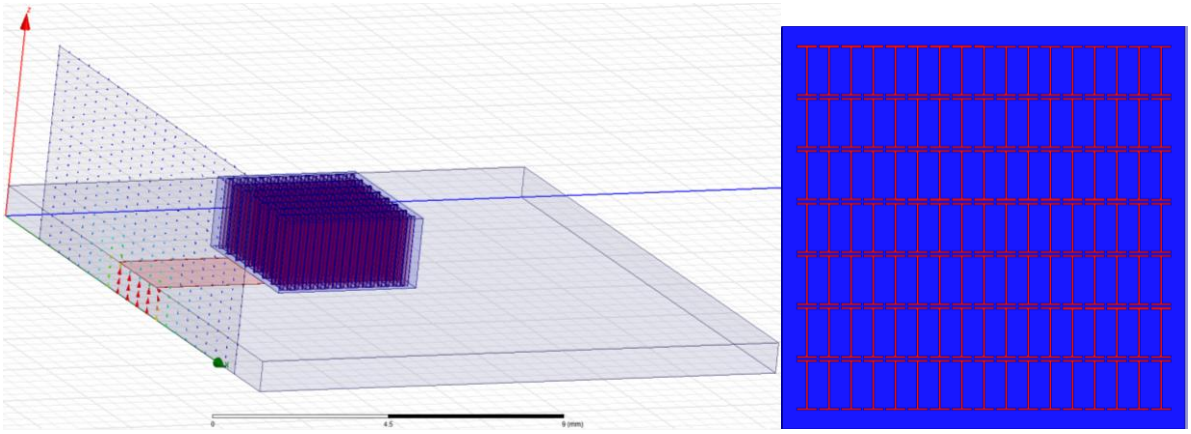

Figure A.4 The meta-DRA design and top-view of H_4.

Design 5 (H_5):

Element Size: 200 by 500µm

Gap: 50µm

Internal Width: 50µm

Dimension of DRA: 4mm by 4mm by 1.8mm

Dimension of Substrate: 15mm by 15mm by 0.781mm

Feed Dimension: 2.2mm by (3.16 + Δl) mm by 0.003mm

ΔL for Feedline: 0mm to 0.15mm, step of 0.03mm.

Number of Inclusions: 6 by 15

Waveport Dimension: Position [2,0,0]; Size => X=11.5mm Z=5mm.

Air box Dimension: Position [-1,0,-1]; Size => 17mm by 16mm by 8mm.

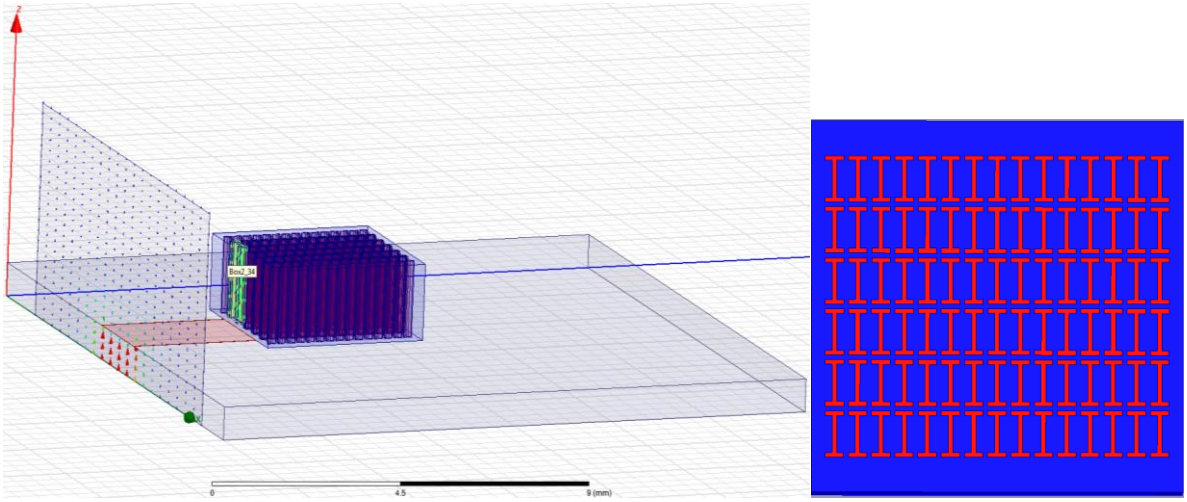

Figure A.5 The meta-DRA design and top-view of H_5.

A.2 Window Inclusions

The next set of designs include metal inclusions in the shape of a window. The following sub sections give the designs made with these inclusions.

Design 1 (W_1):

Element Size: 200 by 200µm

Gap: 20µm

Internal Width: 20µm

Dimension of DRA: 4mm by 4mm by 1.8mm

Dimension of Substrate: 15mm by 15mm by 0.781mm

Feed Dimension: 2.2mm by (3.16 + Δl) mm by 0.003mm

ΔL for Feedline: 0.03mm to 0.15mm, step of 0.03mm.

Number of Inclusions: 17 by 17

Waveport Dimension: Position [2,0,0]; Size => X=11.5mm Z=5mm.

Air box Dimension: Position [-1,0,-1]; Size => 17mm by 16mm by 8mm.

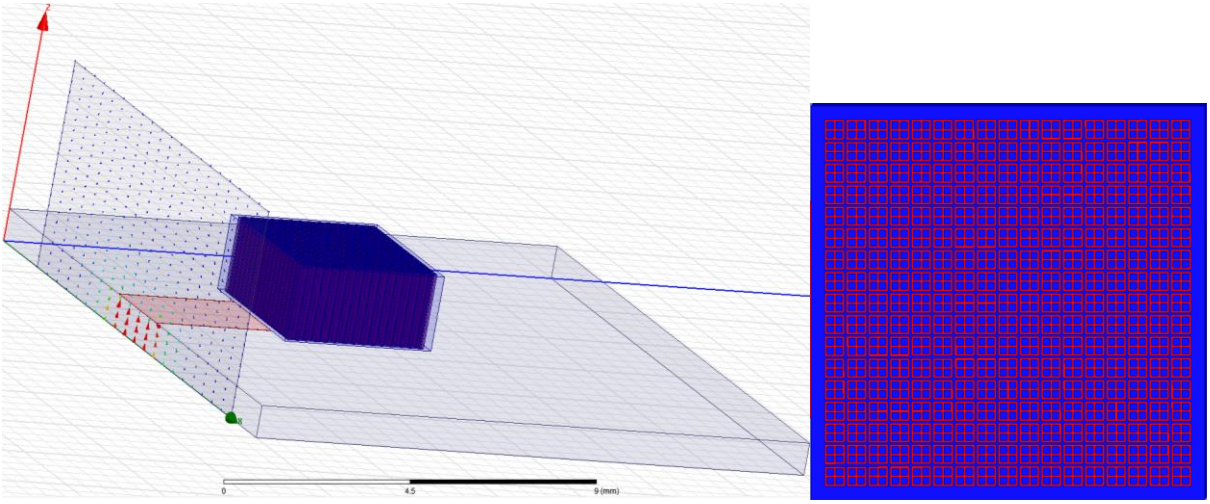

Figure A.6 The meta-DRA design and top-view of W_1.

Design 2 (W_2):

Element Size: 200 by 200µm

Gap: 30µm

Internal Width: 30µm

Dimension of DRA: 4mm by 4mm by 1.8mm

Dimension of Substrate: 15mm by 15mm by 0.781mm

Feed Dimension: 2.2mm by (3.16 + Δl) mm by 0.003mm

ΔL for Feedline: 0mm to 0.15mm, step of 0.03mm.

Number of Inclusions: 16 by 16

Waveport Dimension: Position [2,0,0]; Size => X=11.5mm Z=5mm.

Air box Dimension: Position [-1,0,-1]; Size => 17mm by 16mm by 8mm.

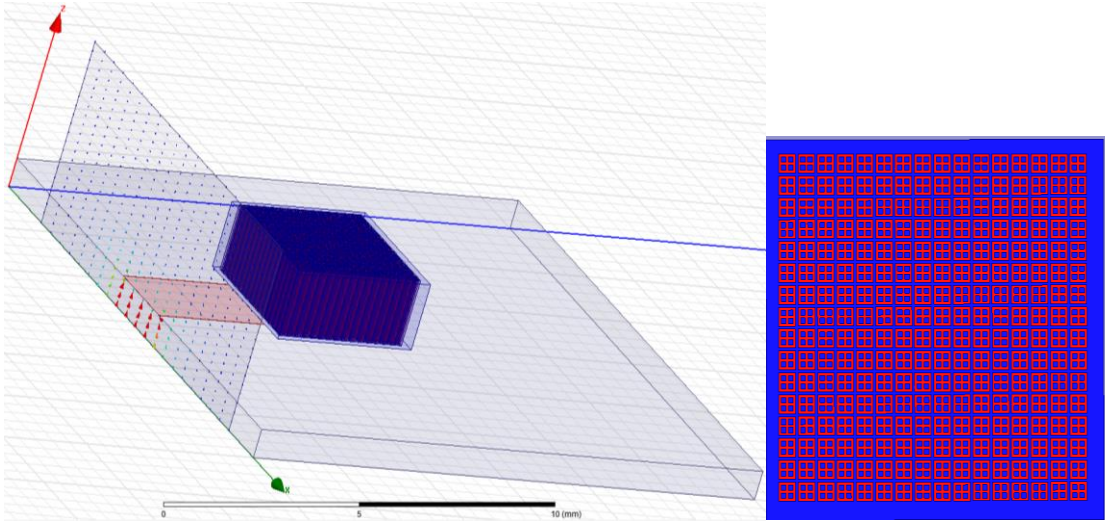

Figure A.7 The meta-DRA design and top-view of W_2.

Design 3 (W_3):

Element Size: 200 by 200μm

Gap: 20μm in the X-axis and 50μm in Y-axis.

Internal Width: 20μm in the X-axis and 50μm in Y-axis.

Dimension of DRA: 4mm by 4mm by 1.8mm

Dimension of Substrate: 15mm by 15mm by 0.781mm

Feed Dimension: 2.2mm by (3.16 + Δl) mm by 0.003mm

ΔL for Feedline: 0mm to 0.25mm, step of 0.05mm.

Number of Inclusions: 17 by 15

Waveport Dimension: Position [2,0,0]; Size => X=11.5mm Z=5mm.

Air box Dimension: Position [-1,0,-1]; Size => 17mm by 16mm by 8mm.

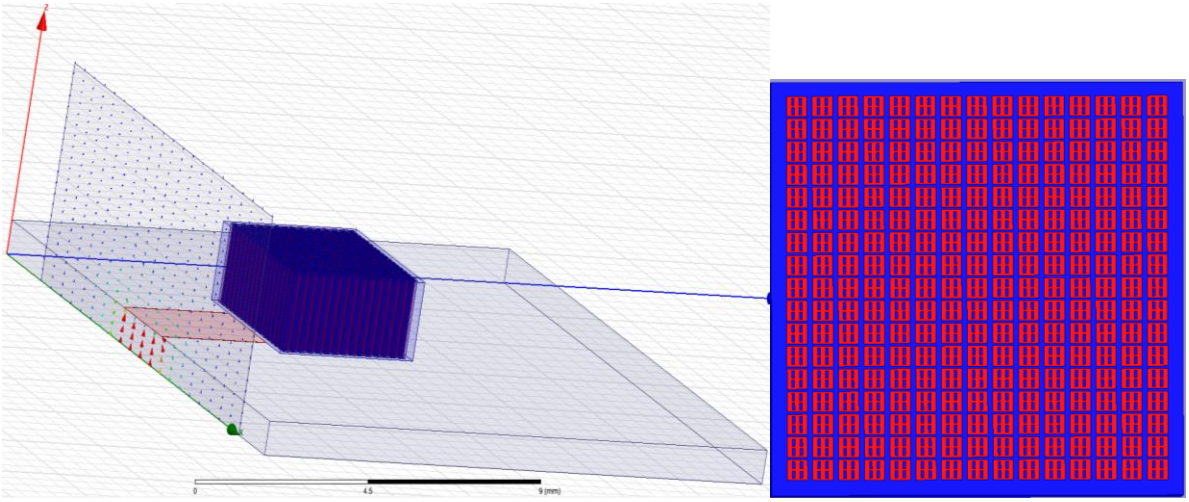

Figure A.8 The meta-DRA design and top-view of W_3.

Design 4 (W_4):

Element Size: 200 by 500µm

Gap: 20µm

Internal Width: 20µm

Dimension of DRA: 4mm by 4mm by 1.8mm

Dimension of Substrate: 15mm by 15mm by 0.781mm

Feed Dimension: 2.2mm by (3.16 + Δl) mm by 0.003mm

ΔL for Feedline: 0mm to 0.15mm, step of 0.03mm.

Number of Inclusions: 17 by 17

Waveport Dimension: Position [2,0,0]; Size => X=11.5mm Z=5mm.

Air box Dimension: Position [-1,0,-1]; Size => 17mm by 16mm by 8mm.

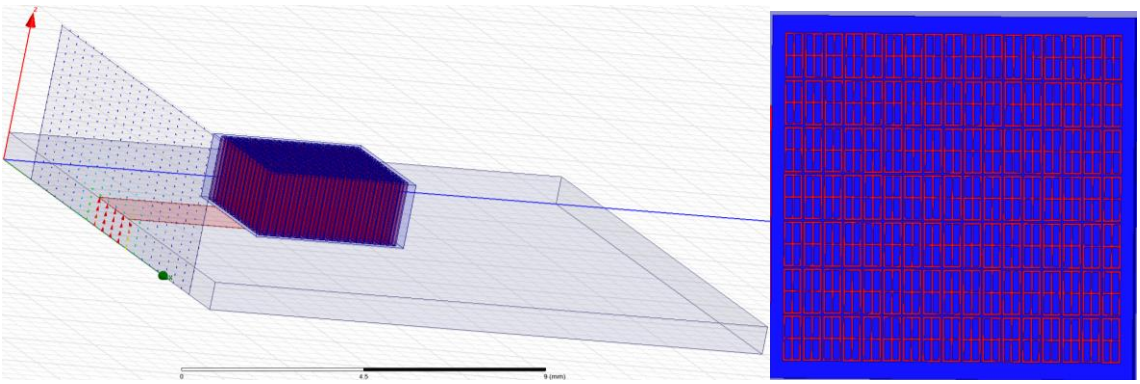

Figure A.9 The meta-DRA design and top-view of W_4.

Design 5 (W_5):

Element Size: 200 by 500µm

Gap: 50µm

Internal Width: 50µm

Dimension of DRA: 4mm by 4mm by 1.8mm

Dimension of Substrate: 15mm by 15mm by 0.781mm

Feed Dimension: 2.2mm by (3.16 + Δl) mm by 0.003mm

ΔL for Feedline: 0mm to 0.15mm, step of 0.03mm.

Number of Inclusions: 6 by 15

Waveport Dimension: Position [2,0,0]; Size => X=11.5mm Z=5mm.

Air box Dimension: Position [-1,0,-1]; Size => 17mm by 16mm by 8mm.

Design 6 (W_6):

Element Size: 200 by 500µm

Gap: 20µm in the X-axis and 50µm in Y-axis.

Internal Width: 20µm in the X-axis and 50µm in Y-axis.

Dimension of DRA: 4mm by 4mm by 1.8mm

Dimension of Substrate: 15mm by 15mm by 0.781mm

Feed Dimension: 2.2mm by (3.16 + Δl) mm by 0.003mm

ΔL for Feedline: 0mm to 0.15mm, step of 0.05mm.

Number of Inclusions: 7 by 15

Waveport Dimension: Position [2,0,0]; Size => X=11.5mm Z=5mm.

Air box Dimension: Position [-1,0,-1]; Size => 17mm by 16mm by 8mm.

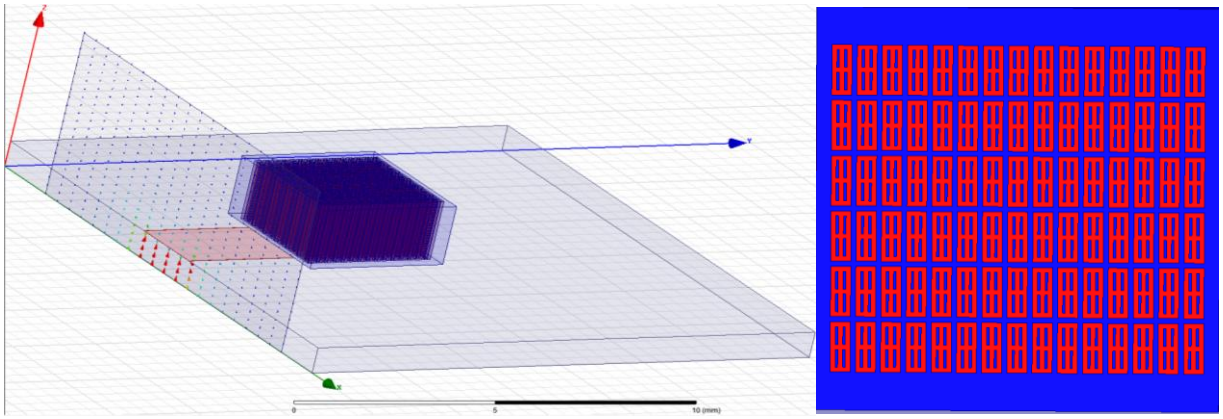

Figure A.10 The meta-DRA design and top-view of W_5.

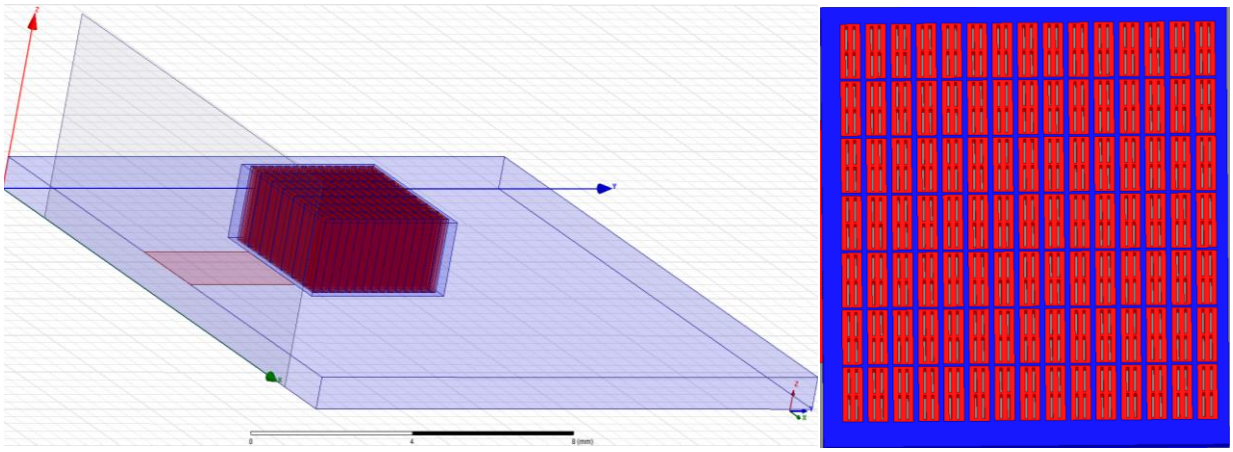

Figure A.11 The meta-DRA design and top-view of W_6.

Appendix B

Design Specifications of H and Window meta-DRAs resonating around 60 GHz

B.1 H Inclusions

These meta-DRAs are formed by metal (Nickel) inclusions in the form of *H* shape as shown in section 3.3.1. The design parameters are given as below:

Design 1 (h_1):

Element Size: 100 by 100μm

Gap: 20μm

Internal Width: 20μm

Dimension of DRA: 1.5mm by 1.5mm by 0.7mm

Dimension of Substrate: 5mm by 5mm by 0.281mm

Feed Dimension: 0.923mm by (0.889 + Δl) mm by 0.001mm

ΔL for Feedline: 0mm to 0.12mm, step of 0.02mm.

Number of Inclusions: 10 by 10

Waveport Dimension: Position [5.1,0,0]; Size => X=4.5mm Z=2.8mm.

Air box Dimension: Position [4,0,-1]; Size => 7mm by 6mm by 8mm.

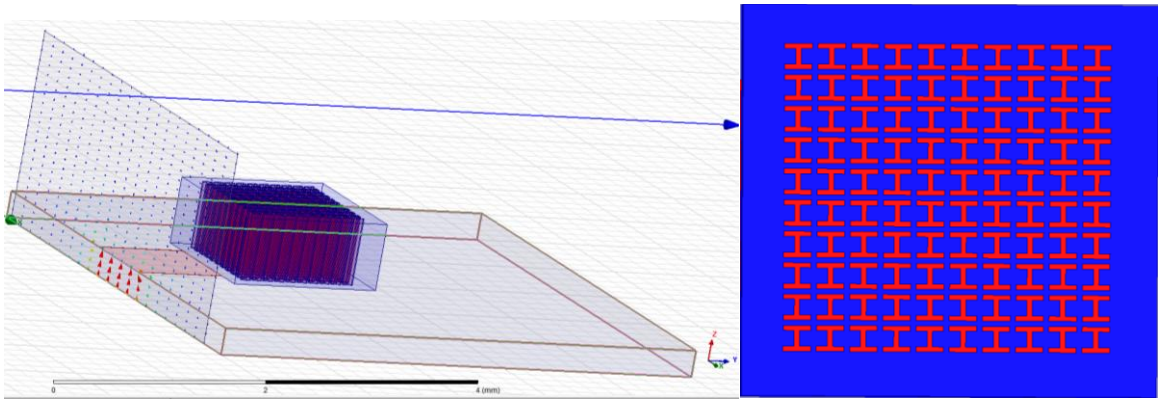

Figure B.1 The meta-DRA design and top-view of h_1.

Design 2 (h_2):

Element Size: 100 by 100μm

Gap: 30μm

Internal Width: 30μm

Dimension of DRA: 1.5mm by 1.5mm by 0.7mm

Dimension of Substrate: 5mm by 5mm by 0.281mm

Feed Dimension: 0.923mm by (0.889 + Δl) mm by 0.001mm

ΔL for Feedline: 0mm to 0.1mm, step of 0.02mm.

Number of Inclusions: 10 by 10

Waveport Dimension: Position [5.1,0,0]; Size => X=4.5mm Z=2.8mm.

Air box Dimension: Position [4,0,-1]; Size => 7mm by 6mm by 8mm.

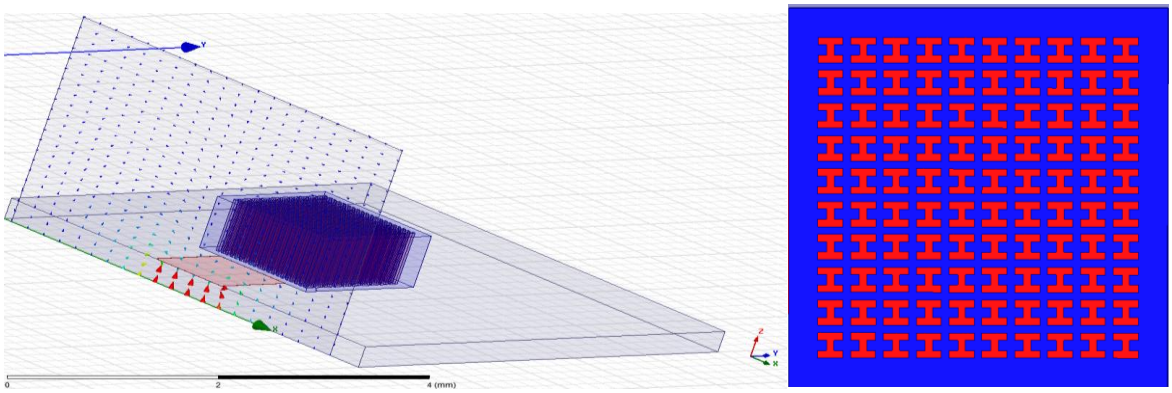

Figure B.2 The meta-DRA design and top-view of h_2.

Design 3 (h_3):

Element Size: 100 by 100μm

Gap: 20μm in the X-axis and 50μm in Y-axis.

Internal Width: 20μm in the X-axis and 50μm in Y-axis.

Dimension of DRA: 1.5mm by 1.5mm by 0.7mm

Dimension of Substrate: 15mm by 15mm by 0.281mm

Feed Dimension: 0.923mm by (0.889 + Δl) mm by 0.001mm

ΔL for Feedline: 0mm to 0.1mm, step of 0.02mm.

Number of Inclusions: 11 by 9

Waveport Dimension: Position [5.1,0,0]; Size => X=4.5mm Z=2.8mm.

Air box Dimension: Position [4,0,-1]; Size => 7mm by 6mm by 8mm.

Design 4 (h_4):

Element Size: 100 by 200μm

Gap: 30μm

Internal Width: 30μm

Dimension of DRA: 1.5mm by 1.5mm by 0.7mm

Dimension of Substrate: 15mm by 15mm by 0.281mm

Feed Dimension: 0.923mm by (0.889 + Δl) mm by 0.001mm

ΔL for Feedline: 0mm to 0.1mm, step of 0.02mm.

Number of Inclusions: 5 by 10

Waveport Dimension: Position [5.1,0,0]; Size => X=4.5mm Z=2.8mm.

Air box Dimension: Position [4,0,-1]; Size => 7mm by 6mm by 8mm.

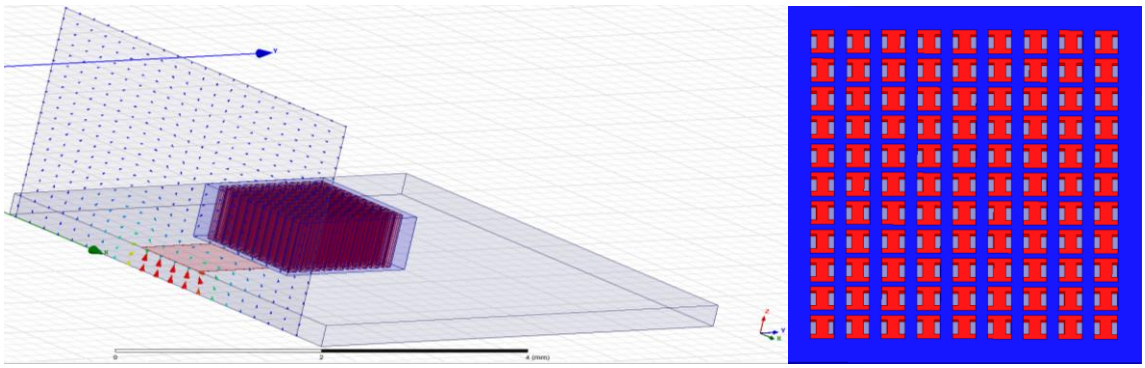

Figure B.3 The meta-DRA design and top-view of h_3.

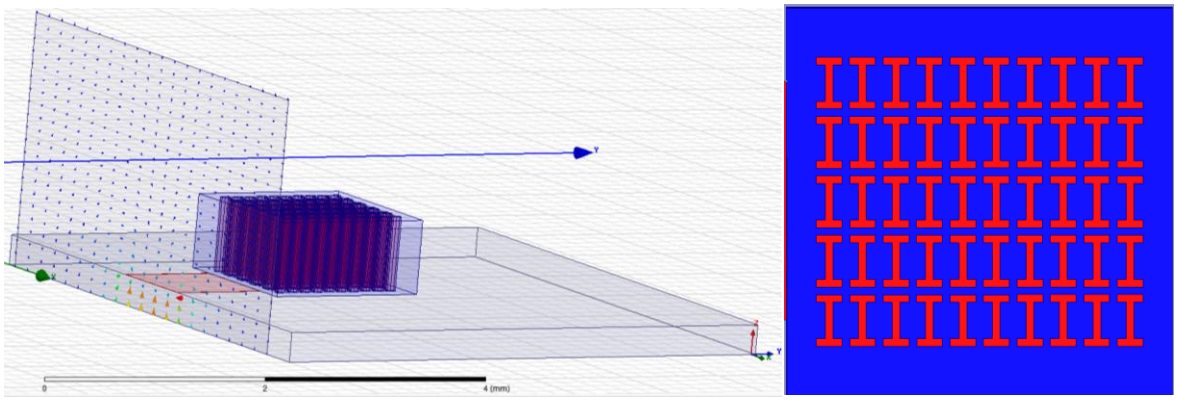

Figure B.4 The meta-DRA design and top-view of h_4.

Design 5 (h_5):

Element Size: 100 by 200μm

Gap: 50μm

Internal Width: 50μm

Dimension of DRA: 1.5mm by 1.5mm by 0.7mm

Dimension of Substrate: 15mm by 15mm by 0.281mm

Feed Dimension: 0.923mm by (0.889 + Δl) mm by 0.001mm

ΔL for Feedline: 0mm to 0.175mm, step of 0.035mm.

Number of Inclusions: 8 by 6

Waveport Dimension: Position [5.1,0,0]; Size => X=4.5mm Z=2.8mm.

Air box Dimension: Position [4,0,-1]; Size => 7mm by 6mm by 8mm.

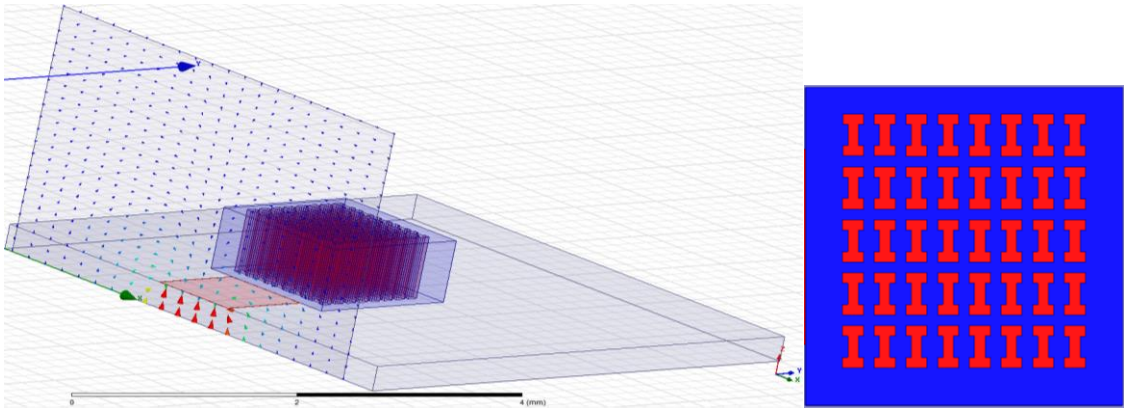

Figure B.5 The meta-DRA design and top-view of h_5.

Design 6 (h_6):

Element Size: 100 by 200µm

Gap: 20µm in the X-axis and 50µm in Y-axis.

Internal Width: 20µm in the X-axis and 50µm in Y-axis.

Dimension of DRA: 1.5mm by 1.5mm by 0.7mm

Dimension of Substrate: 15mm by 15mm by 0.281mm

Feed Dimension: 0.923mm by (0.889 + Δl) mm by 0.001mm

ΔL for Feedline: 0mm to 0.1mm, step of 0.02mm.

Number of Inclusions: 11 by 5

Waveport Dimension: Position [5.1,0,0]; Size => X=4.5mm Z=2.8mm.

Air box Dimension: Position [4,0,-1]; Size => 7mm by 6mm by 8mm.

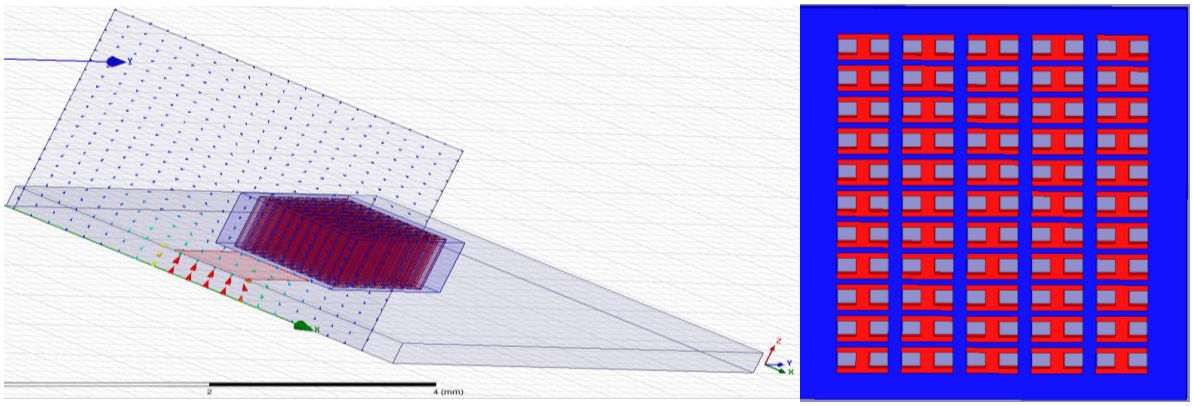

Figure B.6 The meta-DRA design and top-view of h_6.

B.2 Window Inclusions

The next set of designs are window inclusions in the DRAs. The design parameters for the 60 GHz meta-DRAs are given as follows:

Design 1 (w_1):

Element Size: 100 by 100μm

Gap: 20μm

Internal Width: 20μm

Dimension of DRA: 1.5mm by 1.5mm by 0.7mm

Dimension of Substrate: 5mm by 5mm by 0.281mm

Feed Dimension: 0.923mm by (0.889 + Δl) mm by 0.001mm

ΔL for Feedline: 0mm to 0.09mm, step of 0.018mm.

Number of Inclusions: 11 by 11

Waveport Dimension: Position [5.1,0,0]; Size => X=4.5mm Z=2.8mm.

Air box Dimension: Position [4,0,-1]; Size => 7mm by 6mm by 8mm.

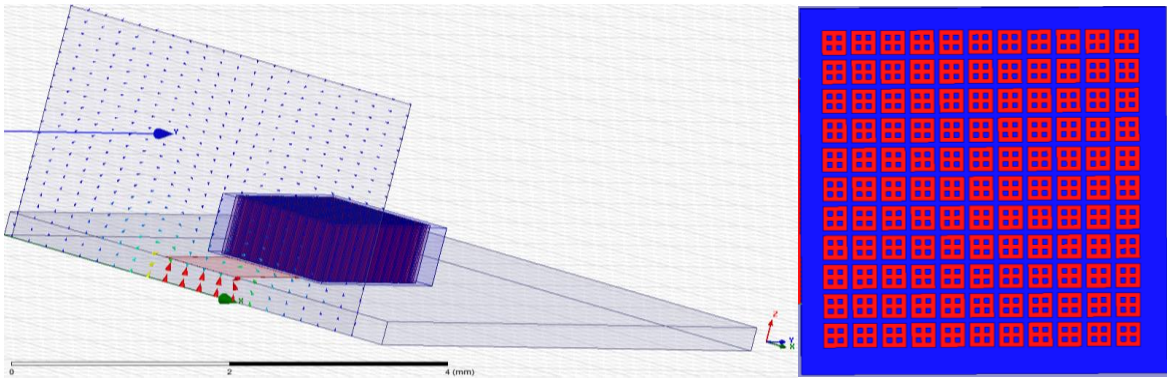

Figure B.7 The meta-DRA design and top-view of w_1.

Design 2 (w_2):

Element Size: 100 by 100µm

Gap: 25µm

Internal Width: 25µm

Dimension of DRA: 1.5mm by 1.5mm by 0.7mm

Dimension of Substrate: 5mm by 5mm by 0.281mm

Feed Dimension: 0.923mm by (0.889 + Δl) mm by 0.001mm

ΔL for Feedline: 0mm to 0.125mm, step of 0.025mm.

Number of Inclusions: 10 by 10

Waveport Dimension: Position [5.1,0,0]; Size => X=4.5mm Z=2.8mm.

Air box Dimension: Position [4,0,-1]; Size => 7mm by 6mm by 8mm.

Design 3 (w_3):

Element Size: 100 by 100µm

Gap: 20µm in X-axis and 30µm in Y-axis.

Internal Width: 20µm in X-axis and 30µm in Y-axis.

Dimension of DRA: 1.5mm by 1.5mm by 0.7mm

Dimension of Substrate: 5mm by 5mm by 0.281mm

Feed Dimension: 0.923mm by (0.889 + Δl) mm by 0.001mm

ΔL for Feedline: 0mm to 0.1mm, step of 0.02mm.

Number of Inclusions: 11 by 10

Waveport Dimension: Position [5.1,0,0]; Size => X=4.5mm Z=2.8mm.

Air box Dimension: Position [4,0,-1]; Size => 7mm by 6mm by 8mm.

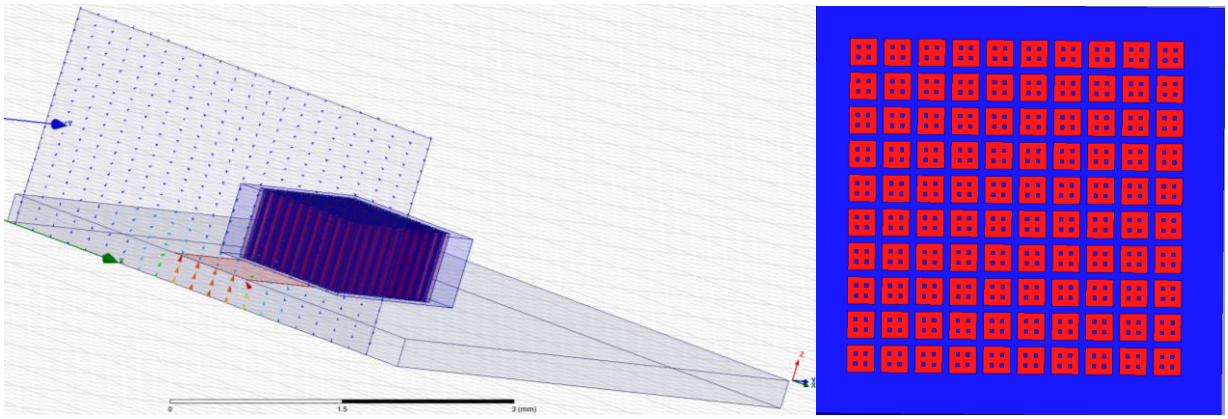

Figure B.8 The meta-DRA design and top-view of $w_{2.}$

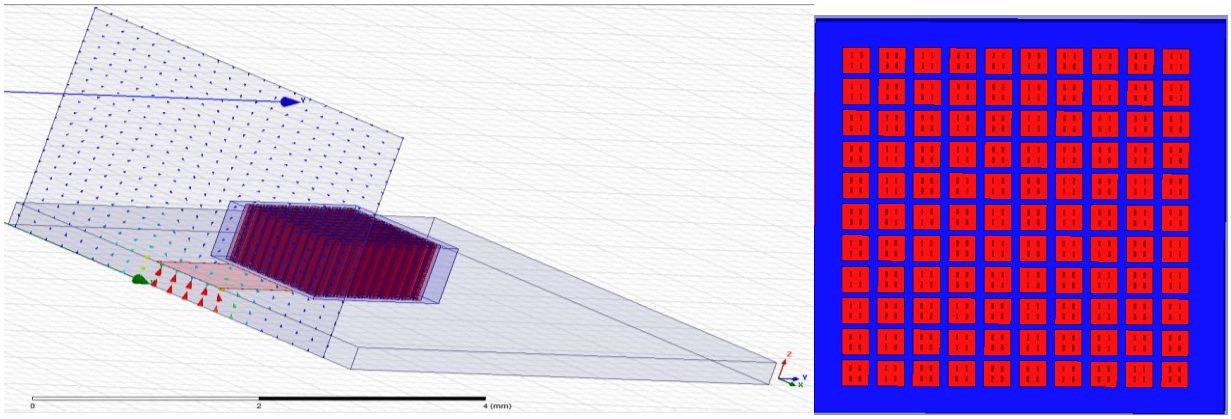

Figure B.9 The meta-DRA design and top-view of $w_{3.}$

Design 4 (w_4):

Element Size: 100 by 200µm

Gap: 20µm

Internal Width: 20µm

Dimension of DRA: 1.5mm by 1.5mm by 0.7mm

Dimension of Substrate: 5mm by 5mm by 0.281mm

Feed Dimension: 0.923mm by (0.889 + Δl) mm by 0.001mm

ΔL for Feedline: 0mm to 0.15mm, step of 0.03mm.

Number of Inclusions: 6 by 10

Waveport Dimension: Position [5.1,0,0]; Size => X=4.5mm Z=2.8mm.

Air box Dimension: Position [4,0,-1]; Size => 7mm by 6mm by 8mm.

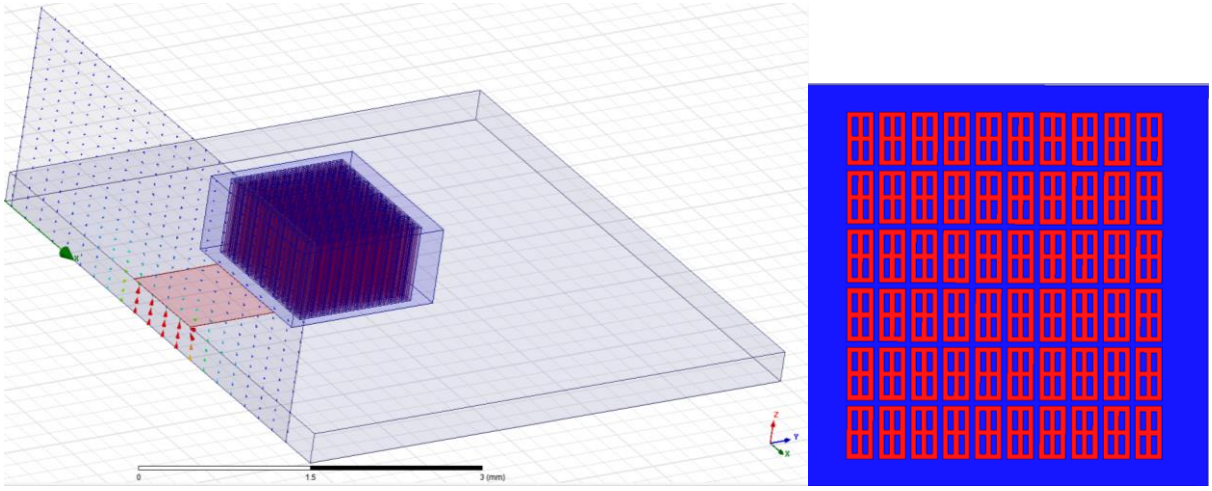

Figure B.10 The meta-DRA design and top-view of w_4.

Design 5 (w_5):

Element Size: 100 by 200µm

Gap: 25µm

Internal Width: 25µm

Dimension of DRA: 1.5mm by 1.5mm by 0.7mm

Dimension of Substrate: 5mm by 5mm by 0.281mm

Feed Dimension: 0.923mm by (0.889 + Δl) mm by 0.001mm

ΔL for Feedline: 0mm to 0.09mm, step of 0.018mm.

Number of Inclusions: 6 by 10

Waveport Dimension: Position [5.1,0,0]; Size => X=4.5mm Z=2.8mm.

Air box Dimension: Position [4,0,-1]; Size => 7mm by 6mm by 8mm.

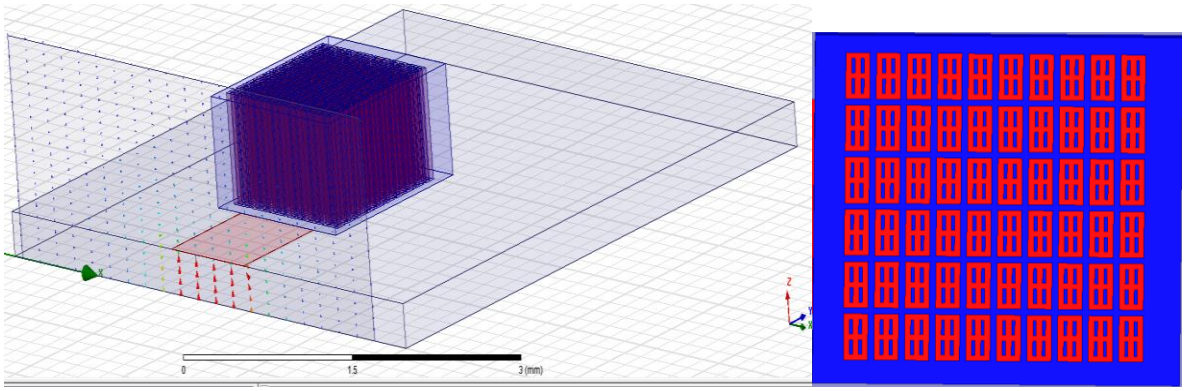

Figure B.11 The meta-DRA design and top-view of w_5.

Design 6 (w_6):

Element Size: 100 by 200µm

Gap: 20µm in X-axis and 50µm in Y-axis.

Internal Width: 20µm in X-axis and 50µm in Y-axis.

Dimension of DRA: 1.5mm by 1.5mm by 0.7mm

Dimension of Substrate: 5mm by 5mm by 0.281mm

Feed Dimension: 0.923mm by (0.889 + Δl) mm by 0.001mm

ΔL for Feedline: 0mm to 0.09mm, step of 0.018mm.

Number of Inclusions: 6 by 10

Waveport Dimension: Position [5.1,0,0]; Size => X=4.5mm Z=2.8mm.

Air box Dimension: Position [4,0,-1]; Size => 7mm by 6mm by 8mm.

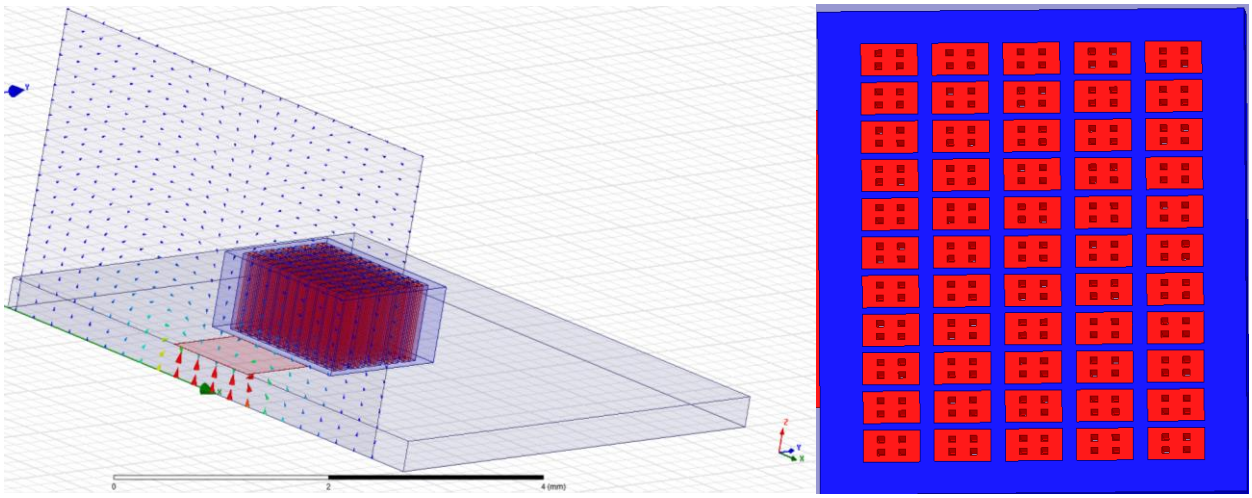

Figure B.12 The meta-DRA design and top-view of $w_{6.}$